FORMATION of DROPLETS from the LIQUID WALL FILM PASSING THROUGH the INLET PORT of a SPARK IGNITION ENGINE

MOHAMED ELMURTADA IBRAHIM

MASTER of PHILOSOPHY

THE UNIVERSITY of ASTON in BIRMINGHAM

AUGUST 1988

The University of Aston in Birmingham

The formation of droplets from the liquid wall film passing through the inlet port of a spark ignition engine.

Thesis submitted for the degree of Master of Philosophy
by Mohamed El-Murtada Ibrahim
August 1988

Summary

The available literature has been surveyed to determine the parameters affecting fuelling requirements of spark ignition engines and their relation to engine performance and emissions. Theories and experiment relating to two phase and multi-component flows have also been examined and the techniques employed in the measurement of droplet sizes and liquid wall films have been reviewed.

Following preliminary steady flow visualisation experiments to examine the trajectories of droplets discharging from the valve port an extensive practical investigation of the spectrum of droplet sizes formed by the break up of the wall film has produced results which have been correlated in terms of the important fuel and airflow parameters.

It is concluded that the Sauter mean diameter of droplets formed by the break up of the wall film will vary between 70 and 150 μm, depending on the operating conditions of the engine. The spectra of droplet sizes measured show that a significant proportion of the total mass of the wall film breaks into drops which will be too large to burn completely and, by comparison with measurements of unburned hydrocarbon emissions from engines supplied with a homogeneous mixture of air and gaseous hydrocarbons, it is concluded that the droplets from the wall film are likey to increase emissions by 50%.

Key words: carburation; wall film; droplets; inlet port.

DEDICATION

To Almighty from Whom the truly faithful acquire their will and hope when there is none.

To my parents,
Faki Ibrahim Taha, my late father
and Zeinab Diab, my mother,
for their determination to give their son a good education
and to my wife and family, without whose
tolerance, self-sacrifice and support
the completion of this work would not have been possible.

Acknowledgements.

The author wishes to record his gratitude to the Government of the Republic of Sudan, to the Chevron Oil Company, and to the Arab-British Charitable Foundation for their financial support; also to the academic and technical staff of the Department of Mechanical and Production Engineering of University of Aston for their help and guidance in the execution of the research.

To his supervisor W.L. Flint for his non failing guidance and technical advice throughout the course of this research.

To his colleagues for being willing to help without any expectation.

LIST OF CONTENTS

LIST OF FIGURES, PLATES AND TABLES

PLATES

TABLES

CHAPTER 1.

INTRODUCTION

1.1. Mixture quality in spark ignition engines

The spark ignition engine is supplied with a mixture of fuel and air which is ignited by the energy of an electric spark and burns to release the chemical energy of the fuel. The pressure of the burnt mixture rises due to the energy release and acts on the moving piston, converting part of the chemical energy into mechanical work.

The mixture which is ingested into the cylinder must be capable of propagating a flame and the rate at which the flame travels out through the mixture must be sufficient to insure not only the combustion is completed before the working stroke of the piston is complete but the energy is released in a manner to obtain the optimum conversion into mechanical work. In the homogeneous charge type of engine the mixture of fuel and air is created by a carburettor or by the injection of spray of fuel droplets into the air stream. In order to propagate a flame the ratio of fuel to air must lie between the limits of weak extinction, when there is insufficient fuel to sustain the combustion process and rich extinction, when there is insufficient oxygen. An indication of the relationship between these limiting states and the temperature of the mixture is given in fig.1.1 for a homogeneous mixture of air and methane.

The charge which enters the spark ignition engine is compressed, whether in the two-stroke or the four-stroke engine, so that its

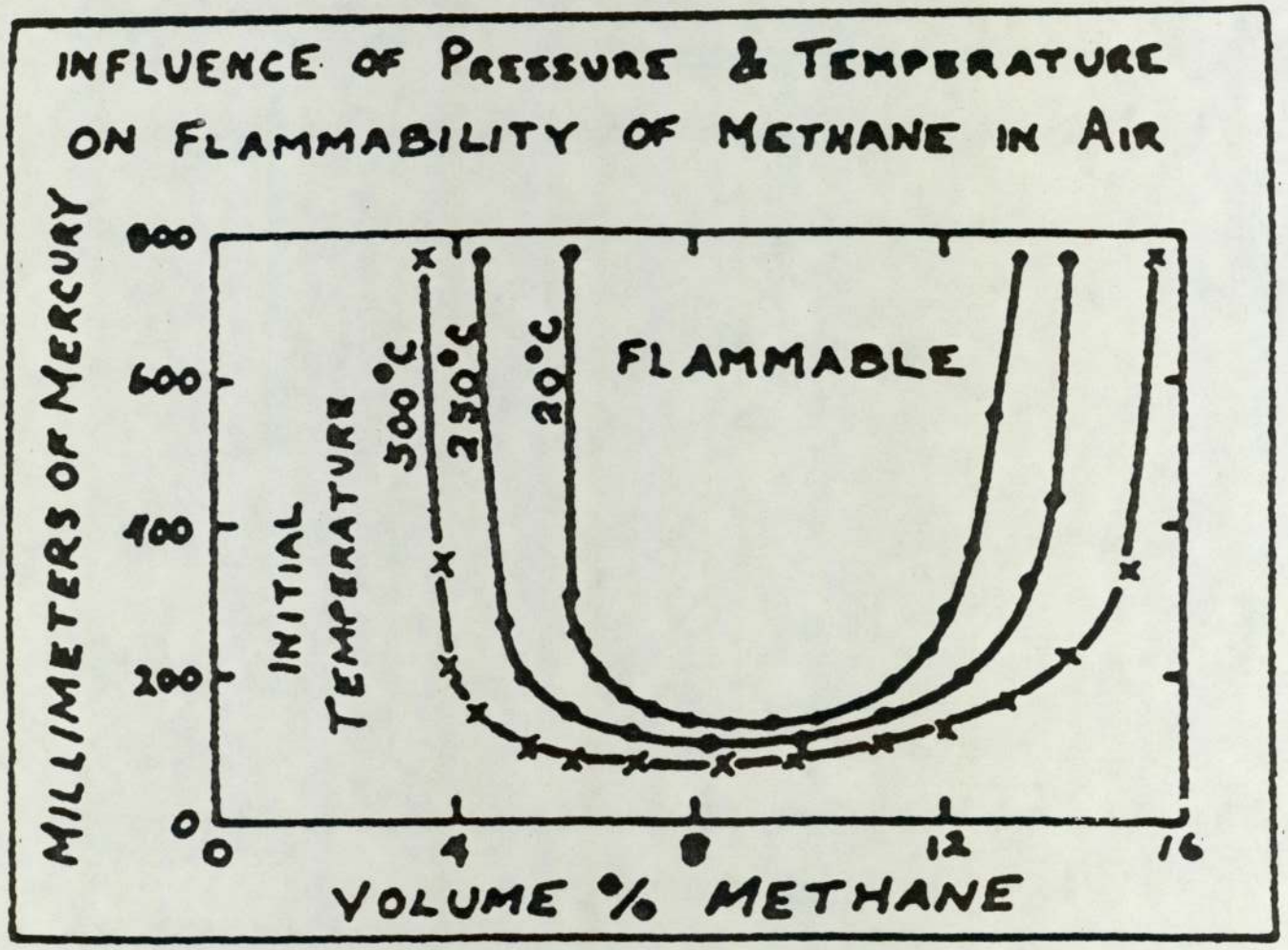

Figure 1.1., Influence of pressure and temperature on flammability of fuel/air mixture [after Stull (64)]

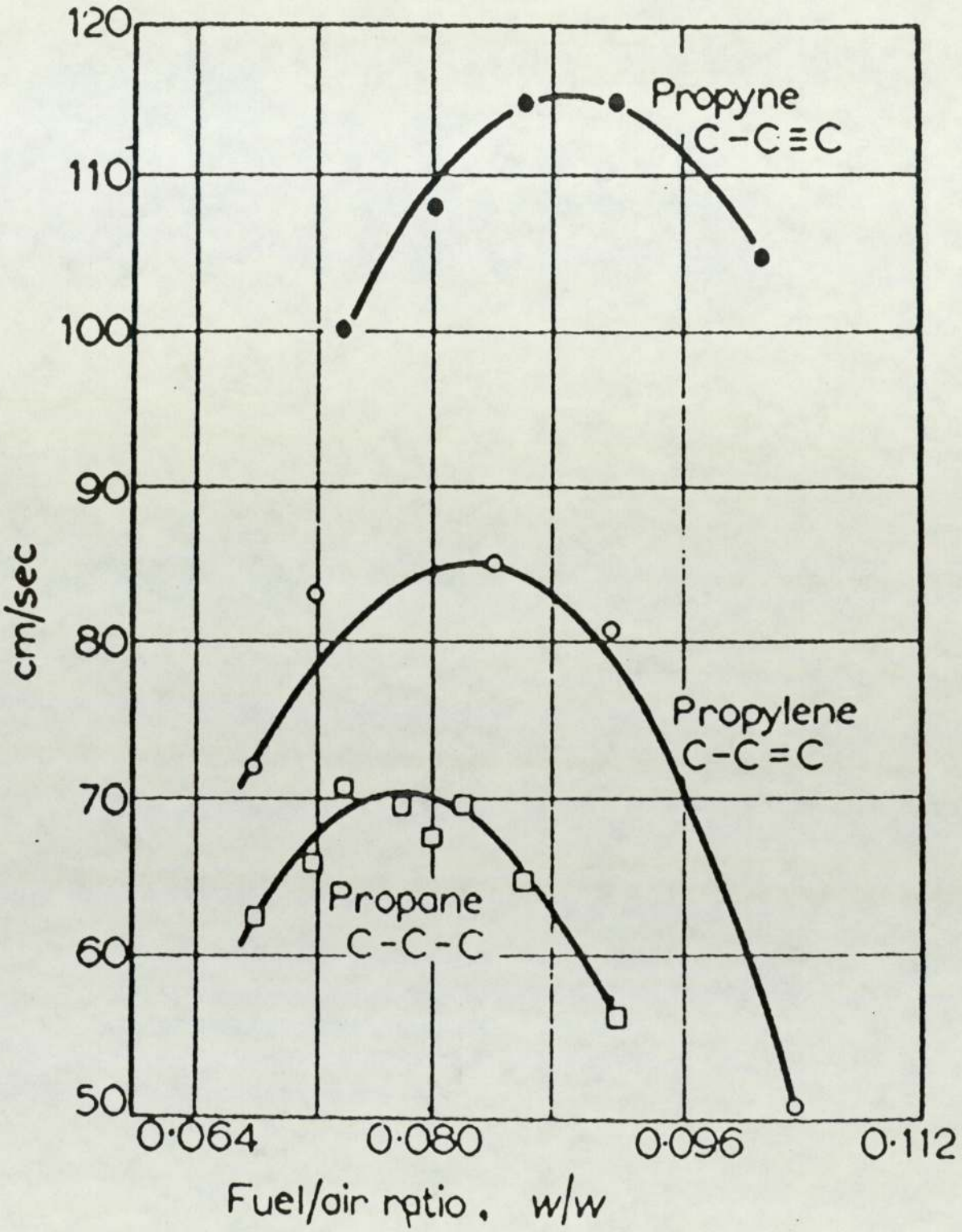

Figure 1.2., relation between flame speed and fuel/air ratio for three gaseous fuels [after Reynolds and Gerstein (77)]

temperature is raised above that of the atmosphere before the spark is passed. The compression process also increases the density of the charge which further affects the rich and weak extinction boundaries for the air fuel mixture.

The velocity with which a flame is propagated through the mixture is dependent principally upon the air/fuel mass ratio but also upon the temperature and density of the mixture. The nature of this relationship is shown in fig. 2 for homogeneous mixtures of air and three different gaseous hydrocarbons. Therefore, in order to ensure that the flame will travel throughout the mixture to give complete combustion in the time available, it is necessary to ensure that the 'correct' air/fuel ratio is supplied to the engine and that this mixture is ignited at the optimum time for maximum energy conversion.

It has long been appreciated that the complete evaporation of liquid fuel into the air stream is undesirable on account of the accompanying reduction in density of the mixture. This limits the mass of mixture which can be drawn into the cylinder and thereby limits the total energy which can be released during the combustion process.

1.2. Ingestion of liquid fuel

Neither the carburettor nor the petrol injection system produce a truly homogeneous air and fuel mixture. Motor gasoline is a blend of more than 30 separately identifiable hydrocarbons and when liquid droplets are sprayed into the air stream in the induction tract the

'light fractions' of the petrol mixture evaporate very rapidly but the heavier fractions much less so, leaving a mixture of air, hydrocarbon vapours and liquid droplets to be ingested into the engine. The droplets which enter the cylinder continue to evaporate as the mixture temperature rises during the compression stroke, although there is some evidence that the increasing pressure will lead to re-condensation of mid-range petrol vapours onto droplet surfaces during the late stages of the stroke.

Following the passage of the spark, evaporation continues in the unburned mixture as the flame front propagates and ideally the original droplets will be of such a size that all the fuel is burned completely .

A number of practical and theoretical investigations have shown that the optimum size of liquid droplet entering the cylinder is in the range 15 μm to 35 μm. Larger droplets will not burn completely and the heavier hydrocarbons are simply exhausted from the engine as unburned vapours formed by heat transfer from the combustion gases in the very late stages of the expansion stroke and during the exhaust process.

The spectrum of droplets sizes produced by carburation contains a significant proportion which are larger than this optimum -- and while the modern low pressure injector spray can be designed to ensure that the droplets are of the correct size, it is only the smallest of the droplets, about 4 μm, which will be carried along in

the air/vapour mixture and follow the same path Larger droplets are liable to be deposited on the walls of the induction manifold by gravity or by inertial separation of the main stream at bends in the tract. The problem is particularly acute in the case of single carburettor or single injector, multicylinder engines but much less significant in the port injected engine where the fuel is injected into each individual induction port immediately before the cylinder head.

A potentially serious problem is created by the presence of the wall film, which comprises the heavier components of the petrol. The film, which is not continuous but has been described as rivulets of liquid streaming randomly on the walls of the manifold, breaks up in an uncontrolled manner as it passes through the inlet valve port and enters the cylinder as a stream of droplets formed by shear forces and surface tension. If this stream contains droplets larger than 35μm then these can be expected to contribute to unburned hydrocarbon emissions from the engine. The reduction of such emissions is the subject of increasingly stringent legislation world wide.

1.3. Unburned hydrocarbon emissions.

Recent investigations into the source of unburned hydrocarbon emissions have identified the small crevices in the region of cylinder head gaskets and the clearances between the piston and cylinder wall as particularly important. The flame front cannot propagate into these crevices to burn the ingested mixture which has been compressed into them and this mixture re-expands, unburned, to mix

with the exhaust gases leaving the cylinder. The investigations from which these findings arose were carried out largely using homogeneous mixtures of gaseous fuel and air. The increased potential for the generation of unburned hydrocarbon vapours from liquid fuel entering these crevices warrants the close examination of the size and nature and destination of liquid droplets ingested into the cylinder, which is one objective of the work described in the following chapters.

CHAPTER 2.

LITERATURE ON CARBURATION AND PERFORMACE.

2.1. Fuelling, carburation and engine performance.

2.1.1. Mixture preparation and distribution.

The bulk of spark ignition engines use carburettors for fuel addition but the principal problem with carburettors is that they do not give a homogeneous mixture. In the carburettor air is the atomizing fluid and has a far greater velocity than the ingested fuel. When air comes in contact with fuel, the shear force of the air breaks up the ligaments of fuel, thrown from the jet of the carburettor, into droplets which will subsequently break into smaller droplets through the action of the surface tension of the fluid and main air stream drag force. The relative velocity between droplets and air promotes the required rapid evaporation.

An experimental study was made by Yokio Hohsho et al [1] of the evaporation of a group of droplets, made to fall freely in a quiescent air under the sub atmospheric pressure conditions encountered in the intake manifold of a spark ignition engine. With an ultrasonic atomiser providing a spray of fine droplets, the evaporation rate was determined by measuring the falling droplet diameters at different heights.

Although the study assumed quiescent air conditions and does not represent the aerodynamic conditions in an engine cylinder, the same relative results could be inferred.

A mathematical model was suggested in which each droplet was assumed to be enclosed with a spherical shell whose diameter was equal to the distance between the centres of two neighbouring droplets. The shell is also assumed to be thermodynamically isolated, so that no heat or mass transfer occurs across it.

From their experiments the investigators showed that the evaporation rate drastically increased with the temperature of the air. A remarkable reduction in evaporation was noticed when the distance between droplets was reduced but the evaporation quadrupled with the increase in the distance between droplet centres.

Petrol (motor gasoline) is a mixture of different hydrocarbons of different boiling ranges [boiling range approximately between 30 °C and 200 °C] **(2,3)**, whose individual rate of evaporation after carburation is determined by their vapour pressures, the surface area of the droplet and the relative velocity with which it is moving through the air. The light fractions evaporate quickly and the drops reduce in size correspondingly. The smaller droplets follow the motion of the flow of air and vapour passing through the manifold. The larger droplets, comprising the heavier fractions of the gasoline, either fall by gravity to the bottom of the manifold or are deposited on the walls at bends, where their momentum overecomes the aerodynamic drag of the main air stream flow. These heavy depositing fractions are the main source of the wall film which will flow along the wall until the major part of it is ruptured at valve exit, the rest of it will flow unperturbed forming rivulets along the cylinder walls

and is believed to be the major source of hydrocarbon emissions in spark ignition engines [4].

The power output from a spark ignition engine is limited by controlling the quantity of mixture entering the cylinders and hence the fuel energy available per cycle. This is normally achieved by means of a simple butterfly-type throttle valve immediately downstream from the carburettor, which has the effect of reducing the density of the mixture. In all but the fully open position a proportion of the fuel droplets produced by the carburettor impinge on the valve plate, where they agglommerate with others to produce larger drops which are increasingly likely to be deposited on the walls of the inlet manifold. At very low throttle openings there will be secondary atomisation of the liquid at the throat of the throttle valve, but at wider openings it has been shown that the wall film quantity is increased by liquid deflected at the throttle. [5,6]

When the mixture which has been prepared by the carburettor is to be supplied to a multi-cylinder engine then the manifold which distributes that mixture to the individual cylinders must ensure that each is supplied with the same mass of air, petrol vapour and liquid droplets, mixed homogeneously and in proportions which will ensure the optimum performance from the engine in terms of power, economy and emissions. Various methods of vapourising the liquid gasoline in the inlet tract have been described employing heat energy, either from the exhaust gases or from engine coolant, to promote vapourisation and improve distribution; while such methods have the effect of increasing evaporated fuel in the mixture and improving emissions they also result in a decrease of power output.

The work reported by Trayser et al [7] showed that complete evaporation of the fuel in the intake system can almost eliminate fuel maldistribution but this will drastically affect the volumetric efficiency by changing the negligible volume of fuel to a significant volume of vapour. They also report that vapourising fuel resulted in extended weak limits and that emissions were lower both at half load and full throttle, ie. unburned hydrocarbons and Carbon monoxide were significantly reduced.

The effects of complete fuel evaporation have been investigated by Hughes and Goulburn [8] who worked with very lean mixtures. They found that the mixture uniformity of the charge was considerably improved by the vapourising approach but the mixture of gas and vapour was not homogenous at entrance to cylinders. They concluded that the engine can run on a lean mixture with reduced exhaust emissions, but a power reduction of 25 to 30% was reported. They advise the need for greater homogeneity of the mixture to achieve a fast flame propagation and a longer duration for combustion [to be increased by a factor of two] subsequent to ignition, to eliminate the slow burning accompanied with partial burn cycles.

Vapourisation has very little effect on rich mixtures but Harrow [3] reports that experimentally it has been proven that the leaner a mixture becomes the more is the improvement on brake specific fuel consumption (bsfc). He concludes that with very lean mixtures an improvement of 25% in fuel consumption can be obtained over the ordinary carburetted engine. He also confirms that smaller benefits are reported to have been obtained from fuel injection systems.

Beale and Hodgetts [4] reported that good mixture quality and homogeneity was by no means a guarantee of low fuel consumption and low carbon monoxide emissions .

2.1.2. Effect of liquid droplets on performance and emissions.

It was stated in section 2.1.1 that the presence of liquid droplets increased the mass of fuel which could be ingested and hence the power output of the engine. Many researchers have published evidence that droplets of the correct size are beneficial in stabilising the combustion process and minimising exhaust emissions.

Peters and Quader [9] reported that homogeneous mixtures are not necessarily the best feed stock for lean engine operation as they resulted in higher hydrocarbon emissions and increased fuel consumption, and it was the heterogeneous charge which was better for lean burn operation.

Induction of rich mixture near the spark plug with an over all lean mixture has reduced emissions more than using a homogenous mixture [10]. The reason is believed to be that the relatively high mean temperature promotes oxidation of carbon monoxide and hydrocarbon but the lower peak combustion temperature inhibits Nox formation .

In Ottocycle engines it has been found useful to introduce easily ignitable fuel droplets to act as distributed ignition sources. Mizutani

and Nakajima [11] found that addition of small kerosine droplets to lean propane air mixtures increased the burning velocity for a mixed fuel/air ratio and also extended the region of stable burning towards leaner mixtures, but this could only be done to an optimum value beyond which the burning velocity fell below that of propane - air mixture. The lower the flow velocity and the weaker the intensity of turbulence, the larger were the kerosine drops and the less was the effect on higher velocities. Separate studies by both experimenters have shown that the combustion promoting effects were due to the liquid droplets. They gave the following reason why kerosine droplets assist in accelerating the combustion process :

1 - the interaction of the droplets with flame and changing the front from smooth to wrinkled, increasing its surface area resulting in an increased burning velocity.
2 - burning droplets act as a high temperature heat surface which accelerates instantaneous burning velocities, or act as stablisers for the flame at the limit of lean air/ fuel ratios.
3 - randomly located burning droplets generate turbulence which leads to increased burning velocities attributed to higher rates of diffusion.

Subba Rao and Lefebvre [12] performed a very interesting experiment and very relevant to the current research. The experiment was carried out on the ignition of kerosine sprays in an air stream at air velocities of similar magnitude to those encountered in the intake

manifold (37 to 46 m/s). A spectrum of sizes was investigated and different Sauter mean diameters were plotted against ignition energies. The test clearly manifested that the weak limit of ignition was considerably improved by the reduction of mean drop size. Rao and Lefebvre plotted minimum ignition energy against fuel-air ratio and noted that the curve grows steeper with the increasing drop size; a much greater increase in spark energy is needed to extend the weak limit.They also noted when air-fuel ratio was reduced towards the stoichiometric, a more rapid reaction within the flame kernel will liberate more heat in the mixture and extend into a region of larger droplets. On the contrary when air-fuel ratio is increased towards the weak limits smaller drops were needed for ignition and the fresh mixture had a more drastic effect in quenching the flame kernel. At levels richer than stoichiometric the ignition limits become totally independent of fuel drop size.

Subba Rao and Lefebvre give the following explanation for the phenomenon: the total fuel contained within the spark kernel can produce local mixture strengths that are close to stoichiometric and hence more conductive to ignition. The authors postulate that under these conditions an increase in droplet size, with consequent decrease in surface area per unit mass of fuel and fuel evaporation rate, will actually improve combustion (see fig. 2.1).

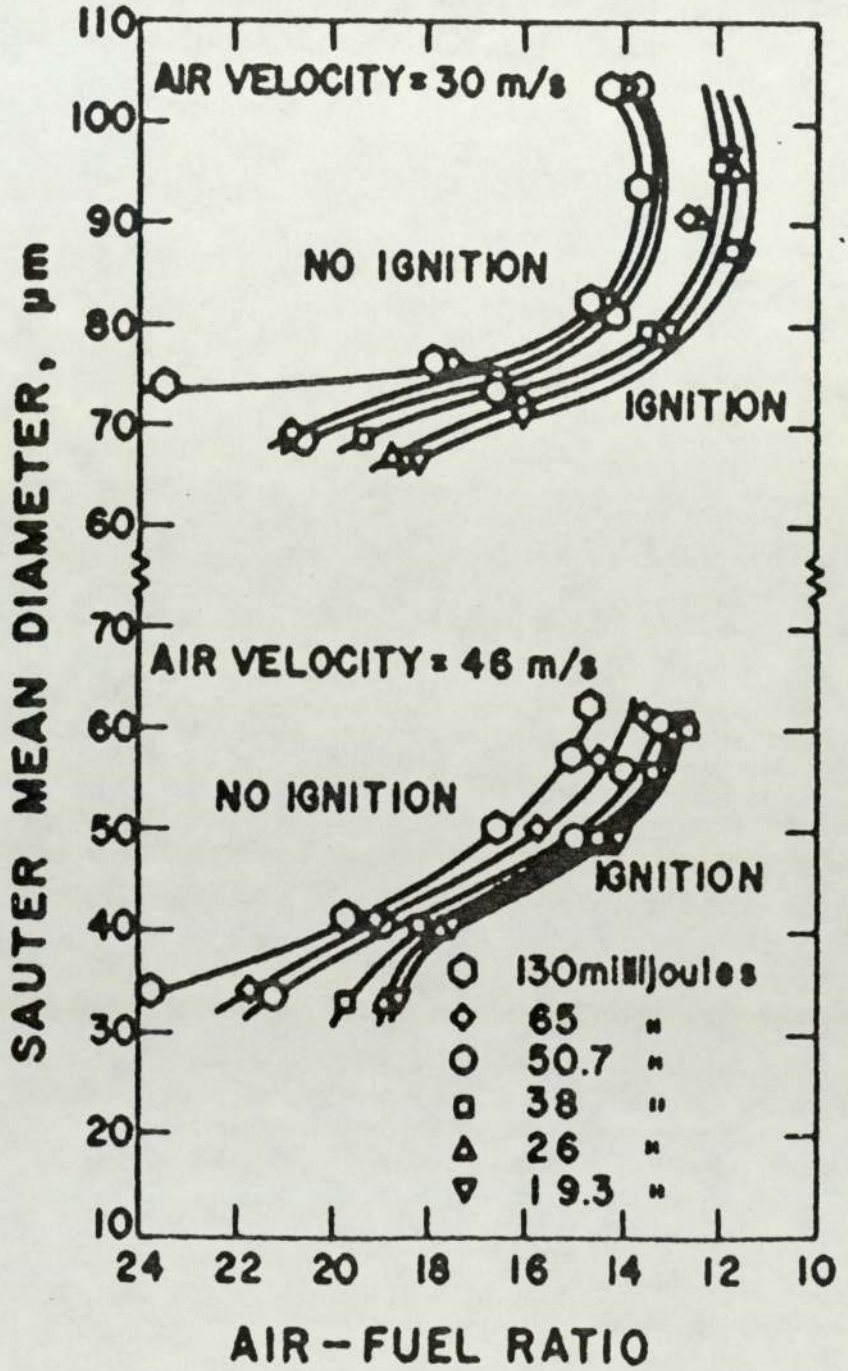

Figure 2.1., effect of fuel droplet diameter and air/fuel ratio on ignition energy requirement [after Subba Rao and Lefebvre (12)]

Lefebvre [13] in a theoretical model has also speculated that the minimum ignition energy is affected most by droplet sizes, air velocity and air-fuel ratio. He developed expressions for the ignition of both stagnant and moving mixtures of air and fuel.
Elwakil et al [14] in their study of core and peripheral temperatures of an evaporating droplet subjected to convection, declared that their measurements show no significant differences between these two temperatures, even during the initial transient heating period. These authors' observations revealed the existence of internal circulations, which imply that the assumption of a uniform temperature may be realistic during droplet convective vapourisation and for combustion.

Be'er and Chigier [15] reported that tests performed on evaporating monodisperse droplets had shown that they obey a law which confirms that the square of the droplet diameter varies linearly with time and obeys the relation:

$$t = -4 \, (\delta m / \delta t) / \pi \, \rho \, d$$

which means that reduction of d^2 is directly proportional to time.

The above equation holds true until approximately 90% of the fuel is burnt, which is taken to be an indication that the combustion of the volatiles is completed and the heavy hydrocarbon residuals have begun to burn. The significance of this relation is that it gives a very positive indication of the effect of the initial droplet size on burning time or evaporation time. The gradient of this relationship for the residual heavy fractions is less than that of the bulk combustion gradient.

Williams [16] [17], Agoston et al.[18] and Sjognen [19] have given data confirming the variation of the extinction velocity with droplet diameter, and although Williams [20] points out that there is an uncertainty about the interpretation of the data, yet he confirms that their relation between extinction velocity and droplet diameter appears to be valid, viz. $v_c \quad \alpha \quad d_l^{1/2}$

Williams goes on to say that 1mm droplets have extinction velocities of about 50 cm/s in air and this implies that extinction velocities for droplets of about 100 μm diameter burning with air in a spray would have an extinction velocity in the range of 5 to 10 cm/s. The extinction velocity drops to zero when oxygen content drops to between 14 and 16 mole %.

Williams also reports that a number of studies have been under taken to obtain information on the drag coefficient of evaporating and burning droplets which have been restricted to pure relatively volatile fuels. He summarized the findings as follows :

$0 < Re \leq 80 \qquad Cd = 27 / Re^{0.84}$

$80 < Re \leq 10^4 \qquad Cd = 0.271\ Re^{0.217}$

$10^4 < Re \qquad Cd = 2$

The author asserts that in practical terms in the combustion of light fuels the (d^2) law is sufficiently accurate for design purposes.

Putnman [21] has proposed the following expression for the standard drag coefficient of a sphere for Reynolds numbers of less than 1000:

$$Cd \times Re/24 = 1 + Re^{2/3} / 6$$

Faeth [22] reports that this expression has been used extensively by other researchers.

Ranz and Marshal [23] correlation for evaporative mass and heat transfer is also frequently used by many researchers:

$$Nu = h D/k = 2 + 0.3 Re^{1/2} [Pr^{1/3}, Sc^{1/3}]$$

where

k is the thermal conductivity of surrounding fluid.

Re is the Reynolds number

Nu is the Nusselt number (heat or mass transfer)

Sc is the Schmit number (mass transfer)

Pr is the Prandtl number

2.1.3. Effect of fuel properties and manifold geometry.

A major parameter in gasoline specifications is the volatility, which determines vapour pressure and specific gravity and is controlled by the recovered volumes at specified temperatures.

Petrol (motor gasoline) contains three different categories of hydocarbon -- paraffins, naphthenes and aromatics. Although it is generally accepted that specific gravity is the principal factor which determines volatility this is not absolutely correct. The highest gravity among the above mentioned groups is that of the aromatics and varies between 0.860 to 0.885; the average gravity of naphthenes is 0.770 and the average gravity of paraffins is 0.771 .

Ricardo [2] established that the aromatic content could be taken as a more appropriate measure for volatility despite the fact that the gravity of the aromatics is the highest of the three groups. Ricardo confirms that the highest power and efficiency is obtained by maximizing the aromatic content of the fuel, which is mainly attributed to the lesser tendency to knock and the reduced need for a higher compression ratio.

Restrictions on exhaust emissions introduced since 1970 have resulted in general engine modifications and consequent change of vehicle performance. These changes, although effective in improving general economy as well as emissions, did not result in specification change for specific gravities. Little information is known on the correlation of specific gravity with fuel economy. Most of the literature available is related to richer than stoichiometric levels. Caddock [24] expects a similar dependence on specific gravity to apply to the economy of lean burn engines, operating in conjunction with improved mixture preparation and modified ignition systems, providing good distribution of the fuel mixture exists and an appropriate fuel is used, having suitable aromatic content and distillation range.

Goodger [25] has shown that sharp bends give better uniformity of mixture than do smoother bends with large radii of curvature. With the gentle bends it has been found that heavier fractions deposit on the outer wall due to centrifugal force and this may also occur due to the decrease in velocity of the gas stream, the heavier the component

the earlier it will be deposited - (ibid). The fuel reaching the inner wall of a sharp bend or elbow has the tendency to be thrown into the main stream as droplets. Basically the change of radius of curvature weakens the effect of surface tension and hence it may result in the rupture of the film and subsequent formation of droplets.

Andreussi and Azzopardi [26] refer to the work of James et al. [27] who concluded that eddies in an airstream only affect droplet sizes below 80 μm. This point, if proven, true could be very important in the study of combustion variables, because it will determine the maximum size beyond which attempts to improve fuel/air mixture in the manifold will not be productive of any substansial effect. On the other hand turbulence is needed in internal combustion engines for flame propagation and good fuel/air mixing.

The rate at which droplets evaporate affects not only the combustion characteristics of the charge but also the emission of unburned hydrocarbons and, indirectly, of carbon monoxide and oxides of nitrogen. All these products are damaging to the environment and are the subject of regulations to limit their emission in most countries of the world.

2.1.4. Sources of emissions from spark ignition engines.

Heywood [28, 29], the Sandia report [30] have reviewed work on the sources of unburned hydrocarbon and other emissions. They report that liquid fuel and unburned charge may accumulate in crevices such as the small volume, between:

1- piston rings and cylinder walls
2- threads around the spark plug
3- space around the plug centre
4- intake and exhaust valve
5- cylinder head and head gasket

Gas flows into and out of these crevices during the course of the engine operating cycle. The largest of these crevices are the volumes between the piston, piston rings and cylinder wall. Some gas flows from there to the crank case and is referred to as the 'blow-by'. The total crevice volume is a small percentage of the swept volume, but during compression, unburnt mixtures are forced into these crevices. Since these volumes are thin, they have a large surface/volume ratio which extinguishes combustion. When pressure drops in the cylinder these gases will flow back out of the crevices and are the major contributing factor to unburnt hydro carbon emissions. The re-expanded gases also contribute to replace air or air/fuel mixture in the fresh mixture and results in loss of power and efficiency.

The thin film boundary layer (some times termed as the quench layer) plays an important role in the heat transfer to chamber walls and in hydrocarbon emissions, is thickest during the latter part of the expansion stroke, and is scraped off by the action of the piston from the walls. It is then entrained by the combustion products and exhausted to atmosphere. It is reported that the mass of gas in this boundary layer can exceed 30 to 40 % of the total charge.

2.1.4.1 Exhaust emissions and air-fuel mixture

Before the serious consequences of exhaust pollution were properly appreciated only power, efficiency and economy were sought in designing the spark ignition engine. The introduction of stringent restrictions on pollutant limits have made it necessary to reduce exhaust emissions to the minimum practical level consistent with advancing technology.

Heywood illustrates the process of formation of the emissions in the spark ignition engine in three stages :

1- When spark is initiated causing fuel to ignite and flame to proceed and then quench as it reaches the wall, nitrogen oxide is formed in the high temperature combustion products throughout the cylinder. Carbon monoxide is also formed during the combustion process.

2- during the expansion stroke the piston will recede and falling temperature will stop any reaction of carbon monoxide with oxygen (termed as freezing the reaction).

3- the exhaust valve will then open and the gases (carbon monoxide, nitrogen oxide and unburned hydrocarbons caused by unburnt gases from the quench layer) will then be exhausted to atmosphere.

A strong correlation was found to exist between the three emissions concentrations and the equivalence ratio, see fig. 2.2, defined as the ratio

(Actual fuel/air ratio)/(stoichiometric fuel/air ratio)

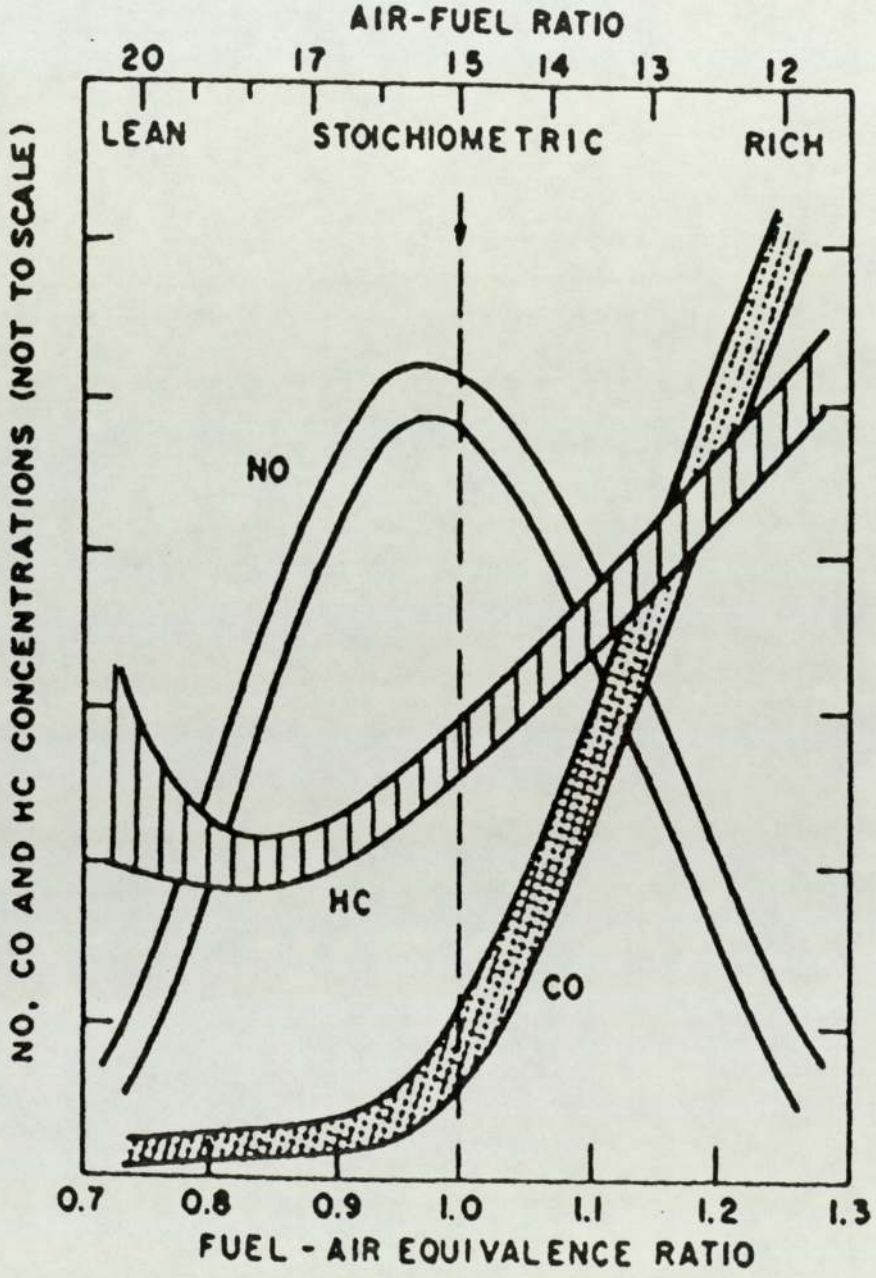

Figure 2.2., engine exhaust emissions and fuel/air equivalence ratio

Formation of Nox (nitrogen oxides) increases with increasing temperature and oxygen concentration with the maximum rate occurring at slightly lean air/fuel ratios, although a significant Nox reduction is achieved with very lean burn configurations.

Hydrocarbon emissions decrease with increasing air- fuel ratio as the fuel density in crevice gases decreases and the availability of excess oxygen increases in combustion products enabling post combustion oxidation of gas which expands out of crevices. Hydrocarbon emissions may increase with very lean mixtures because the flame speed is reduced and incomplete combustion causes partially burned charges to be exhausted or the charge may misfire, when the spark cannot ignite too weak a mixture. It has been reported by Germane et al. **(10)** that considerable hydrocarbon emissions will occur as the weak extinction limit is approached, leading to misfire and flame propagation failures.

Multicylinder engines depend on the ability to distribute the mixture uniformly and consistently to individual cylinders. For lean burn engines the need to have good distribution is greater than is the case for engines operating close to the stoichiometric air-fuel ratio, because the effect of maldistribution is proportionally more serious for leaner ratios.

2.1.4.2. Measures employed to reduce emissions:

Nitrogen oxides (Nox).

Exhaust gas recirculation (**EGR**) is used for cutting down on nitrogen oxides formation but this has led to penalties in fuel consumption which necessitated proportional control of the recirculating quantity.

Spark retarding also partly reduces nitrogen oxides emissions but a more complete solution requires the use of a catalytic reactor, which is a complex system that has to cope with carbon monoxide and hydrocarbon emissions at the same time [(3)].

Hydrocarbons:

Hydrocarbons are controlled by air- fuel ratio to a point beyond which retarding the ignition could be attempted as a second step, but even this has to be done carefully or else it will result in more damage to economy.

Carbon monoxide:

The emission of this pollutant strongly depends on air-fuel ratio: the leaner the mixture the less will the carbon monoxide be and the more fuel economy might be reached. The removal of carbon monoxide from exhaust involves afterburning in the exhaust pipe, either thermally or catalytically, with air injection into the reactor. The rich mixture used and the power expended in operating the air pump will both result in more fuel consumption.

Blackmore [31] summarises the efforts employed for improvements, that could be attained and where they are mostly required in spark ignition engines. His table also gives an indication to the economical feasibility of the improvements.

2.1.4.3. The lean burn approach.

Most research on spark ignition engines is currently concentrated on lean burn engine development. The two main reasons are the anticipated improvement in fuel economy and the likely reduction in emissions. Another less important reason is that it is the preferable mode for the investigation into the use of alcohols in spark ignition engines.

Cyclic Variations in lean burn engines:

Cyclic variations are predominant in lean burn engines and more attention is constantly drawn towards that field of research. Efforts are however being made to stabilize the combustion process. Fast burning mixtures do not suffer from large variations because energy release takes place close to top dead centre, where piston velocity and cylinder volume are changing slowly.

Generally cyclic dispersion is dependant on the homogeneity of the Air-Fuel mixture (drops, etc..), turbulence at the time of and within the vicinity of the ignition process. Two main parameters greatly influence increase cyclic variations in lean burn engines :

1- Ignition variability which is caused by combustion starting before ±10% of the total combustible mass is burnt [10]. Variations in this region are caused by the low ignition energy, which leads to poor formation of the flame kernel. Near the critical flame radius, high turbulence around the spark gap at time of spark discharge causes heat transfer out of the developing flame kernel.

2- The other parameter is the time of spark discharge in the compression cycle, which affects the temperature and pressure of the mixture. These causes of variability are most difficult to measure.

2.1.5. Effect of the liquid wall film of emissions.

Hasson [6] reported that the removal of the wall film improves the overall performance of the engine and reduces emissions, especially hydrocarbons. From his theoretical investigation of the effect of the size of the liquid droplets on performance and emissions, he advises that for optimum level of emissions, the large film droplets formed by rupture of the wall film at valve exit should be broken down to smaller droplets the size of 20 to 35 microns.

Hasson states that the film alters according to engine speed and operating conditions. When the throttle is closed suddenly during deceleration most of the film is suddenly flashed off as the manifold pressure decreases; the additional film which enters the cylinders passes through the engine without burning completely. If the throttle is then snapped open, a liquid has to replace the one flashed off before re-establishing equal amounts of fuel to all cylinders .

Hayashi and Sawa [32] studied transient characteristics of a carburetted engine during a gradual closing of the throttle plate. The following was observed:

1 - Mean wall film thickness mainly depends on the intake air velocity and air fuel ratio, its value ranging between 0.05 and 0.2 mm.

2 - Wall film rate increases proportionally with air velocity and inversely with air/ fuel ratio.

3 - In small engines mean wall film velocity is equal to about 1 to 6 m/s. and that corresponds to 1/ 100 to 1/ 200 of air velocity.

4 - The percentage of wall film increases with the increase in engine speed, air / fuel ratio and intake manifold length.

Servatti and Yuen [33] studied the behaviour of liquid fuel in an intake manifold. They assumed the film to be a couette flow at the lower part of the pipe. They also found that the wall film decreases with the decrease of the air velocity. Their findings also showed that percentage wall film can be more than 90 % of the total fuel flow.

Nightingale and Tsatsame [34] measured the wall film using separators at the branch ends of a four cylinder engine manifold during a cold start. Their findings indicated that wall film can reach as much as 50 % of the total fuel feed for a 50 seconds cranking time at 2 / 3 choke condition.

2.2. Carburettor research and modelling.

Finlay et al [35], major contributors in this field of research, measured fuel distribution in the region of throttle plate of an air valve carburettor, and used an isokinetic probe for wall film measurement.

Their findings were :

1 - There is more concentration of droplets in the core than near the wall and the droplets are not evenly distributed.

2- The distribution of either droplets or wall film is better immediately down stream of the throttle plate than further down stream or prior to the engine.

3- Drop mass flow rate upstream of the throttle plate is greater than that down stream.

4 - Wall film quantity down stream from the throttle plate is less than that upstream at 1500 /3000 rev/min, full throttle.

As Boam and Finlay [5] suggest in their computerized model the reduction wall film quantity down stream from the throttle plate agrees well with their finding that secondary atomization occurs at by the throttle plate, with droplets being entrained into the core flow. They concluded that for the mixture quality to be improved, film quantity has to be reduced as far as possible.

Hasson [6] measured wall film quantities downstream from the carburettor af a single cylinder engine, using a wall film separator to remove the film. He investigated the effect of throttle opening,

straight duct length and typical bends and found that the wall film is thickest in half throttle operation, the quantity being reduced by secondary atomisation at lower throttle openings and by reduced deflection by the throttle plate at wider openings. The wall film quantity was found to reduce along the length of a straight duct, due to entrainment of droplets, but tended towards an eventual equilibrium between entrainment and deposition within ten pipe diameters from the throttle plate. The effect of a sweep bend of radius to diameter ratio 2/1 was to increase the wall film quantity by a factor of three in all but quarter throttle operation, while the mitre bend caused a reduction of up to 50%.

2.2.2. Theoretical models of carburation.

Boam and Finlay [5] base their carburation model on a multi-component analysis of the petrol. They reduce the 36 identifiable hydrocarbon constituents of petrol into 16, which adequately represent the major components of the gasoline fraction. It is worth mentioning that this model was the first model to treat petrol as a multi-component fuel and satisfies the heat and mass transfer equations between the three components of the fuel mixture, the wall film, the droplets and the gas core (air and vapour).

The authors also considered the effect of adding heat to the mixture in three different ways --- to the fuel before entry to carburettor, to the air and to the wall of the induction pipe down stream from the throttle plate. They conclude that the most effective application was that of wall beating, which acts directly on the heavier components

flowing along the wall. Application of heat to the fuel was effective in that it caused the lighter components to flash off but its effect died out gradually along the induction pipe.

The work of Servatti and Yuen [33], already discussed, represents an earlier stage in efforts to produce a complete computer model and included the effect of droplet evaporation and the liquid wall film.

2.2.3. Alternative carburettor designs, lean burn engines and alternative fuels.

Several attempts have been made to improve the quality of the mixture delivered by carburation systems. Harrow [3] reviews the following:

1 - Ethyl Corporation rectangular hot box.

The carburettor is sunk in the exhaust pipe cross over of the engine, the air-fuel mixture emerging from the primary barrel passes through the hot box . Under all driving conditions the fuel air mixture from the secondary barrels by-passes the hot box because a high velocity air/fuel mixture can be relied upon to keep a good quality distribution even without evaporation. The outcome is said to be an improvement across the full spectrum of driving conditions. Also because the main flow of the combustion air is not heated, therefore the volumetric efficiency is maintained.

2 - The Vapipe.

A heat exchanger conveys heat from the exhaust system to vapourise the fuel under all operating conditions. Because there

is a lack of evaporative charge cooling, there is a loss of the volumetric efficiency, to counteract this effect a larger carburettor can be used.

3 - The Dresserator.

This is a variable carburettor with a mechanically actuated sonic throat, which has proven to be very efficient for fuel atomization and mixture quality:

a - by introducing the fuel over a large surface area subjected to sonic flow .

b- by passing the combustible mixture through a shock wave to atomize and improve homogeneity.

c- by eliminating flow variation caused by a down stream throttle plate .

4- Fuel injection :

There is a lot of controversy about the benefits of fuel injection in gasoline engines. Generally the system operates with a low injection pressure spraying fuel into the manifold immediately upstream from the inlet valve of the individual cylinder, although somewhat higher pressures are used with EFI (Electric Fuel Injection) controlled systems. It is however, established that the maximum power outputs are improved in fuel injection systems. It is reported that the EFI manifold is better aerodynamically because it allows better mixing than carburetted manifolds .

Mixture quality increases in importance the leaner the mixture

becomes. Good mixture uniformity eliminates or cuts down maldistribution and allows carburettors to be tuned for optimum economy. For short trips fuel consumption is considerably reduced by improved mixture quality under cold running conditions. Many devices have been introduced for improving mixture quality on condition that spark timing and mixture strength are optimally adjusted.

CHAPTER 3

Droplet Formation and Two Phase Flows.

Droplets are formed by the break up of a liquid jet or sheet, or by entrainment from a liquid surface into a passing fluid stream. Therefore droplets will be formed at three different stages during the carburation and ingestion of the petrol/air mixture into the cylinders of a spark ignition engine. The carburettor (or the modern spray injector) is designed specifically to produce very small droplets, giving a high surface area per unit mass ratio to ensure rapid evaporation and mixing of the fuel and air. The larger droplets fall to the walls of the inlet manifold and stream as rivulets or a thin liquid film and droplets are torn from waves on the surface of these liquid streams. Finally droplets are formed from the wall film as it flows through the inlet port and into the cylinder.

3.1. Droplet formation in sprays and atomisers

Nukiyama and Tanasawa [36] made extensive drop size measurements with a twin fluid atomizer. The liquid (usually water) was introduced into the air stream at a relatively low velocity. Air velocity was varied from 150 to 1000 ft/s and the sizes of the liquid tube and air nozzle varied from 0.2 to 2 mm and 2 to 5 mm, respectively. Drop samples were taken on the axis of the nozzle at a distance of 150 to 250 mm. The Sauter mean diameter, d_{32}, was given by:

$$d_{32} = (585 \sqrt{\sigma}) / (u \rho) + 597 (\mu / \sqrt{\sigma \rho})^{0.45} (1000 V_l / V_a)^{1.5}$$

where

u = air velocity relative to the liquid (m/s)

σ = liquid surface tension (dyne/ cm)

ρ = liquid density (g / cm^3)

μ = absolute viscosity of liquid (Poise)

v_l = volume flow rate of liquid

V_a = volume flow rate of of air

For water at 15 deg. C this becomes

$$d_{32} = (16{,}430 / u) + 4\ 1.0\ (Q_w / Q_a)$$

where

Q_w = weight flow rate of water (lb/hr)

Q_a = weight flow rate of air (air pressure = 1 atm) (lb/hr)

u = air velocity relative to the liquid (ft/s)

The Sauter mean diamete, d_{32}, mentioned above is defined as the diameter of the drop having the same (surface /volume) ratio as that of the whole spray.

Wigg **(37)** measured the distribution from an atomiser by using the freezing wax method, described in chapter 4. Based on his own measurements and the measurements of other researchers he concluded that the Nukiyama- Tanasawa equation overestimated the ratio of liquid to air flow. He later on developed an equation to describe the median diameter:

$$dm = 0.004\ \upsilon^{0.5}\ W^{0.1}\ (1+ W/A)\ h^{0.1}\ \sigma^{0.2}\ \rho^{-0.3}\ \partial u^{-1}$$

where υ is Kinematic viscosity m^2/s

W is liquid mass flow rate kg/sec

h is height of air annulus. mm

ρ is the fluid density kg/m^3

σ is the surface tension N/m

∂u is the relative velocity

Mullinger and Chigier [38] made comprehensive study of the effects of changing geometrical variables in atomizer design and the thickness of oil film in the mixing chamber. They verified that Wigg's equation for the determination of mean drops sizes agreed closely with experimental results. Their tests included values of air/fuel ratios of 0.005. Those experimental results were taken as proof that the geometry of the atomizer plays little part in determining the droplet size. The equation has been used to analyse sprays for many designs of twin fluid atomiser and it has been shown that only density and velocity change had any effect on the droplet size.

3.2. Droplet formation from a liquid surface

A major cause and source of droplet generation has been identified as the shearing off of the roll wave crests. The idea that the droplets are atomized into the gas flow by rupture of wavelets was thought to be originated by Woodmansee [39], who suggested that wavelets are caused by the imbalance of pressure variations of the gas over the wave surface interacting with the retarding forces of surface tension and gravity according to Helmholtz' instability criterion. He suggested that wavelets are accelerated towards the front of the roll wave, and while this is happening, the wave is lifted as a ligament in the form

of an arch. The centre part of the arch ruptures while the end of the arch, which is still attached to the liquid film, falls back into the film. (fig. 3.1). Hall Taylor [40] also reported that liquid droplets are entrained by the crests of disturbance waves which are torn off due to the gas core.

Dombrowski [41] idealized the drop formation from aerodynamic waves using the model shown in fig. 3.2, which assumes that waves will continue to grow until the crests are blown off. The waves will be broken up into half wavelengths which shrink to ligaments that subsequently break into drops. This original speculation conforms favorably with very recent theories of drop formation, for example it generally agrees with Woodmansee's postulation of the formation of droplets from rollwaves.
Zannelli [42] showed that the wave lengths which would arise in wall film flow are within the range required by the Helmholtz instability criterion, while Taylor [43], using a sinusoidal wave model, concluded that large waves can occur under these conditions.

3.3. Two Phase Flows.

The flow in the engine inlet system is essentially a two phase, multi-component flow. The general subject of multi-phase flows received little practical or theoretical attention before the middle of the present century, when an understanding of the generation of steam in the riser tubes of steam-generating boilers began to assume greater importance as power ratings and operating pressures increased sharply. The need to ensure adequate safety margins in the design of steam generators for nuclear power plant added to the

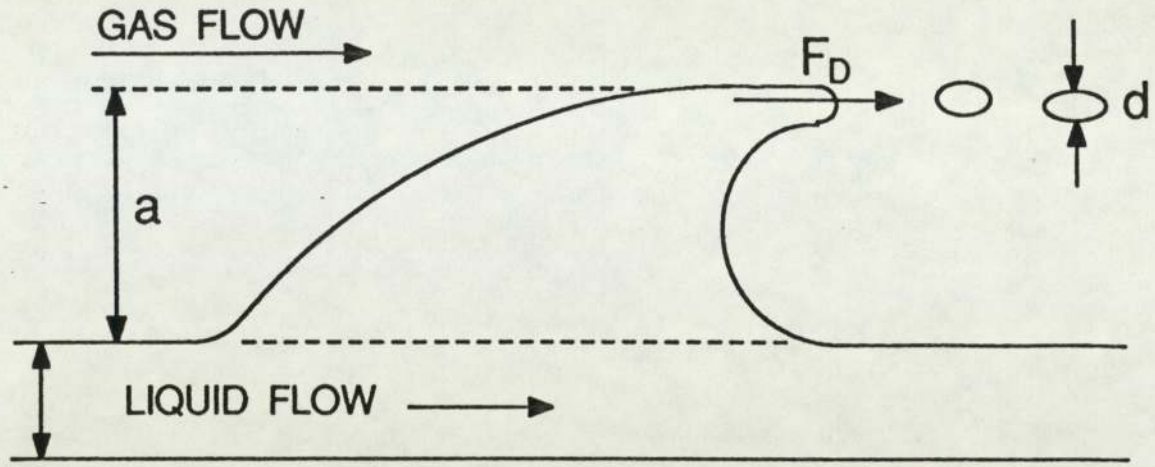

Figure. 3.1 Mechanism of the shearing off of roll-wave

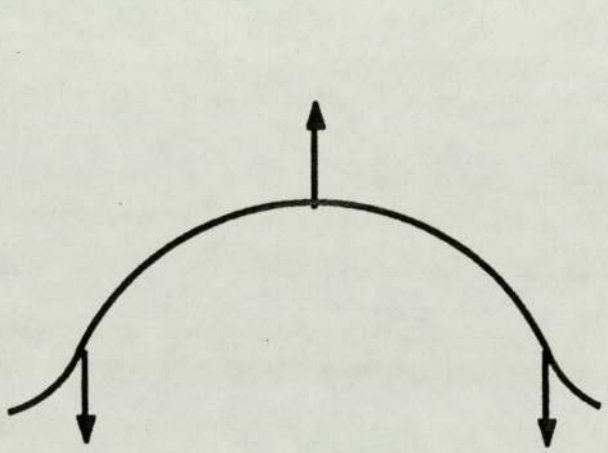

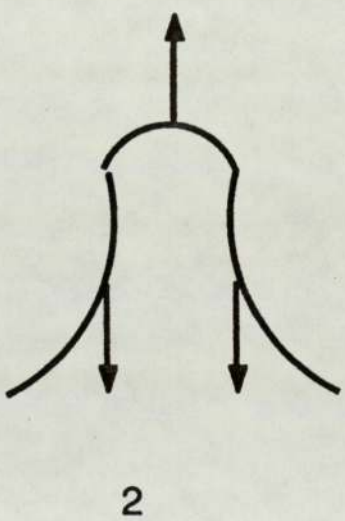

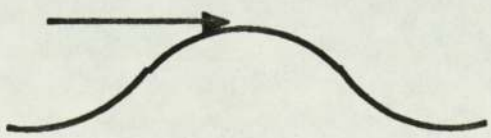

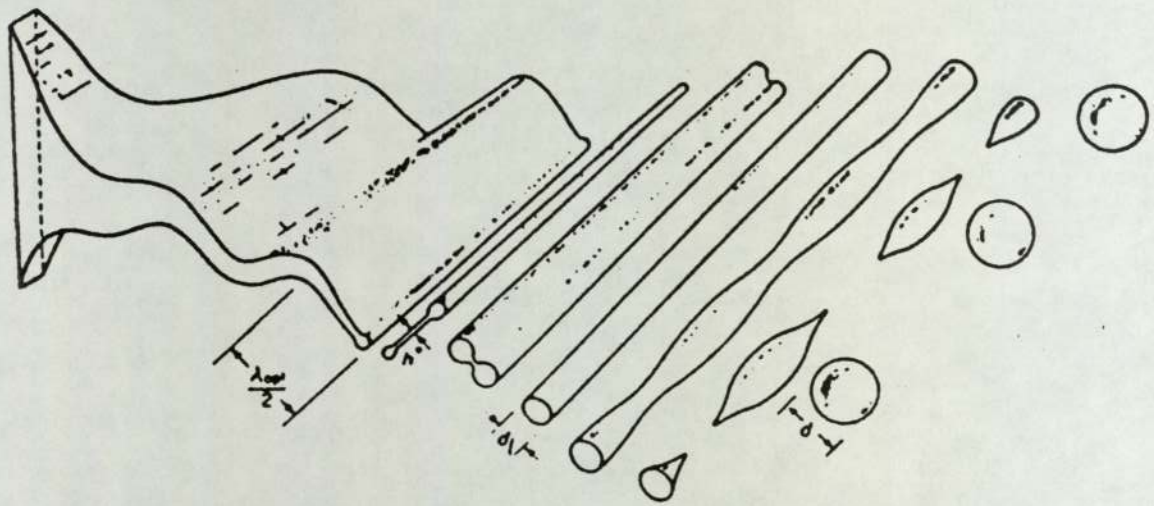

Figure 3.2., droplet formation from a liquid film

[after Dombrowiski [41]]

importance of understanding the nature of the two-phase flow and the energy and momentum transfers involved.

Lockhart and Martinelli [44] identified and examined six different flow regimes illustrated in fig. 3.3 as:

1 - bubble or froth : bubbles dispersed in the liquid.
2 - plug : plugs of liquid followed by plugs ofgas.
3 - stratified : liquid and gas flow in stratified layer.
4 - Wave : gas flows on top of pipe section, liquid in waves in lower section
5 - slug : slugs of gas bubbles flowing through the liquid.
6 - annular : liquid flows in continuous annular ring on pipe wall, gas flows through the centre of the pipe.

The objective of their analysis was to provide working relations for the momentum transfers and corresponding pressure drop encountered in two-phase flow in circular pipes and their theoretical analysis did not make a close examination of the physical origins of the correlations. Indeed the basic assumption was that the pressure drop encountered in two-phase flow could be related by a simple constant factor, the 'Martinelli' parameter, to that which would normally be

expected for gas flowing in the same circumstances. The experimental results of their work are presented in the form of a chart which allows the numerical value of the constant to be determined for the desired flow geometry and other conditions.

Krasikova [45] was the first to discover an eccentricity of the wall film existed, when measuring the wall film thickness in a horizontal pipe using an electrical resistance technique. The length on which the wall film was measured was great and hence an average rather than a point-wise measurement was made.

McManus [46] confirmed that this eccentricity existed and is among the very few investigators who have examined local film thicknesses and its relation to surface characteristics of the pipe wall. He confirmed that the velocity profile of the core flow was influenced by the presence of the wall film and in horizontal flows the maximum velocity occurs at a position above the centre line. The displacement is related to the thickness of the wall film; no correlation was offered.

McManus also showed experimentally that the liquid Reynolds Number varies almost linearly with static pressure drop and he used the Martinelli Parameter "X" to prove experimentally that the ratio of pressure drop to the total pressure drop varies almost linearly with the parameter for the turbulent/turbulent case for high liquid flow rates. See fig 3.4.

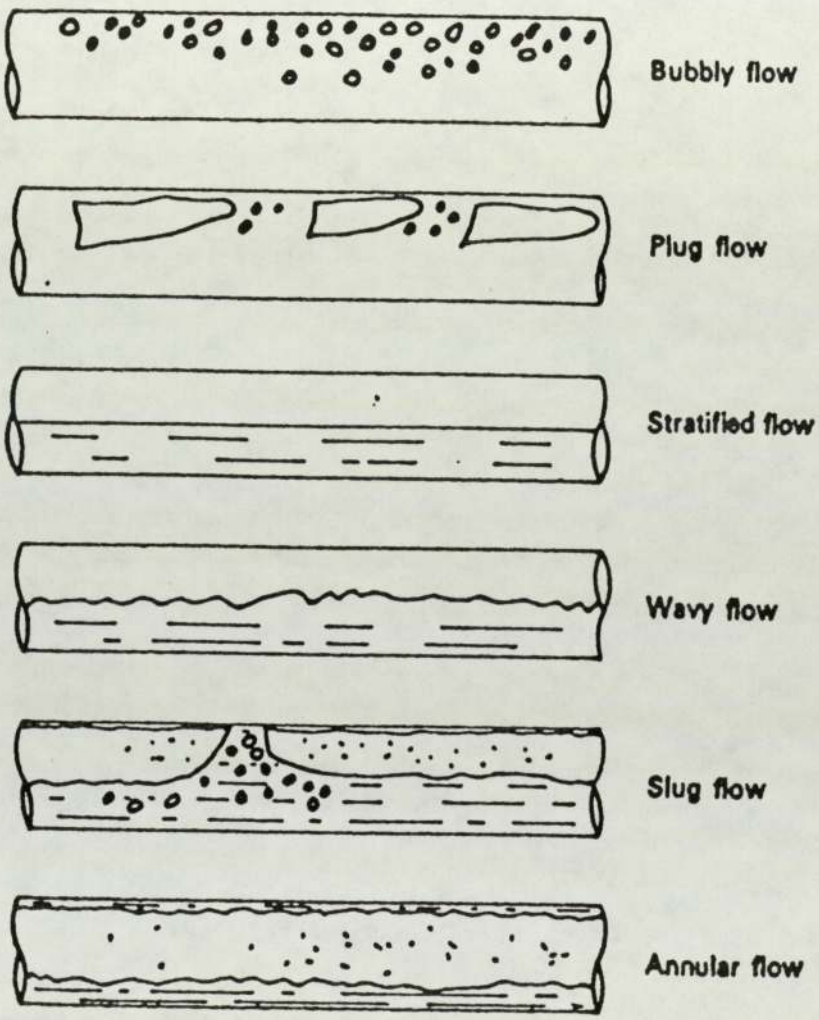

Figure 3.3., regimes of two- phase flow

An important finding of McManus is his correlation for the mean film thickness. The correlation is:

$$\delta / D = k \left[(Re_L)^a / (Re_g)^b \right] (\rho_g / \rho_L)^c (\mu_L / \mu_g)^d \quad \text{---------} \quad (1)$$

where:

δ = Film thickness.

D = Tube diameter.

k = Empirical constant.

Re = Reynolds number.

ρ = Density.

μ = Dynamic viscosity.

L is for liquid.

g is for gas.

a,b,c and d are exponents "undetermined in the available literature ".

Hewitt[47] who has published extensively on the subject of two-phase flow and covers more aspects than any other author in the available literature regarding different aspects of the annular two-phase flow confirms that in horizontal two-phase flow regimes liquid tends to go to the bottom of the pipe and hence film thicknesses are higher in these regions, but he declares that for this to be significant it might require a long tube. Hewitt also mentions that a situation can be postulated where gas flows under shear stress may cause a flow of liquid upwards that balances the effect of the flow regime originating from gravitational forces. Since a thicker film exists at the bottom, it will cause entrainment of droplets and

eventually lead to an equilibrium situation, and redistribution on the upper wall may also occur. He claims that it is possible to have thick liquid films in horizontal flow at low Reynolds numbers, whereas in vertical flow at high gas flow rates, the liquid films are extremely thin. He confirms that naturally the wave formation leading to droplet entrainment is greatly different in the two cases.

3.4. Droplet entrainment and depostition.

As the information on liquid film formation, droplet entrainment and droplet deposition in a two-phase annular mist flow is important for planning and designing nuclear reactors and steam generators Koji Akagawa et al [48] sought to clarify some characteristics on liquid film flow. Since it is uncommon to find a reasonable study that investigates droplet deposition and entrainment and at the same time discusses the variation of film thickness, their work is presented in a very comprehensive way. They suggest a correlation for film thickness, droplet deposition and entrainment.

Koji Akagawa et al used a horizontal rectangular channel, employed a scoop to remove liquid film, and measured entrainment by using an isokinetic probe. The velocity distribution at entry to the channel was almost uniformly distributed but is gradually offset with the increase of horizontal axial distance where liquid flow in the lower part becomes reduced owing to :

1 - The increase on frictional resistance on the liquid face.
2 - The exchange in momentum due to droplet creation.

3 - The effect of distribution of droplets concentration.

The velocity distribution is asymmetrical along the height of the channel and maximises at a distance of approximately:

$$Y/H = 0.6 \quad \text{----------(2)}$$

Y is the vertical displacement.

H is the height of the channel.

This agrees with Krasikova [45]

Koji Akagwa et al express the local droplet concentration using the local droplet flow rate (G_{EY}) and local gas velocity (U_g).

$$C = G_{EY} / U_g \quad \text{----------} \quad (3)$$

G_E usually in g/s (total droplet flow)

They compare their horizontal flow model with that of Gill et al [49] [50] who correlated the dependance of entrainment on the axial distance covered by flow regime. Their findings are similar, as the entrainment showed an axial increase which reaches a fully developed state and steadies out at a distance of approximately 5 meters. Obviously such distances are much greater than those found in engine intake systems.

The same authors suggest an empirical result for entrainment:

$$G_E/G_{EO} = 1\text{-}e^{-0.38\ (x-a)} \quad \text{----------} \quad (4)$$

where G_{EO} is G_E at a state of equilibrium and the constant "a" depends on flow conditions and has a value of 0.22 to 0.43 . [x is the width of the channel].

The cross sectional axial entrainment follows an exponential distribution and is similar to what other researchers have described.

$1/B \; d\, G_E/dZ = W_c - W_d$ ----------(5)

As $d\, G_E/dZ$ = zero at the fully developed region, the rate of deposition equals the rate of entrainment.

W_c (entrainment) = W_d (deposition rate) ----------(6)

Since the scoop removes the film there will be no entrainment:

$W_c = 0$

$W_d = -1/B \; (dG_E / dZ)$ ----------(7)

The axial change of concentration in the vertical direction has a similar shape independent of the horizontal position, the droplets diffuse to the upper part of the duct and concentration increases proportionally as the axial distance Z increases. Concentration can be expressed by the following dimensionless equation:

$(C - C_H)/(C_O - C_H) = \{ e^{(1 - y/H)}] a - 1 \}/\{ e^a - 1 \}$ --- (8)

where : $a = v_f \; H/ \; E_p$

v_f = Settling velocity could be reasonably considered as the terminal velocity, m/ s

H is the height of the channel

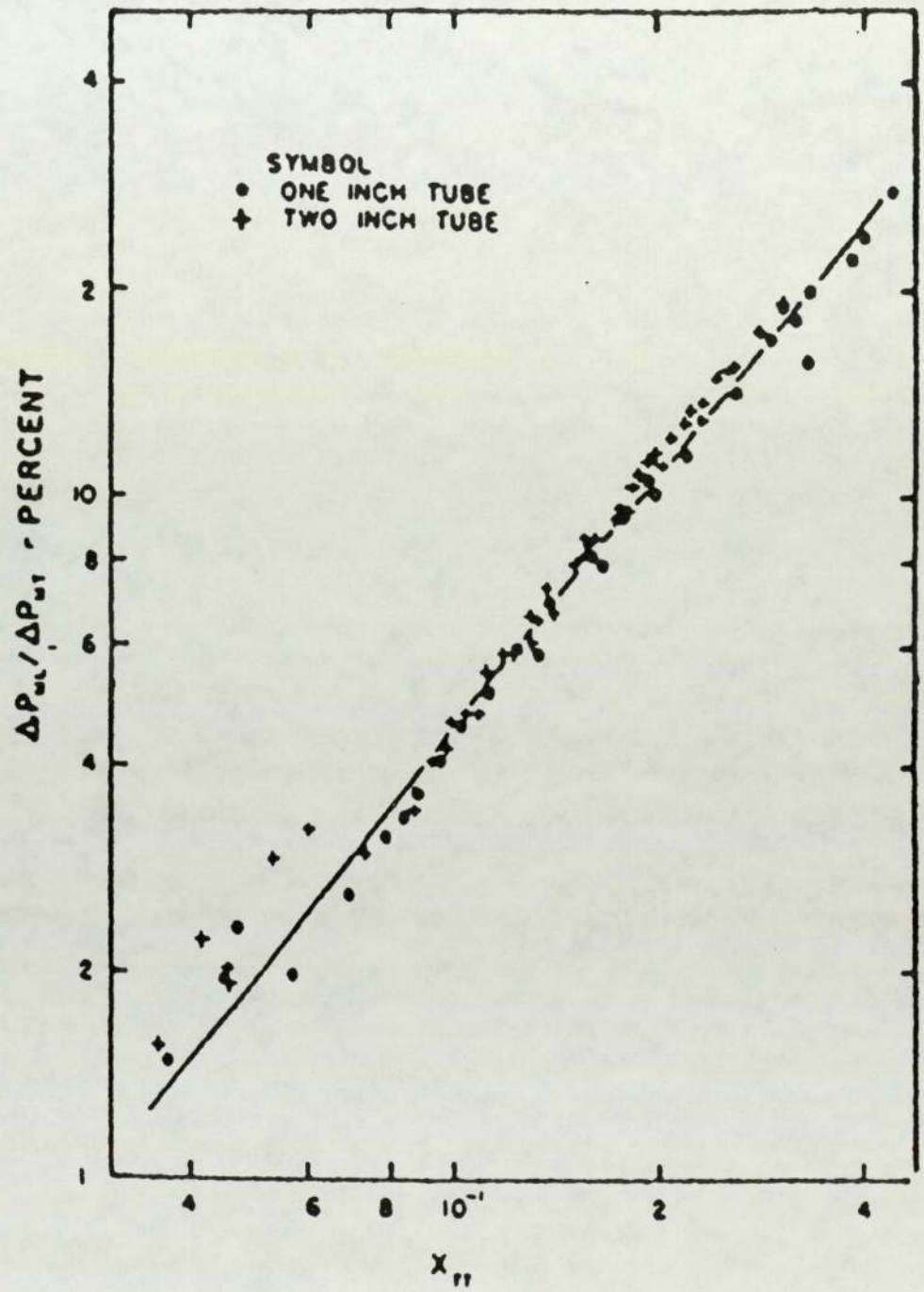

Figure 3.4., correlation of of pressure drop in annular two- phase flow [after McManus [46]]

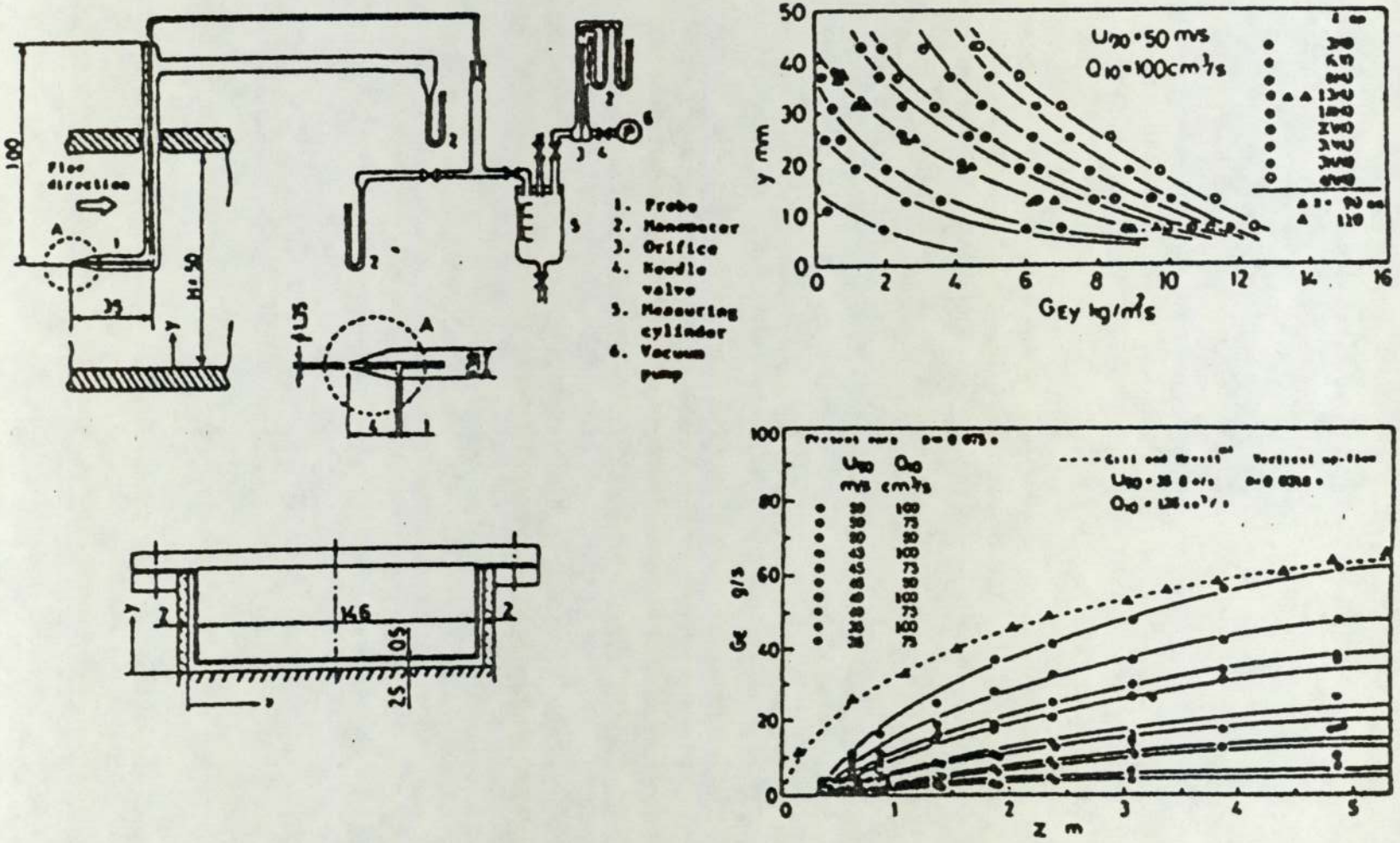

(48)

Figure 3.5., Akagawa et al apparatus and results.

E_p (m^2/s) is the turbulent diffusion coefficient. C_o and C_H are droplet concentrations at Y = 0 and Y = H respectively.

Koji Akagawa et al used correlations formerly used by Ueda [51], Hewitt [47] Dallman and Hanratty [52] for their results, and concluded that the entrainment in the horizontal regimes is larger than that obtained in vertical flows.

The correlations used by Ueda and Hewitt are:

$$(W_c / \{U_{go} \sqrt{(\rho_l \rho_g)}\} \text{ - versus - } G_f)$$

Gf (Liquid film flow rate per unit wetted perimeter)

U_{go} is the gas core velocity m/s.

ρl, ρg liquid and gas densities respectively.

Although the correlation of the vertical tube cannot apply for the horizontal tube, yet the entrainment rate can be expected to be in the form of:

$$W_c = U_{go}^d G_f^f$$

where d and f are constants.

The liquid droplets are strongly affected by turbulent diffusivity and by gravity. Mass transfer in a vertical direction at a height y was assumed to depend on the product of turbulent diffusivity and velocity owing to the gravitational precipitation .

Thus

$$W_c = \{ E_p \ (dc / dy \ )\}$$

where E_p = eddy diffusivity.

c = concentration.

Thus it was deduced that entrainment rate and deposition rate are given by:

$$W_c = - E_p \, (d c / d y)_{y= h\ max.} \quad \text{---------- (14)}$$

$$W_d = U_f \, C_{y = h\ max.} \quad \text{---------- (15)}$$

where h max = maximum thickness

Akagawa et al. quote the relation

$$E_p = (v_f / a) * H \quad \text{---------- (16)}$$

where **a** is a dimensionless parameter determined from their experiment.

At the equilibrium condition when $W_c = W_d$ then the above equations can become:

$$W_c = (U_f / a) \; H \; (d c / d y) \quad \text{----------} \quad (17)$$

Koji Akagawa et al concluded that:

1- Total droplet flow rate can be represented by the following formula:

$$G_E / G_{EO} = 1 - e^{-0.38Z} \quad \text{----------(18)}$$

where Z is the distance from the incipient point of droplet entrainment.

2- The following relationship between the droplet entrainment and

the property (i.e assumed breadth, height, velocity and frequency of occurrence) of disturbance wave was obtained:

$$Wc = 4.88 \times 10^{-8} \{(B \Delta h) / \lambda \} U_{go}^{4.5} \rho_l$$

B is the breadth of wave in Sekoguchi's model (fig. 3.7), U_{go} is the gas velocity, l is for liquid.

The generalised form of the above equation is:

$$W c = 2.93 \times 10^{-5} \{(R_{e g} / 10^{2})^{3.5} (R_{e g} / 10^{5})^{5.5}\}$$

3 - An equivalent diffusivity coefficient depending on gas velocity and liquid flow rate (Ep) was suggested. This coefficient is higher than the diffusivity coefficient in the single component gas flow.

Gill et al[50] reported that the flow of entrained droplets increased in the axial direction of the flow and that the deposition of entrained droplets equalises with entrainment flow at approximately two hundred diameters from point of introduction of the fluids.

A notable relation quantifying the entrainment was the correlation by Wicks and Dukler[53]: see fig. 3.6

$$R = (B W_{LE} V_L / V_G) / (dP_F/dz)_G \quad \text{----------(19)}$$

in which the parameter R is related to the Martinelli Parameter X by:

$$X = \text{Martinelli parameter} = 0.069\ R^{0.39} \quad \text{----------(20)}$$

W_{LE} = Flow rate of entrained liquid.

$(dP_F/dz)_G$ is the frictional pressure gradient for the gas flowing alone in the tube.

B is an empirical constant having a value of 22 for smooth injection

of fluid and a value of 13 for pulsed injection.

Alexander and Coldren [54] carried out experiments on the deposition of 27 μm water droplets on the walls of a horizontal pipe. The deposition was estimated by the rate of change of radial profile of the droplets mass flux and determined by :

$Q_d = K_d C$

K_d = is the mass transfer coefficient

$= 0.834338 \times 10^{-4} Vg^{1.17}$ ----------(21)

C is the concentration of the droplets within the gas stream (kg/m^3)

McCoy and Hanratty [55] have tried to find a general correlation applying to both vertical and horizontal regimes. They conclude that gravitational settling can have important effects on this type of flow under scrutiny, yet they say that the settling or deposition could be different from that for vertical flow regimes [an argument also put forward by Hewitt [47]].

Correlations obtained from vertical flows can only be used for horizontal flows within certain limits. Provided k_{DV}/V_t is greater than 10, McCoy and Hanratty quote:

$$N = k_{DV} \rho_G W_{LE} / W_G \quad \text{---------- (22)}$$

where k_{DV} is the deposition rate constant and V_t is the terminal velocity.

N = Mass rate deposition per unit area

W_{LE} = is the mass flow rate of the dispersed droplets,

W_G = is the mass flow rate of the gas.

In their analysis of the work of other researchers, McCoy and Hanratty derived an average figure of 1.7 for the ratio of deposition rate constant over the frictional velocity for vertical flow regimes, based on a large volume of data. However they arrive at an important relation, and that is the straight line relation between the vertical and horizontal deposition constants over the corresponding frictional velocities.

Andreussi et al [26] measured the sizes and ejection velocities of droplets in both annular vertical and horizontal flows. The velocities and direction of trajectories (paths) were found to be independent of each other. The mean values of ejection velocities were related to a model extended from James et al [27] which shows that large droplets entrained by the gas are ejected from large disturbance waves which are formed on the film and continue to travel at about their initial velocity in a constant direction until they are deposited ; a mechanism which can be called direct impaction.

It was found by Andreussi et al that the larger droplets achieve lower axial velocities because of their shorter residence time in the flow . The authors claim that a number of entrained droplets deposit by a random diffusion like mechanism caused by successive trajectories of gas phase eddies. It was mathematically represented that droplets whose original transverse velocities were zero deposit according to an exponential decay law, and that 20 diameters from film removal section, it was found that deposition occurs due to droplet

concentration through a drag coefficient, and is almost independent of flow conditions and tube diameter.

The authors introduce the following equations:

$$f = .079 \left(\mu_g / 2 \rho_g U_g R \right)^{0.25} F_i$$

But since they assume that F_i is equal to 1 then the equation reduces to Blasius equation $f = 0.079 \, Re_g^{-0.25}$

f has the usual notation of coefficient of friction.

R is the tube radius.

(where F_i is a correlation factor .)

Other symbols have their usual meaning

Using the laser axial view technology the authors introduce the following correlation for the mean droplet diameter:

$$V_i = 11.1 \, U^* \sqrt{(\rho_G / \rho_l)}$$

U^* = Frictional velocity

$= \sqrt{(\tau / \rho)}$

They used $U^* \sqrt{(\rho_G / \rho_l)}$ to correlate the above equation .

They conclude by :

1 - Commenting on the difficulty of horizontal flow due to the complication caused by the asymmetry of the liquid film. The thick film flows along the bottom of the channel and that is the main source of entrainment.

A very important remark is quoted:

"However it has been observed that data from higher gas rates are similar to vertical flow data for the same pressure if the area occupied by the liquid at the bottom of the channel is deducted from the cross sectional area."

2 - Ejection velocity of drops is independent of the direction and drop size.

3 - It has been found that larger drops achieve lower axial velocities than smaller drops because of their shorter residence time in the flow.

3.4.1. Droplet entrainment and deposition rates

Tatterson (56) asserts that no complete model exists that can predict the rate of atomisation or drop size distribution. However he implies that pressure variations cause waves to grow leading to the shearing of droplets from wave crests, that surface tension is the principal force retarding this process and that viscosity has a minor effect. He refers to atomization from roll waves as one of the factors which contribute in the process of making droplets. Larger droplets will be sub divided into smaller ones depending on the balance between normal gas forces, surface tension and viscosity of the liquid in question. This subdivision will continue to occur until the ratio of "gas resistance pressure" $\rho (U_G - U_d)^2$ to "surface tension pressure" (σ / ρ) is greater than some critical value

This ratio is the Weber number

$$We = \rho_G (U_G - U_d)^2 \, d / \sigma$$

where: U_G = Gas velocity

U_d = Drop velocity

d = Drop diameter

σ = Surface tension

ρ_G = gas density

Hinze **(57)** found the critical value of the Weber number varies between 10 and13 for rough pipes and 22 for smooth pipes.

Koji Akagawa et al used a model referred to by Sekoguchi **(58)** (see fig. 3.7) to correlate the droplet entrainment characteristics which are obtained from the experiment. The droplet flow rate created by the shearing off from a disturbance wave by the gas stream per unit width is expressed as:

$$\{ K_1 B' k_2 \Delta h \rho_l /2\} \quad (kg / m) \qquad \text{---------- (9)}$$

where K_1 and K_2 are constants .

The passing frequency of the disturbance wave is :

Ud/ λ (s^{-1}) and residence time is $1/U$ (s/m)

If the frequency of droplet entrainment from disturbance wave is n, the liquid droplet flow rate W_c can be expressed as:

$$W_c = \{ K_1 B' K_2 \Delta h\} * \rho_l [(U_d /\lambda\ 1) * (1/ U_d)] n$$

$$= \{ K_1 K_2 \rho_{l/2}\} [(B' \Delta h) / \lambda] n \quad \text{---------} \qquad (10)$$

It is clear from above that W_c is a function of $B' \Delta h/\lambda$ and the relation is shown in fig. 3.8a.

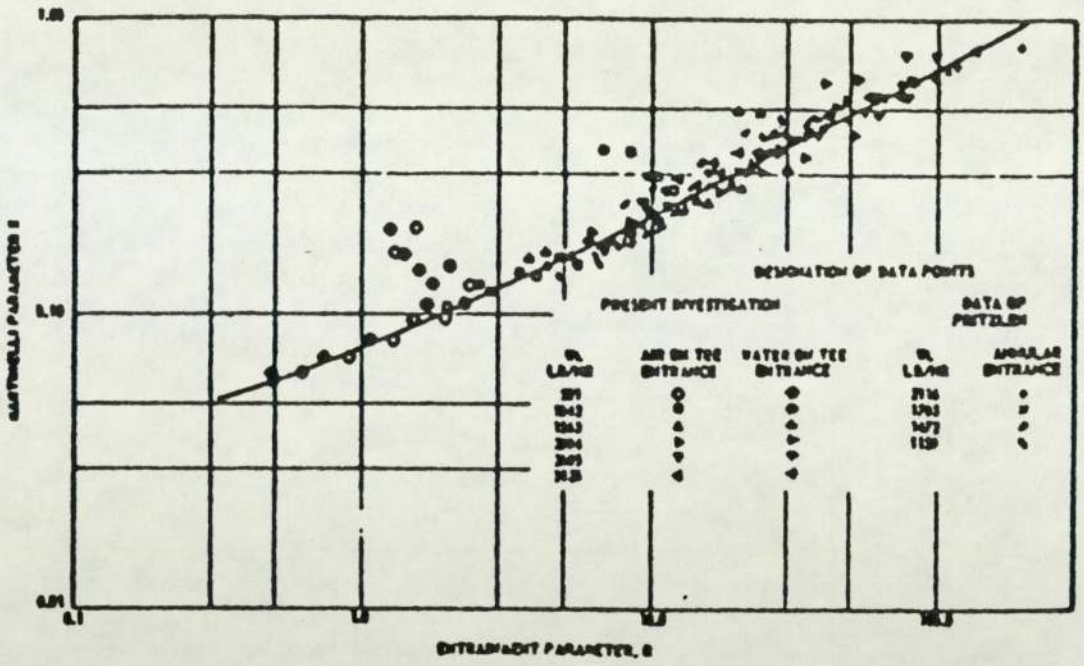

(53)

Figure 3.6.a, Wicks and Dukler entrainment parameter.

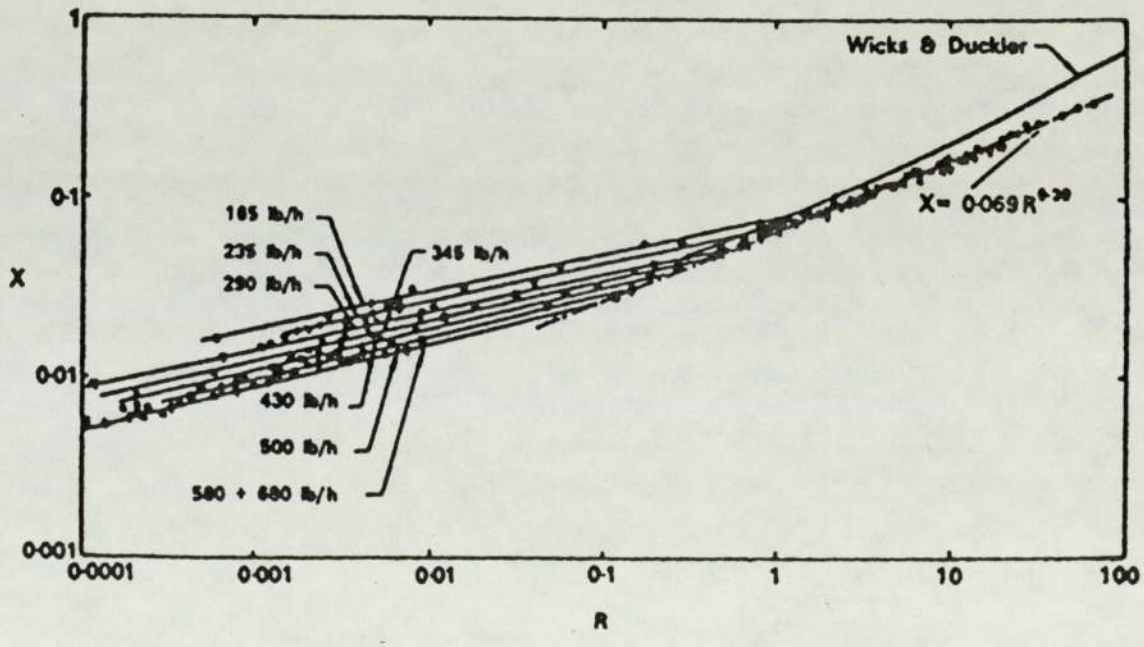

Figure 3.6.b., Wicks and Dukler entrainment correlation [after Hewitt and Taylor (47).]

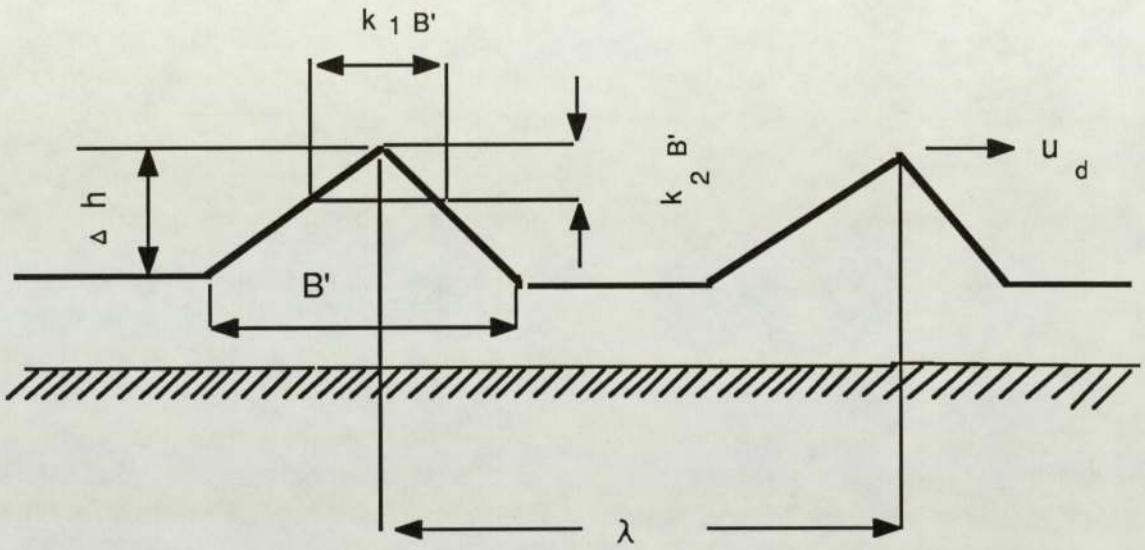

(58)

Figure 3.7., Sekoguchi's Model of droplet entrainment.

The frequency of the liquid droplet entrainment, n, is a function of superficial gas velocity, U_{go}

from the relation of $\tau_i \propto U_{go}^{4}$.

$$\therefore \quad Wc = 4.88 \times 10^{-8} (B \Delta h / \lambda) U_{go}^{4.5} \rho_l \text{------} (11)$$

where the unit of W_c = kg / m^2 s

B Δ h and λ are m

U_{go} is m / s

ρ_l is Kg / m^3

The relation between the average film thickness h_m and W_c is shown in figure 3.8b.

Evidently the value of W_c is affected by the average film thickness and the authors derived the following equation to show dependence on h_m and U_{go}

$$W_c = 4.5 \times 10^{-7} h_m U_{go} \rho_l \quad \text{---------- (12)}$$

Koji Akagawa et al express this equation in a more generalized form by introducing the Reynolds number of thel iquid flow to give :

$$Re_l = U_f h_m / \nu_l = Q_f / B \nu_l \quad \text{----------(13)}$$

U_f = average velocity of the film

Q_f = liquid film flow rate

The above equation can be written as:

$$Wc = 2.93 \times 10^{-5} \left[\left(Re_f / 10^2 \right)^{3.5} \left(Re_g / 10^5 \right)^{-5.5} \right]$$

Attempts have been made by a Japanese team, Isao Kataoka and co-workers[59], to investigate the major cause of droplet formation and the size of droplets by applying empirical relations. After surveying the work of different experimenters in the field and examining a large quantity of experimental data they concluded that the standard Weber criterion, based on the relative velocity between droplets and gas flow, predicts excessively large drop sizes. Therefore it was assumed that the majority of the droplets were generated by shearing off from the roll wave. They show analytically that their postulated mechanism is the dominant factor in determining the drop sizes. Their model allows all the available data to be correlated satisfactorily and although they produced no experimental work of their own, they approached the problem analytically and finally arrive at the conclusion that the diameter largely depends on the turbulent gas flow, because the Weber number is not a strong function of the liquid Reynolds number.

Hence in their correlation, they finally omit the dependance of the Weber number on the Reynolds number, providing that the Reynolds number does not vary widely.

Isao Kataoka et al quote:

$$We\ (d_{vm}) = 0.028\ Re_f^{-1/6}\ Re_g^{2/3} (\rho_g/\rho_f)^{-1/3} (\mu_g/\mu_f)^{2/3} \text{---(23)}$$

This expression may be reduced to:

$$= 0.01\ Re_g^{2/3}(\rho_g/\rho_f)^{-1/3}(\mu_g/\mu_f)^{2/3} \quad \text{----------(24)}$$

Therefore the recommended mean diameter becomes:

$$D_{vm} = 0.01\sigma/\rho_g j^2_g Re_g^{2/3}(\rho_g/\rho_f)^{-1/3}(\mu_g/\mu_f)^{2/3} \quad \text{---------(25)}$$

and the average maximum size becomes:

$$D_{max} = 0.031\sigma/\rho_g j^2_g Re_g^{2/3}(\rho_g/\rho_f)^{-1/3}(\mu_g/\mu_f) \quad \text{---------- (26)}$$

(The experimental data fit the log normal distribution, and were correlated within plus or minus 40% error.)

Where:

We = Weber No.

Re = Reynolds No.

μ = Viscosity.

ρ = Density

D = Droplet diameter.

j = Volumetric flux.

σ = Surface tension.

g = Gas.

f = Liquid.

vm = Volume mean.

max= Maximum.

Azzopardi **(60)** deduced a formula to correlate the droplet size of two-phase annular flows. He used a laser diffractor for his experimental work, proving by comparing his results with those of other workers that the machine gave accurate comparable results. However the empirical formula, which has a similar form to that of

Nukiyama and Tanasawa, has a major limitation in that it is specific to flow situations in which drop sizes increase with the liquid flow rate, hence the formula cannot be generalised. He concluded that the drop sizes had been found to depend on gas velocity, which agrees with the findings of Kataoka and co-workers. He also went on to say that the droplet sizes depend on drop concentration but not on the tube diameter.

Azzopardi quotes:

$$d_{32}/\lambda = 15.4/We^{0.58} + 3.5\ G_{LE}/\rho_L U_G \qquad \text{----------(27)}$$

where:

d_{32} is the Sauter mean diameter.

$$= \Sigma (d^3 \Delta N_d)/\Sigma (d^2 \Delta N_d)$$

We = is a Weber number= $\rho_L U_G^2 \lambda / \delta$, $\lambda = \sqrt{\sigma/\rho_L g}$

U = is the gas velocity.

G_{LE} = is the entrained liquid mass flux.

σ = is the surface tension.

ρ_L = is the liquid density.

N_d = proportion of droplets in size range

The findings of Kataoka et al could be expected to be more useful, because they could be used for general situations, since their analysis does not apply only to any one particular mode of annular two phase flow.

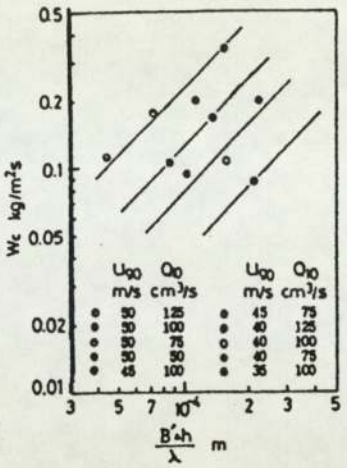

Figure 3.8.a., entrainment / geometric correlation.

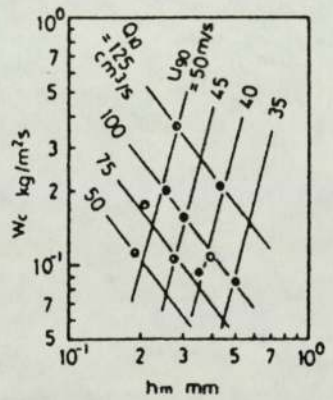

Figure 3.8.b., entrainment / film thickness correlation.

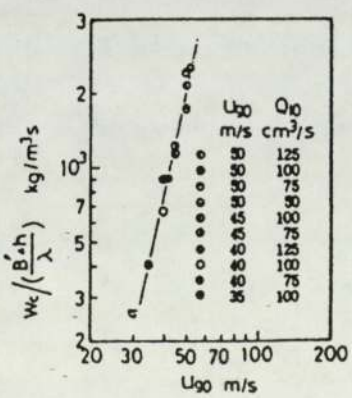

Figure 3.8.c., entrainment / core flow velocity correlation.

for annular flow. [after Akagawa (48)]

The literature survey on this chapter has covered the theory on droplet formation, the behavior of the film and the way it flows and breaks up due the action of drag force (air, gas). The viscosity and surface tension have been shown to be the main influences controlling the formation of the droplets and the film break up, especially at the very initial stages.

It has also been found that most of the analyses used to describe two-phase flow are postulations mostly based on empirical relations. In horizontal two-phase flows it has been shown that the main source of droplet formation is the film which runs along the wall of bottom part of a channel or pipe.

For the flow field to reach a fully developed form, it requires lengths of pipe or channel exceeding 200 diameters. However, at high rates of gas flow it has been found that the horizontal and vertical two-phase flow regimes could be described by the same empirical relations.
Inspite of the fact that trajectories and velocities are governed by undefinable factors (random-like and eddying effects), the entrainment of the droplets has been found to conform with the empirical relations and mostly described by exponential decay laws.

The main fact is that the survey on this chapter has given an insight on the behavior of liquid films and formation of droplets in two-phase multi-component flow fields, such as that existing in the induction pipe and cylinder of a spark ignition engine.

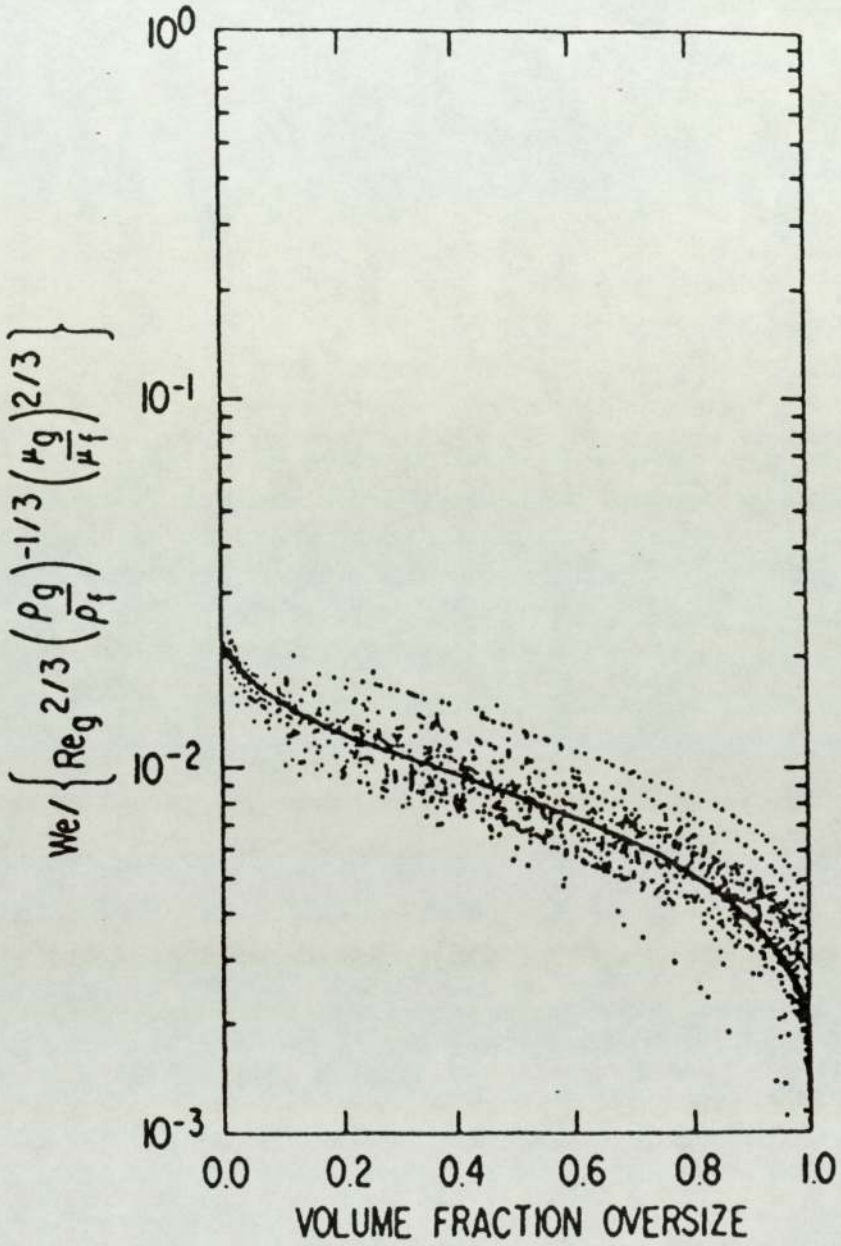

Figure 3.9., Weber / Reynolds number and volumetric fraction over size correlation [after Kataoka et al. (59)]

CHAPTER 4

Wall film and droplet measurement techniques.

In the literature review of chapter 3 certain of the measuring techniques commonly employed in wall film measurement have been referred to by name and droplet size limitations have been quoted. The principal measuring techniques will now be reviewed, in order to clarify later details of the experimental programme and design of the test equipment, discussed in chapter 5.

4.1. Wall film measurement [47].

Since the wall films involved in most types of film flow are rather thin (<2.54 mm) their measurement is not easy, a variety of alternative methods have been practiced. They can be classified into three main groups:

(a) **film average method:**

The average thickness is measured over a considerable length of liquid film. This includes making an instantaneous average, obtained over a fixed length of the film or by conductance methods where averages over both distance and time are obtained.

(b) **localised methods:**

Involves techniques for obtaining a reasonably localised measurement of film thickness without being able to obtain an

instantaneous value. These methods include radio active absorption and emission, conductivity probe and capacitance measurements. Using these methods makes it possible to obtain information on the temporal variations of film thickness.

(c) **fixed point methods:**

Involves methods whereby statistical or continuous information can be obtained at a point in the liquid film. This will include the needle contact method, the light absorption method, the photographic techniques and the fluorescence technique method.

4.1.1 Film average methods

Hold-up measurements

The technique consists of isolating a section of the pipeline, draining it and then measuring the volume, normally two isolation valves are needed for smooth control of flow. To avoid excessive shock, the flow stream may be diverted through a by-pass. This method neglects entrainment which renders it inaccurate at high flow rates.

Weighing methods

These are similar in principle to the draining method except that it is arranged to measure the hold-up in the experimental section. Normally this method is inaccurate for vertical conditions with gas flow.

Film conductance method

This depends on the conductance of a certain length of film, which could be made conducting by adding electrolytes, and is made to flow over an electrical insulator. Electrical connections are then made to the length in question by inserting the electrodes in the wall. This method has been used by many experimenters but although the results are reproducable yet the presence of surface waves may lead to an error thought to be in the order of 30%.

4.1.2 Localised methods:

Radioactive absorption and emission:

A radioactive substance is dissolved in the flowing liquid, the amount of radiation detected will depend on the amount of the liquid in the locality, and hence on the film thickness, the intensity of radiation is detected as a function of the thickness. All radiation methods suffer from lack of accuracy, and special attention has to be given to safety aspects.

Conductance probe method:

Electrodes are placed in close proximity on the surface over which the film is flowing and are connected flush with the wall. The specific advantage of this over other methods is that it can give limited information about instantaneous variation of film thickness and enters the time factor into consideration. The dependence of conductance upon the film thickness is initially linear except for high thicknesses.

Measurement of capacitance:

Use of the capacitance method has proved difficult and it is not recommended because corelations are geometry dependant.

4.1.3 Local measurement methods

(a) Needle contact method

When the needle is made to contact with the film, the distance between the needle point and solid containment is noted. If no waves exist, the first measurement will represent the film. When waves are present , then the troughs of the waves will be touched. The point of contact can either be determined by electrical or optical methods. The electrical method is the more reliable and consists of measuring the conductance between the needle tips and pipe wall. This method can provide statistical information but it has to be noted that it does not give continuous information about the changes in the film. One disadvantage of this method is that contact hysteresis might occur. (Surface tension might cause the film to stick to the needle) resulting in more delay of signal. Another disadvantage is that the flow must be disturbed to introduce the contact needle.

(b) Light absorption method

The idea is to pass a beam of light and then detect its intensity on the opposite side. The amount of light absorbed will be a function of the film thickness. Normally special dye stuffs are added to

increase the light absorption. The disadvantage of this method is that wavy films cause light to scatter resulting in reflection.

(c) Photographic, shadow and Interferometric methods

The measurement is carried out in a glass section and the glass must have the same refractive index as the flowing liquid, the advantage of this method is that it does not interfere with the flow hydrodynamics of the liquid film, further more it is not necessary to add any dye material or electrolytes to facilitate the film thickness measurement.

Polarised light.

None of the afore mentioned methods is capable of measuring liquid films in the anticipated thickness range (10^{-3} to 10^{-4}) mm. An optical method using polarized light is capable of indicating changes of liquid films of molecular dimensions (10^{-6} to 10^{-7}) mm has been used. It makes use of the fact that polarized light when reflected from clean metallic surfaces is elliptically polarised and the presence of a thin film will cause a change in the eccentricity by an amount related to the film thickness.

Fluorescence spectrometer method

A beam of light of a given wave length is passed into the liquid film, a fluorescing dye material is added to the liquid and the

incident light excites fluorescence of different wave lengths. The amount of fluorescence increases with the increasing film and can be metered by first separating the fluorescent light from the reflected components of the incident light by means of a spectrometer. (See fig 4.1). Blue light from a mercury vapour lamp is passed through a microscope illuminator, and then focused in a conical beam into the liquid film. The circulating water contains fluorescing dye stuff in small concentrations, which has negligible effects on liquid physical properties and does not influence wave formation. The incident beam will excite green fluorescence in the film. The fluorescent light is emitted isotropically through the illuminated region of the film and some of this light is picked up by the objective lens of the microscope illuminator, it then passes through the half silvered mirror and to the collimator of the spectrometer. The spectrometer separates the green light from any reflected blue light. A photo multiplier (substituted for the eye piece of the spectrometer) records the intensity of light, and the signal obtained is sensitive to the geometrical arrangement of the optical system.

Main advantages:

Good frequency response Gives highly localised measurement

No interruption to flow

Disadvantages:

Unstable for complex geometries.

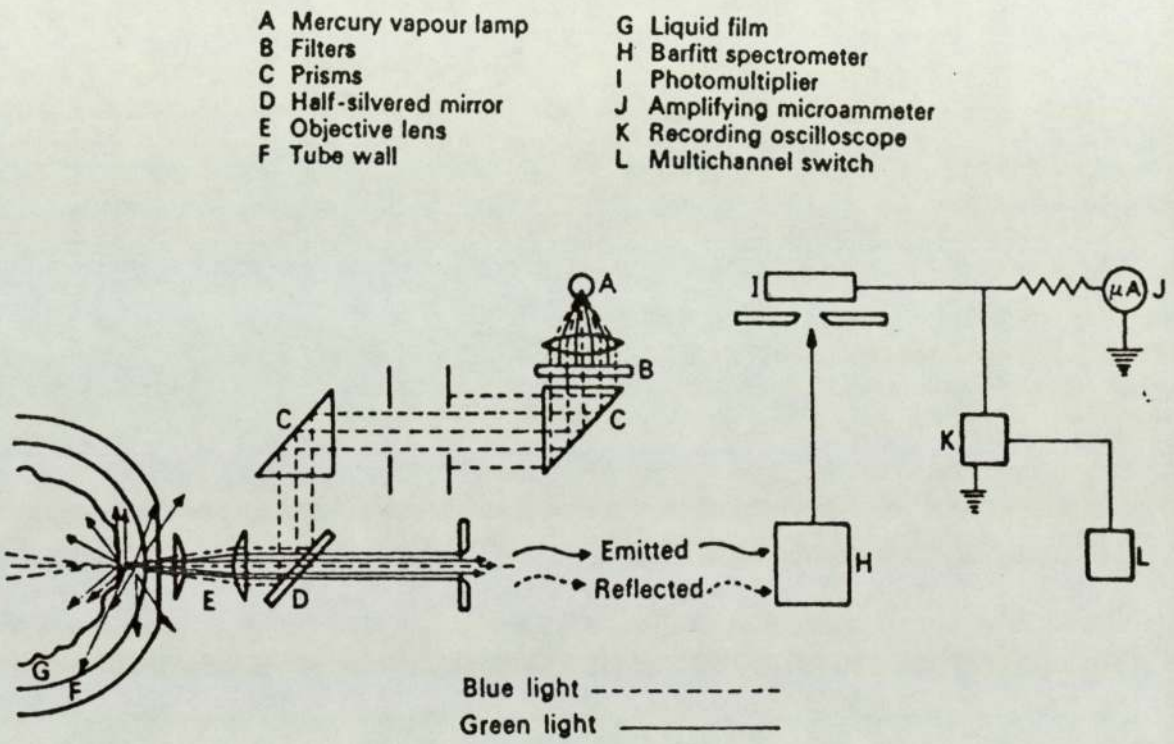

Figure 4.1, fluorescence spectrometer Method

Adding of fluorescent stuff may be good with water but may not be acceptable with other substances.

Many alternative methods are available for measuring film thicknesses but none of them could be said to be completely ideal. The fluorescence method is non-obtrusive and offers some advantage for situations where it can be used: where it cannot, the probe method is recognised as the best alternative.

4.2. Droplet size measurement methods. (74) (75) (76)

Three methods are mainly available for measuring droplet size and distribution:

(a) mechanical methods

(b) photographic techniques

(c) light scattering methods.

4.2.1. Mechanical Methods

4.2.1.1 Coated slide techniques

In this technique the sample is collected on a glass slide coated with a material which shows the mechanical deformation of the coating due to droplet impacting. The materials used for coating slides are either of lamp black or a white vaseline smoothed by heating to 150 °C in an oven for three minutes, or magnesium oxide formed by exposing the slide to magnesium ribbon. The data are

correlated by introducing an empirical factor "the impression coefficient", *I*, such that;

I = 0.86 for 20 to 200 μm range

I = 0.71 for 10 μm drops.

I = 0.77 (We)

where We = Weber No.

However, this method is tedious, and it is very difficult to get a representative sample. Moreover, some of the smaller droplet sizes escape being monitored and tend to flow with gas stream; smaller slides have then to be used, which would reduce the method's capture efficiency. Alternatively the slides may be surface coated with a liquid coating which is immiscible with the spray. It should not allow drop coalescence; the drop liquid aggregate should remain stable, and should be less dense than the sprayed liquid, or else the sample will be coalesced. Liquids which have been used include liquid soap, castor oil and Shell Spirax Oil 250.

In such applications, a correction factor termed the flattening coefficient is used. Oil soluble dyes are sometimes used to facilitate size measurement. This method allows the determination of drop size frequency distribution from the size count obtained when the slide is examined under a microscope.

4.2.1.2. Frozen drops in wax method.

For this technique the sample of droplets is collected by spraying into a freezing bath, freezing the droplets into solid spheres. The collected droplets are separated by sieving and it may be necessary to insulate the sieving system, to keep sizes to standard level. To escape the complications of freezing media, some investigators have used a spray of paraffin wax sprayed at temperature above its melting point. The droplets solidify in the cold gas stream and it must be noted that the drop formation occurs before any alteration in maximum temperature. This method eliminates the need for techniques, which require a microscope to measure the drop size.

4.2.1.3. The cascade impactor

This is based on the principle that when a sample slide is placed in the path of the large droplets, they will impact on the slide because of their momentum, small drops will follow air stream; the air velocity is increased successively by reducing the orifice through which the stream is made to pass, and thus successively smaller drops are made to impact. The relative mass impacting on each stage can be determined by gravimetric methods.

4.2.1.4. Pulse counting technique:

Based on the fact that, voltage pulses are produced when the droplets of a particular size, short circuit the tips of needles across which a potential is applied. The distance between the two needles is micrometer adjusted, the distribution of the droplets is

derived from the relation between pulse count and separation. The fluid in use should have a reasonable conductivity level. Again here, a correlation factor is needed to interpret the signal pulses by short circuiting the needle tips across two points of a droplet which do not represent a measurement of its diameter.

This system is capable of measuring sizes in the range 15 to 100μm., although the interaction between air and probe might lead to errors.

4.2.2. Photographic techniques.

4.2.2.1 Single and double flash illumination.

The single flash illumination technique provides photographic information of drop sizes, using a microscope to measure the image size. By using a double flash system it is possible to provide information about velocity and flight angle of drops. The method has been used for drops sizes between 5μm and 1000μm and velocities in the range from zero to 75m/s, and flight angles from zero to 360°. The idea of the two spark system depends on two spark sources which are fired in an optical system that focuses the light on the test section. A camera is used to record the drop images produced. The resultant negative can be used to measure droplet velocity, angle of flight and size. The method produces two images of the droplet pattern, Successive position of each drop enables the droplet velocity to be determined while the droplet size can be measured with a microscope. See fig. 4.2.

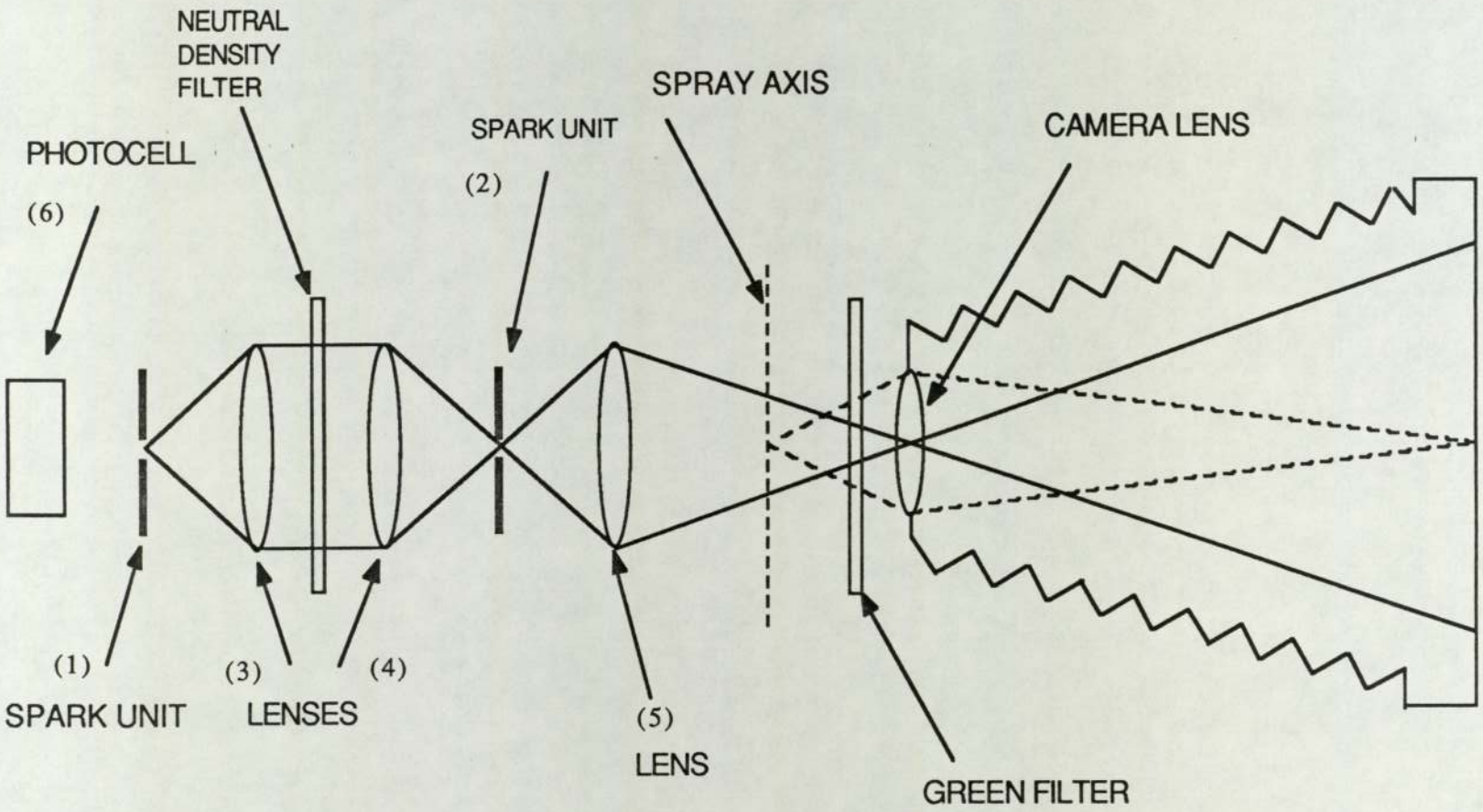

Figure 4.2., Optical system for two sparks

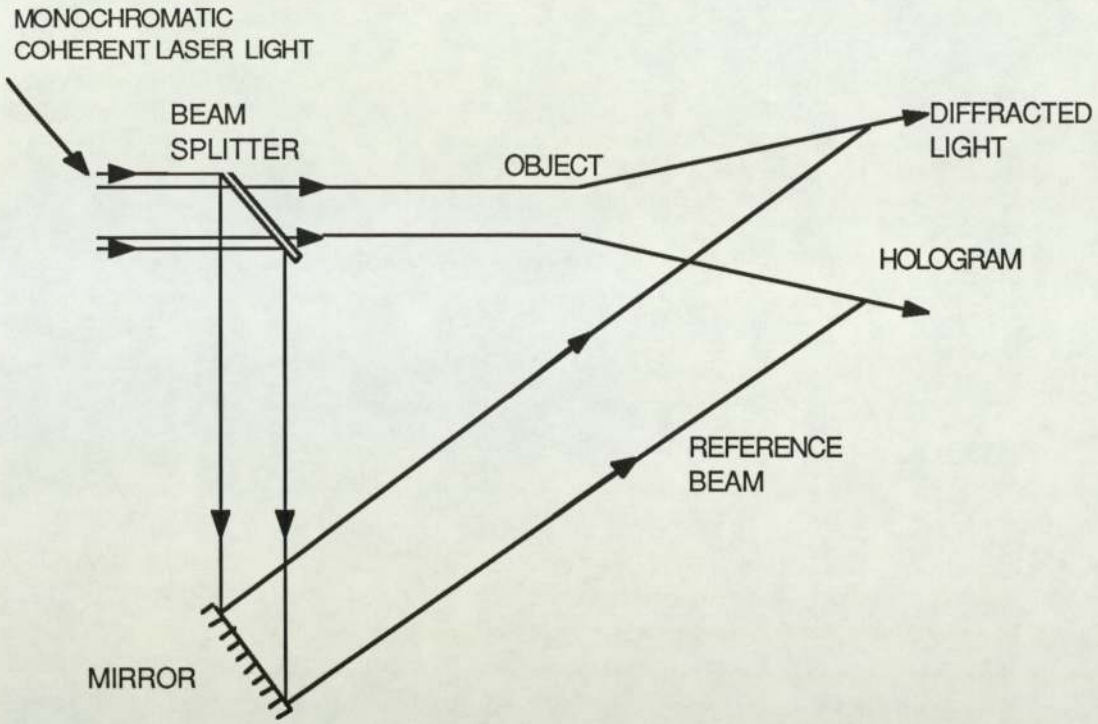

Figure 4.3., laser holography system

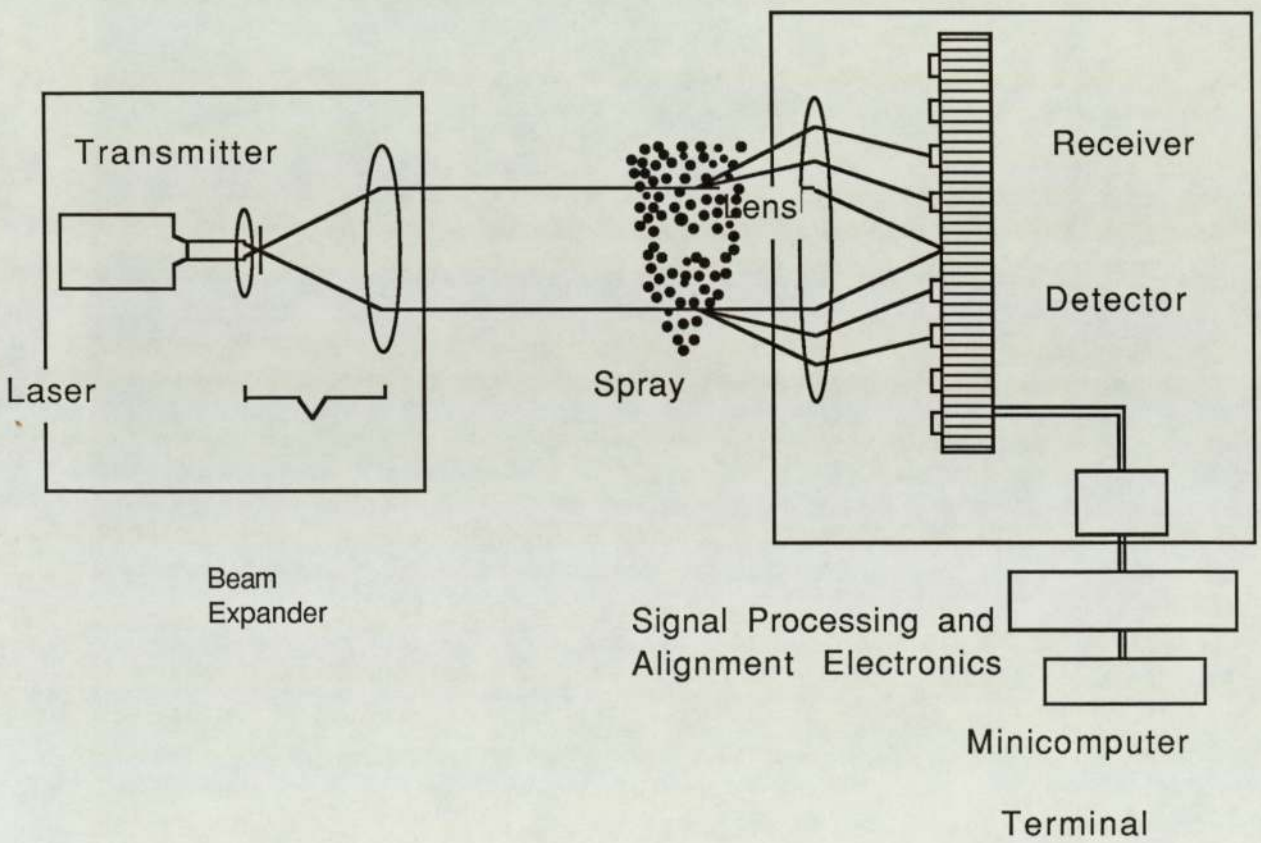

Figure 4.4., laser diffraction system

4.2.2.2. Laser holography: See fig. 4.3.

Holography is the technique of recording the image of an object using the intensity, wave length and the phase of light reflected or transmitted by the object. Photography uses the wave length only, while holography employs the phase content of the light. For the purpose of holography light from a laser is normally split in two beams, the reference beam is reflected unchanged in phase to fall on holographic emulsion. The other beam strikes the object and is reflected from the object to the emulsion which it reaches at the same time as the reference beam, but the two rays are different in phase and this causes interference resulting in a hologram of varying illumination intensity. To reconstruct the hologram, the reference beam from the laser is reconstructed at the same angle. The hologram acts as a refracting screen, and behind it a wave pattern is formed of the object originally seen in position. The droplet size measurement is determined by relating the depth of field of laser holography to droplet size and laser power.

4.2.2.3. Optical-Diffraction technique:

When a parallel beam of monochromatic light falls on a circular disc or aperture a diffraction pattern is created. Some of the light is deflected by an amount depending on the size of the disc and the diffraction pattern is usually inversely proportional to the disk diameter. The diffraction pattern is very large compared to the geometric image. When a lens is placed in the light path beyond the

disk and placed in the focal plane, then the undeflected light will be focused at a point along the axis of the lens and the conical diffracted light will be focused around the central spot. The displacement of the disk will not move the diffraction pattern, since any conical diffraction angle always ends up as the same radial displacement in the focal plane. The diffraction pattern produced on the screen is known as the Fraunhofer diffraction. The light distribution will appear as a series of concentric rings, alternating light and dark. The rings appear at different positions for different sizes of discs, so in the case of droplets or particles an integrated light distribution would be obtained where by the drop size distribution could be entered. The Fraunhofer distributions of rings of light are decreasing in light energy in proportion to $(\sin x/x)^2$.

The annular rings are light sensitive and the intensity of the light falling on each is measured electronically, the allowance for the increase in area of outer rings is made within the computer software used to analyse the results.

The Malvern particle sizer is a commercial device which employs the Fruanhofer fringe technique. It consists of a He/Ne laser source which produces a continuous beam of coherent light which is expended and collimated. The beam behaves as a high quality monochromatic light beam with a wave length of 0.633 μm. The beam passes through the particle stream where it is diffracted and

then passes into the receiver which comprises a single collection lens, a photodiode detecter screen, and an analog to digital convertor. The detector consists of an array of 30 annular detectors on which the diffracted light falls. The computer programme which analyses the diffraction pattern allows the user to analyse the data directly or to fit that data to either of two accepted correlations for the cumulative distribution of droplet or particle sizes.

4.3. Distributions employed in droplet size measurement.

4.3.1. The binomial distribution:

The commonest of many discreet types of variations assuming random distribution of events is the binomial distribution. It has been used successfully in a considerable variety of situations.

In the case of a stream of droplets in which all sizes co-exist the sizes are assumed to exist in proportions of p and q, larger than a particular size "d" and below that size respectively. If a number of "n" drops is withdrawn from the stream, the probability of combination would be, according to Bernoulli by the binomial expression as:

$$(p+q)^n$$

The mean number of sizes larger than "d" is "np" and the standard deviation of the sample quality as $\sqrt{npq}$. The frequency at which the (larger than size d) samples differ from p by more than $\pm\sqrt{pq/n}$ is 5%.

The relations between frequency of sample quality and its difference from the true proportions of the components in the mixture will approximate to the theoretical relation only after a sufficiently long time of mixing ie, the standard deviation will be according to the Bernoulli formula after prolonged mixing.

4.3.2. Normal distribution:

It is modelled by the function:

$$n_d = (1/\sqrt{2\pi})\ \exp\ (d-x)^2/2N^2)$$

where: x the sample mean, nd the relative frequency of size d and N the standard deviation of a particle or droplet. The distribution is a bell shaped curve.

The drawback of the normal distribution is that it is defined to be finite over the interval $-\infty$ to $+\infty$, that means that some weight distributions will give negative values.

4.3.3 Log normal distribution:

The weight frequency distribution is assumed to obey:

$$l_d = 1/\ln(N) * \sqrt{2\pi}\ \exp\ \{\ln d - \ln x^2/2\ln(N)^2\}$$

where: ld is the weight frequency at size d.

x is the geometric mean of the distribution and N is the geometric standard deviation.

No values exist below zero, hence it does not give the same problem as the normal distribution and it can account for a size weight of (1 to 100)%. It can be represented linearly.

4.3.4 Rosin Rammler distribution [76]:

This distribution was originally developed to correlate the cumulative distributions of size of coal particles, and has since been found to apply to many other materials and situations: one of the fields of application is drop size measurement. The authors obtain the following from the probability equation (let the size distribution be R over a certain size x):

$$df(X)/dx = 100n\ bx\ \exp(-bx)$$

where n and b are constants,

1/b is a measure of particle (droplet) size present

n of the substance (fluid) being analysed.

Integration gives: $R = n\ 100\ \exp(-bx)$

This may be reduced to: $\text{Log log } (100/R)\} = \text{const} + n \log x$

If log log (100/R) is plotted against log x, a straight line results with n being the slope of the straight line.

Chapter 5.

Experimental programme and test results

5. General.

The objective of the experimental programme was to examine the size spectrum of droplets into which the wall film broke up as it passed through the inlet valve and entered the engine cylinder. Of the droplet measuring techniques reviewed in the previous chapter only the photographic method and the laser particle sizer were available and because the particle sizer uses light diffraction as the basic principle of its operation, it was clear that it would not be possible to work on a firing engine, since the diffraction pattern would be distorted not only by the droplets in its path but also by the laser beam passing through a region of non-uniform temperature. It was therefore decided to use the cylinder head from a single cylinder engine and mount this on a mock cylinder barrel with suitable holes drilled to allow the laser beam to pass through the stream of air, fuel vapour and droplets leaving the valve port.

To reduce the danger of explosion from the use of normal petrol/air mixture and in order to ensure that the droplets which were measured had been formed only by the break up of the wall film it was decided to inject separated wall film liquid, obtained during a previous research programme, directly onto the walls of the inlet manifold. It was intended that an exhauster should be used to draw air through a carburettor and into the manifold at flow rates in the range normally

employed in working engines; the valve gear would be operated by an auxiliary drive and the wall film injected at an appropriate point ahead of the valve port. Later tests were to be carried out using petrol supplied by the carburettor in the normal way. The problems of operating safety for the tests in which wall film and petrol were to be used were investigated carefully and are the subject of a detailed report attached as Appendix 1

The arrangement of viewing ports for the passage of the laser beam was to be based on the design employed by Finlay et al (61) in their investigation of droplet spectra immediately downstream from the throttle plate of an air valve carburettor. This consisted of diverging cones on either side of the test section, to contain the diffracted beam, each termination closed by an optical flat to seal the inlet system for vacuum operation and allow the undisturbed passage of the laser beam. Finlay worked on a firing engine but it had proved difficult to avoid clouding of the optical flats by droplets entering the cones as a result of the pulsating flow. To overcome this problem the investigators used shutters adjacent to the test section and an "air curtain" to keep the glass clear. A rather simpler system was designed and constructed for the present investigation, but the experimental programme did not progress to the point where this was utilised.

An initial series of tests was performed using air and water to examine the general behaviour of two phase flows in a transparent inlet system connected to the cylinder head of a single cylinder

engine and to obtain some visual evidence of the break up of wall films at the exit from pipes and engine inlet ports. This was followed by steady flow tests in which the same system was fitted with a transparent cylinder barrel to discover the likely trajectory of the droplets within the cylinder. The work of Bican had shown that the path of the gas flow into an engine cylinder was the same in both steady and pulsating flow conditions and the object of these tests was to ensure that the viewing ports would be correctly located in the cylinder barrel of the final test rig for use with the laser particle sizer.

Once the direction of droplet streams had been established the design of the unsteady flow test rig and visualisation system was embarked upon. When the details of this design had been finalised an extensive series of unsteady flow tests was carried out in which air and wall film were discharged through an oscillating valve fitted at the exit from a horizontal pipe of circular cross section and the stream of droplets passed through the beam from the Malvern laser particle sizer. The results from these tests represent the main body of experimental achievement: as stated earlier, time limitations prevented any use being made of the enclosed discharge unsteady flow test equipment with flow induced by the vacuum exhauster facilities.

5.1. Steady flow tests using air and water.

5.1.1. Flow visualisation with open discharge.

The introductory test series referred to above was carried out using a steady flow of air obtained from laboratory services and supplied via a rotameter to the particular inlet configuration being examined. Water was injected either from a spray nozzle on the centreline of the pipe or directly onto the walls of the inlet system from radial holes in the outside surface of an annular distibutor. The arrangement is shown in sketch form in fig. 5.1(a).

Because the object of these tests was to gain some knowledge of the physical nature of wall film flows the apparatus was not equipped with sophisticated instrumentation. The system pressure drop and total flow rates of air and wall film were measured, together with air and water temperatures and laboratory ambient conditions. Because the tests were carried out during the period in which the literature on two phase flows was being reviewed an attempt was made to correlate the present results using the methods of earlier workers.

It was observed that the flow patterns were not affected by the way in which the liquid was injected. The inlet system pipework was all of circular cross section with the centreline in the horizontal plane. At low rates of airflow the injected liquid formed a stream flowing along the bottom of the pipe but at high airfow the liquid spread upwards and flowed randomly in rivulets, or as a film with greater thickness at the bottom of the pipe. The correlations in terms of the

Martinelli parameter are shown in fig. 5.2 and indicate that the analysis is applicable even in the short lenghts of duct which were used in the present tests.

The break up of the wall film at exit from a plain horizontal pipe indicated that the size of the droplets formed was related to the airflow velocity and to the liquid flow rate. No attempt was made to measure the size of the liquid droplets. It was observed at higher liquid flows that a proportion the film flowing on the bottom of the pipe tended to adhere to the lip of the pipe at exit and formed very large drops which fell from the underside when their mass could no longer be supported by the effects of surface tension.

When the inlet pipework was connected to a cylinder head in which the inlet valve was held open the size of droplets was seen to depend on valve opening and air/liquid mass ratio: small drops were discharged at low openings. The direction of discharge was controlled by valve opening: at very low openings the discharge was almost uniformly distributed, but at greater openings the line was established by the path which was followed by the main bulk of liquid flowing along the bottom of the pipe and towards the outside of the 90° sweep bend within the cylinder head. As with the open pipe there was a tendency for the film to follow the solid boundary at the discharge and large droplets were seen to run along the underside of the cylinder head.

These tests established the likely path of droplets at entry to the cylinder, but it was judged necessary to extend the tests to include discharge into a transparent cylinder barrel to establish the effect of enclosing the flow.

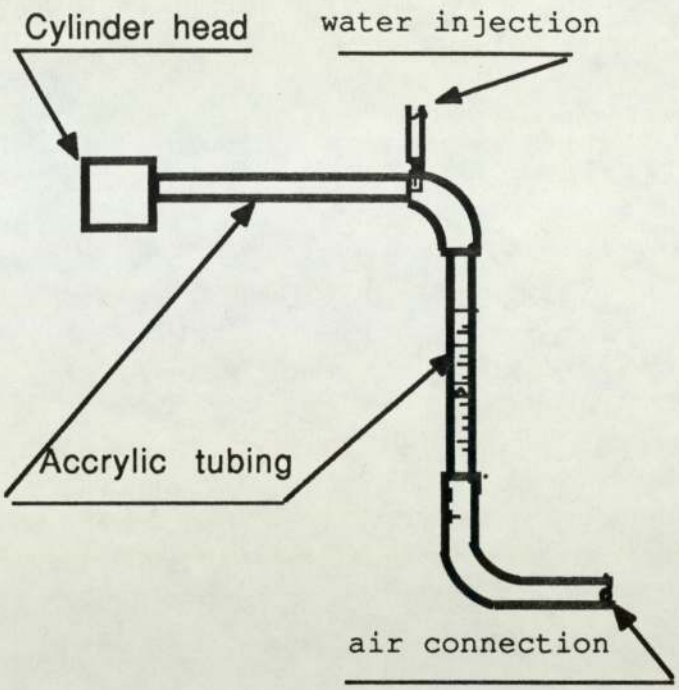

Figure 5.1. a

Horizontal rig for steady flow visualisation

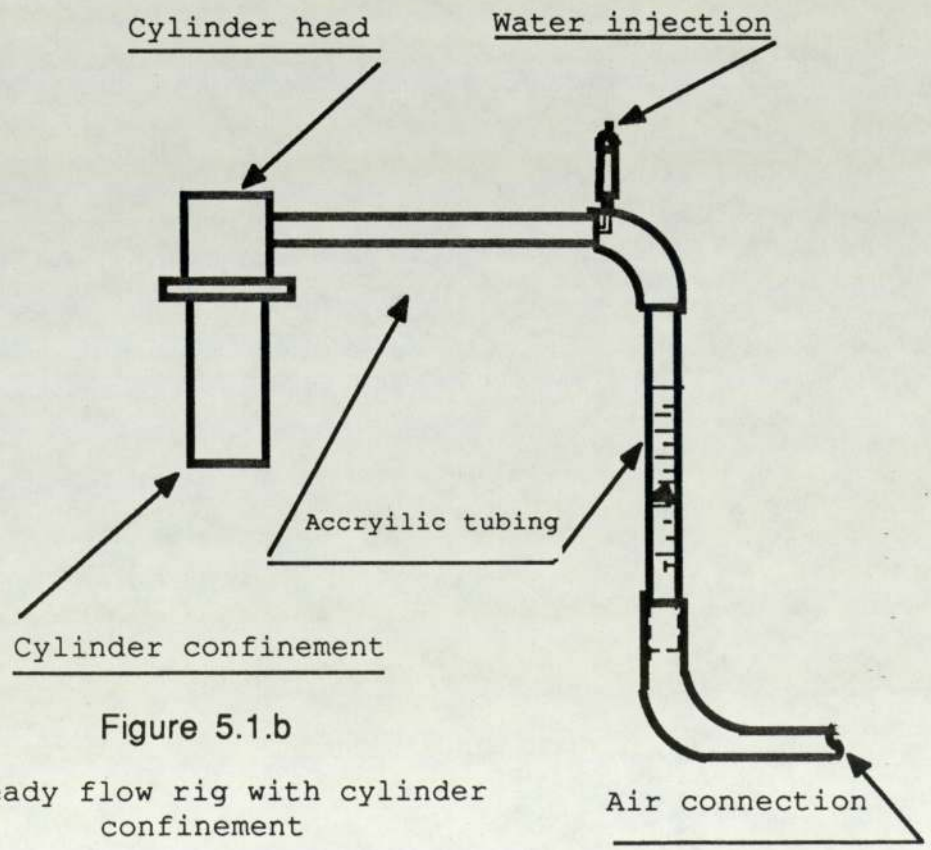

Figure 5.1.b

Steady flow rig with cylinder confinement

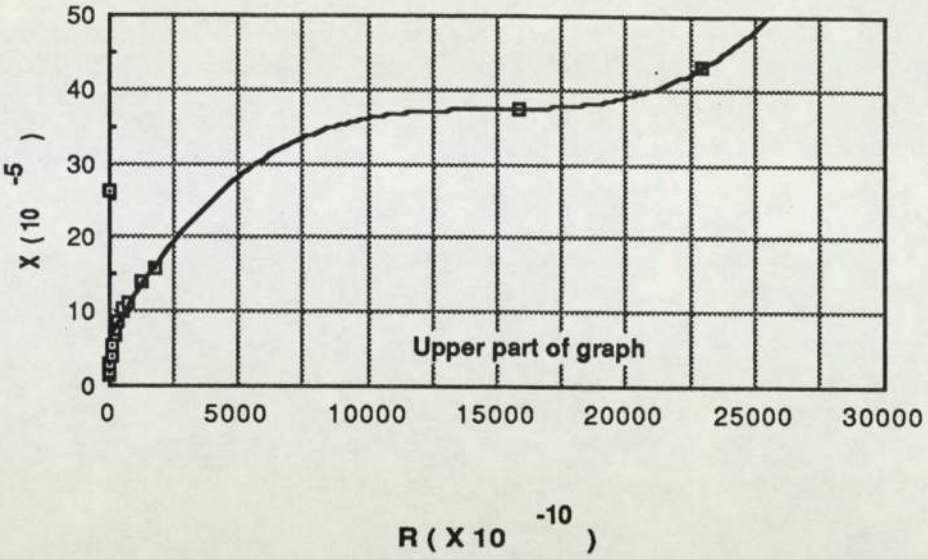

Figure 5.2.a., Martinelli Vs Wicks& Dukler(Parameters)

" current research"

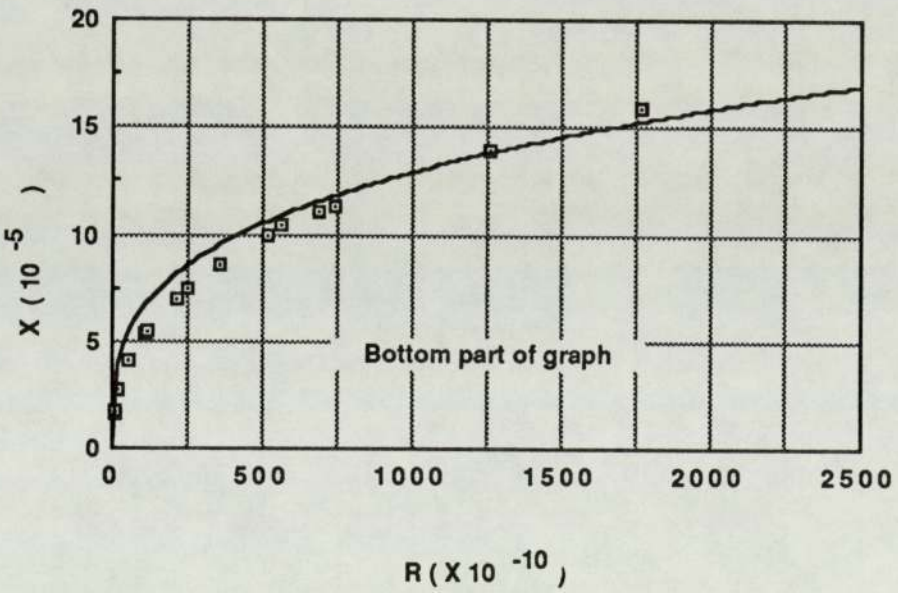

Figure 5.2.b., Martinelli Vs Wicks & Dukler (Parameters)

"current research"

5.1.2. Flow visualisation with enclosed discharge.

A transparent cylinder barrel was fitted to the cylinder head used in the experiments described in 5.1 and further tests were conducted over a wider range of air flows, using both air/water and air/petrol mixtures. The general arrangemet of the apparatus is sketched in fig. 5.1b. The instrumentation used enabled the same experimental data to be recorded, but the observation of flow patterns and droplet formation was supplemented by video-recordings. The frame frequency of the video recorder is too low to permit the discrimination of droplets in the flow and provided no more than a permanent record of the direction of droplet discharge for a range of valve positions under steady flow conditions. Pl. 5.1a and Pl. 5.1b. are photographs taken from the video screen and show clearly the pattern of flow within the inlet pipe and the cylinder.

As in the free discharge tests it was again the case that smaller droplets were formed at low valve openings, while the wall film broke into a clearly directed stream of droplets for wider openings, the size of the drops being governed by the air/liquid mass ratio and the airflow velocity.

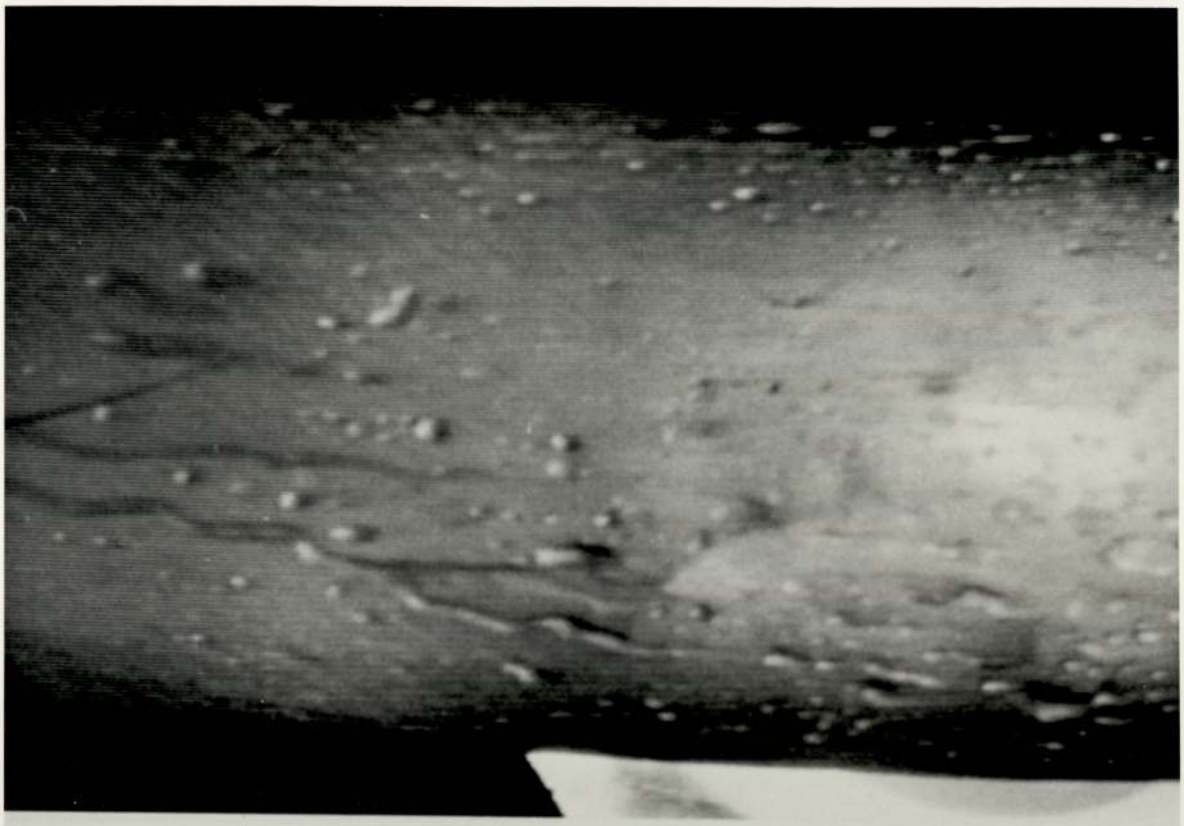

Pl. 5.1a
Annular flow in horizontal pipe.

Pl. 5.1b
Flow pattern of droplets entering
engine cylinder in steady flow

5.2. Droplet size measurement tests.

Two series of tests were undertaken to investigate the effect of pulsations on the formation of droplets. In both cases the wall film liquid was injected at a measured rate into the bottom of a straight length of transparent pipe. Air was supplied from a centrifugal blower which was capable of representing the full range of airflow Reynolds numbers arising in the manifold of a typical spark ignition engine from idling to full power conditions. The ratio of wall film flow to total air flow used in the tests covered the full spectrum reported in the literature. In the first instance the pulsating flow was induced by means of a rotating disc at entry to the blower, while the airflow and droplets were discharged from the open end of the transparent pipe. The beam from the Malvern particle sizer was arranged to pass through the core of droplet flow. The disc causing the flow pulsations was slotted over a full quadrant to represent the induction phase of engine cycle operation and a wide range of rotational speeds was investigated.

In the second test series a typically shaped valve was actuated at exit from the transparent pipe: again the tests were carried out over the full range of Reynolds numbers and valve speeds. The valve was operated using a Scotch yoke mechanism which produced a sinusiodal motion rather than the rapid lift and closure associated with automotive valve action. The likely effects of this choice will be discussed in a later chapter.

5.2.1. Disc valve tests.

For these tests air was supplied from a low pressure blower to a horizontal straight pipe representing the manifold. Wall film liquid was introduced through a hypodermic tube lying on the inner surface and flow pulsations were imposed by rotating a disc over the inlet to the blower. A kidney-shaped hole cut into one quadrant of the disc simulated the breathing operation of a four stroke engine. The rotational speed of the motor driving the disc valve was controlled by a thyristor and the speed of rotation was determined using a stoboscope. The Malvern particle sizer was set up using the 600mm lens. The number of droplets formed due to pulsations created at inlet to the blower was insufficient to give the levels of obscuration which are normally regarded as necessary to ensure 'good' results and tests were carried out using a closely seived size range of silica sand particles falling through the laser beam at similar obsuration levels. The results of the sand particle tests showed that the particle sizer was producing accurate results at these low obscuration levels.

5.2.2. Inlet valve tests.

The facilities used for these tests are indicated in the accompanying photographs, Pl. 5.2a and Pl. 5.2b. Preliminary steady flow tests were undertaken using a number of fixed valve positions before proceeding to investigate the size of droplets formed in the full range of air and film flows and valve operating speeds which represent engine operating conditions. In the steady flow tests the presence of the valve gave rise to significant droplet formation only at low valve

openings: with the valve in operation and creating unsteady flow conditions a wide range of droplet sizes was produced and it was found to be necessary to use the 800mm focal length lens in the particle sizer to ensure that larger drops were correctly identified. In many instances tests were repeated to ensure that repeatable results were being obtained.

5.3. Results.

The results of the tests described above are presented in tabular and graphical form in tables 1 to 8 and figs. 5.2 to 6. The initial steady flow tests did not include any measurement of droplet sizes but show that the data for two phase flow can be correlated using the approach of Lockhart and Martinelli, despite the undeveloped nature of the flow in short pipe lengths. Fig. 5.3 shows the effect of airflow Reynolds number upon liquid droplet entrainment in the free discharge conditions of the steady flow air/water test rig, demonstrating that the rate of increase of entrainment decreases logarithmically towards a constant value at high rates of core flow. The later tests, in which droplet size measurements were taken in steady flow conditions, show that roll wave shearing of the wall film did not produce measurable droplets in the range of Reynolds numbers and air/film mass ratios representing steady flow in the intake manifold. The results for pulsating flow induced by the rotating disc valve indicate that pulsations increased the extent of roll wave shearing to the point where droplets were produced in small numbers, while the tests in which a representative engine inlet valve was operated at exit from the pipe show that a very wide spectrum of droplets was produced. Supporting evidence was provided in a series of photographs, from which the presence of large droplets is clearly evident and it is also apparent that the wall film may follow the geometry of the pipe exit to form very large liquid drops, particularly in the conditions of relatively high film flow which would correspond to cold start-up of an engine.

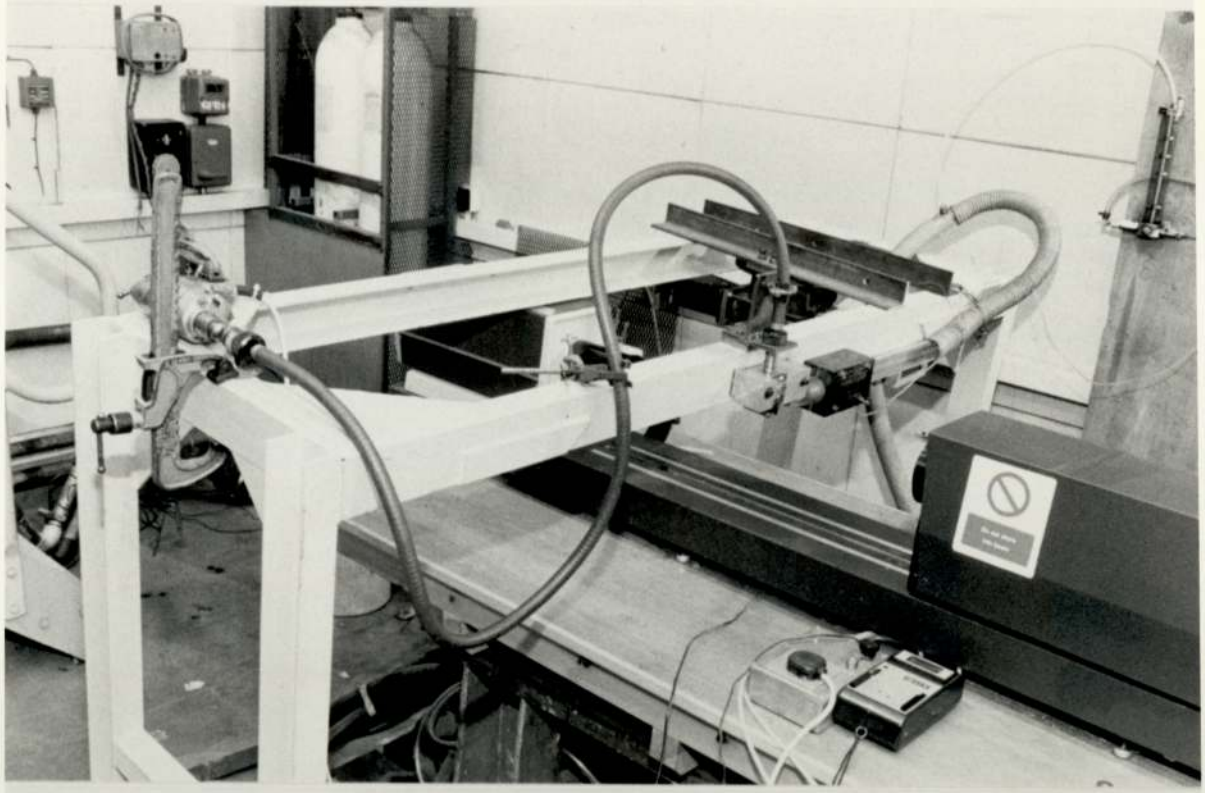

Pl. 5.2a.
General view of Malvern Particle Sizer and Inlet Valve

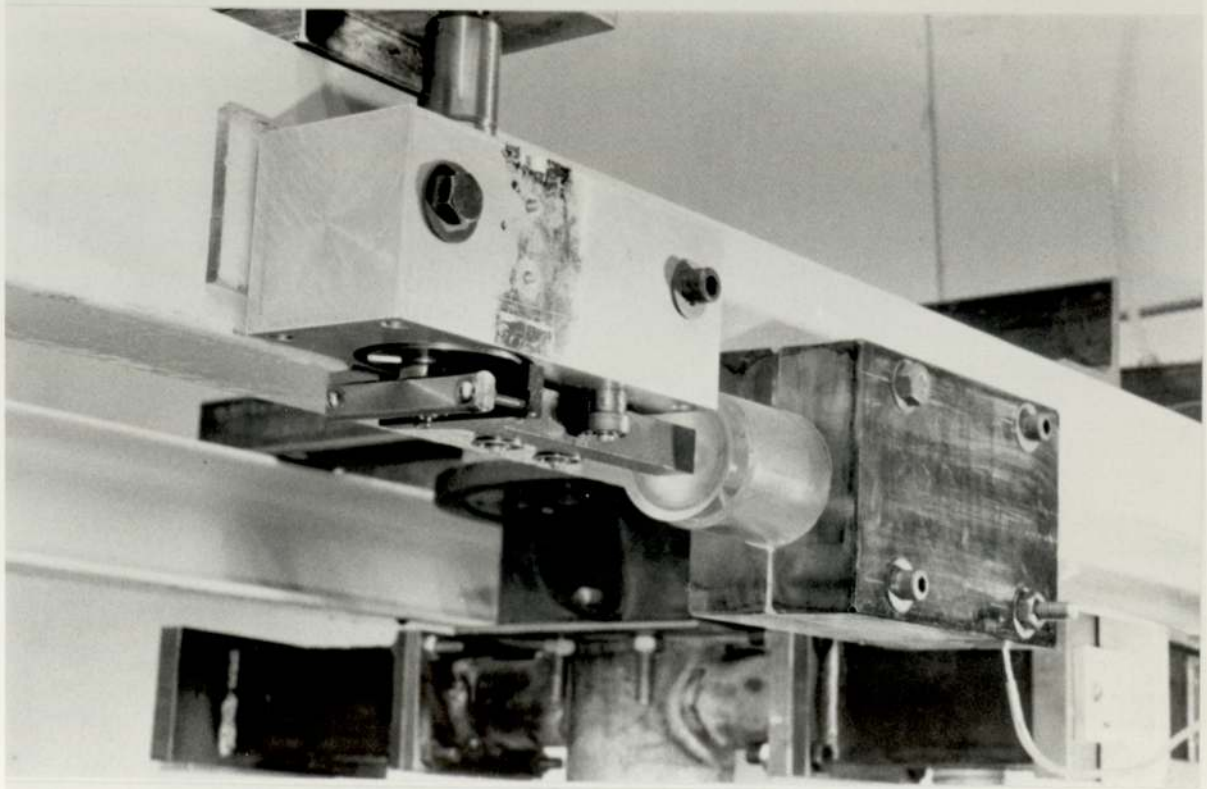

Pl. 5.2b.
Inlet Valve and Actuator

The significance of the findings from all the tests which were carried out is discussed in the following chapter.

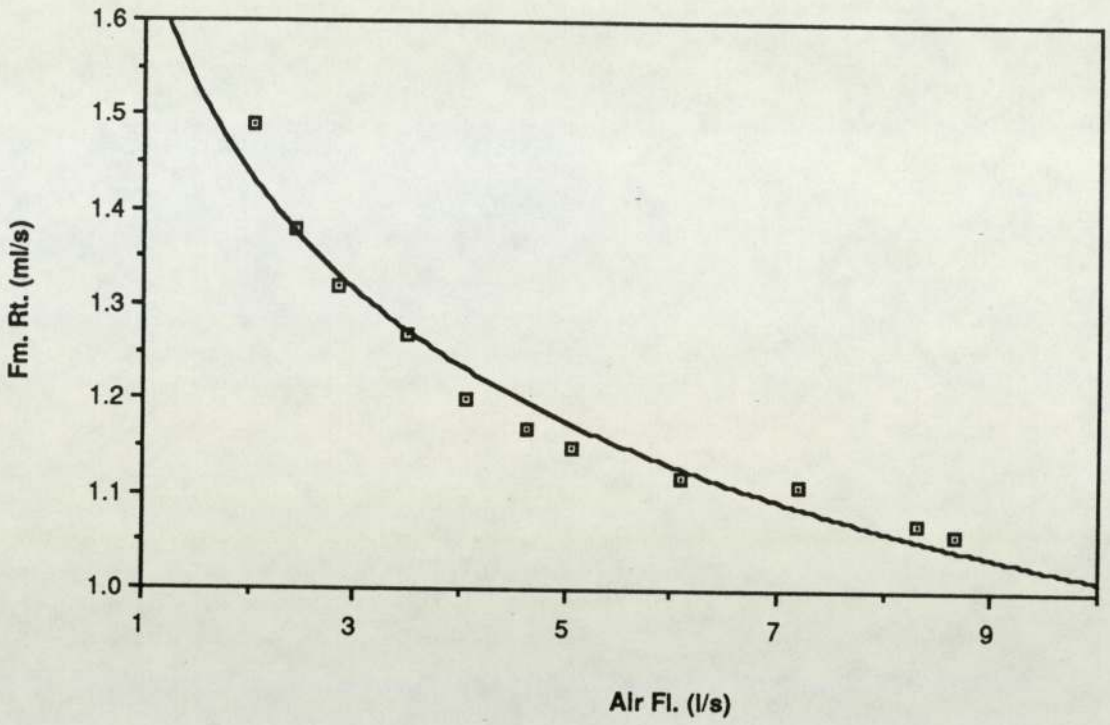

Figure 5.3.a.. film flow versus air flow rate

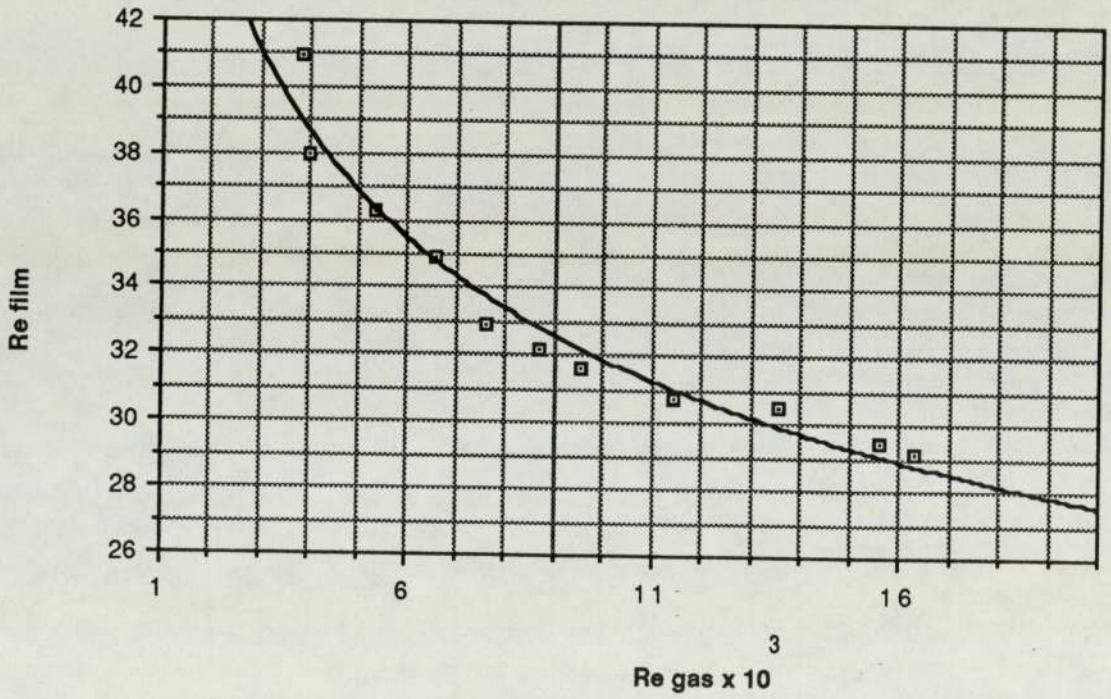

Figure 5.3.b.. film flow Re / air flow Re correlation

CHAPTER 6.

DISCUSSI0N.

6. General.

The literature survey has demonstrated that up to 50% of the total petrol which is carburetted into the cylinders of a spark ignition engine may be streaming on the walls of the inlet manifold rather than air and petrol vapour mixture, or being carried as small droplets entrained in the core flow. The wall film hydrocarbons comprise the 'heavy' aromatic components of the original petrol, with an average specific gravity of 0.86. The size of droplets into which the liquid breaks up will have a vital influence on the power output and emissions from the engine and on cycle to cycle variations in cylinder performance, yet no research has been reported which investigates the spectrum of droplet sizes or their dependence on operating conditions. The present work was undertaken to assess the contribution which the wall film might make to unburned hydrocarbon emissions from spark ignition engines and determine the distribution of droplet sizes formed as the film passes through the inlet valve.

6.1 Literature survey.

The literature survey revealled that most investigations of two phase flow relate to vertical transport with fully developed flow and that the annular flow met in the inlet manifold of a petrol engine is only one of a wider range of two phase flows situations which might arise.

The main conclusion to emerge from the small number of papers dealing with horizontal flow was that empirical relationships deduced from the correlation of vertical flow test results could be applied successfully to horizontal flows only when the Reynolds number of the core flow exceeds 5000 and the gas/liquid volume flow ratio is greater than 2000. The establishment of fully developed annular flow is recognised as requiring a pipe length of up to 200 diameters. This means that the expressions for pressure drop and the rates of entrainment and deposition of liquid droplets which are accepted in the literature will not apply in an inlet manifold, which is typically no more than 10 pipe diameters in length downstream from the carburettor with up to three 90° bends in the flow path, including the geometry of the inlet valve port.

Nevertheless, the computer model of carburation by Finlay and Boam gives a useful indication of the relative proportions of the mixture which will enter the engine as air/vapour mixture, entrained droplets or liquid film. What it does not attempt to predict is the size distribution of droplets entering the cylinder after passage through the inlet valve, nor has it made any allowance for the effect of bends in the manifold.

The evidence of Peters and Quader or of Mizutani and Nakajima clearly shows the important effect of droplets of liquid fuel on cylinder performance through improving combustion characteristics, while the predictions and experimental results of Hasson provide a clear explanation for the effect of large droplets on emissions and the

same author attributes cyclic dispersion to the irregular break up of the wall film.

The literature contains no direct evidence to link cycle to cycle variations in cylinder performance with the droplets formed from the wall film and both the size distribution of these droplets and the cycle to cycle consistency of that distribution remain important unknowns preventing a fuller understanding of the performance and emission characteristics of engines.

6.2. Flow visualisation tests.

6.2.1. Open discharge tests.

6.2.1.1. Open pipe discharge.

The main objective of the visualisation tests was to obtain evidence of the nature of two phase flows within the inlet manifold and of the manner in which the wall film broke into droplets as it left the valve port. Despite the steady flow nature of these tests the results were indicative of certain aspects of the later findings. The low level of visible droplet entrainment from the wall film was verified later, in the tests where droplet sizes were measured (see section 6.3).

The attempted correlation of the flow and pressure drop results obtained during these early tests showed a logarithmic dependence of the Martinelli parameter on the corresponding Wicks and Duckler parameter. Fig. 5.3 shows the effect of droplet entrainment from the walls, indicating that entrainment increases with Reynolds number but at a rate which decreases logarithmically. The close correlation

of these results is of little general value because it relates only to the fixed geometry of the pipework used in the tests. However the findings are in agreement with those of earlier workers, such as Alexander and Coldren.

In the very late stages of this research a model for entrainment by Azbel and Liapis [62] was found. These authors applied the Navier-Stokes and continuity equations to both phases and obtained a dimensionless correlation using similarity techniques. They demonstrated that their solution was capable of correlating their own experimental results. An entrainment example was calculated using their method and compared with another model of entrainment originally by Paleev and Flippovich [63], discussed by Hewitt and Hall Taylor [47]. The comparison produced encouraging results. Details of the two models are in Appendix 3. A new correlation line for petrol and air was assumed to lie between curves for the alcohol/air and water/air mixtures , fig. A3.1, and an eqation for the petrol film is suggested in terms of the parameters used by these authors. In the present situation this correlation suggests that approximately 40% of the petrol will be entrained, a figure which compares well with the values obtained by Finlay et al. in their carburation model.

6.2.1.2. Fixed valve at exit.

The use of a fixed valve at exit from the pipe system and the cylinder head showed that small sized droplets were formed only when there was a high rate of shear between the wall film and core flow, as occurred when low valve openings were employed. These tests also

indicated the possibility that large droplets will be formed and enter the engine during the part of the induction stroke when the valve is fully open. The way in which very large droplets were able to form and remain attached to the underside of the cylinder head is attributed to the steady flow nature of the experiment. In those tests where the valve was actuated in the normal way the formation of such large droplets took place over several cycles of valve operation (see 6.3) and cannot represent what might happen in an engine cylinder, where any liquid which flows across the valve seat and remains attached to the underside of the cylinder head will get evaporated off during the working stroke.

The direction of liquid flow out of the valve port with the valve fixed in position was shown to depend on the mass ratio of gas to liquid and on the valve lift. As stated above, small droplets were formed at low valve lift when a high rate of shear existed between the fluid phases at the valve throat. In this situation the droplets were discharged almost uniformly in a conical pattern, but as the valve lift was increased so the droplet stream was discharged closely in a single direction.

6.2.2. Closed discharge tests.

Many of the observations made in section 6.2.1 apply to the tests conducted with a transparent cylinder barrel attached to the cylinder head. The general behaviour of the steady two phase flow in the manifold was unchanged and the discharge of gas and liquid from the

valve port behaved no differently at corresponding conditions.

The presence of the cylinder wall caused the larged droplets formed at the valve port to break up further upon impact with the wall. Whether the presence of a piston reciprocating in the cylinder and moving away from the cylinder head as the droplets were discharged would have changed this situation would depend on the relative velocities of the piston and the droplet stream. Individual droplets cannot be seen in the still photograph taken from the video film, since the frame speed of the video camera is too low to capture the image of a rapidly moving droplet. No attempt was made to measure the droplet velocity, so it cannot be said whether droplets might impinge on the piston crown.

The main droplet stream was observed to leave in a direction which did not vary greatly with conditions, except at low valve openings, and it was this direction which was chosen when the location of viewing ports was selected in the design of final test equipment.

6.3. Steady flow roll wave shearing.

As stated in chapter 5 the test equipment used to conduct the pulsating flow tests was first used to try to measure the size of droplets produce by roll wave shearing in steady flow conditions. The measurements were made with the laser beam traversing the stream at exit from the straight length of transparent pipe and the wall film liquid was injected from a single hypodermic tube lying on the inner

surface at the bottom of the pipe. The available range of air and liquid flow rates enabled all the normal flow situations observed in the visualisation tests to be represented. By a suitable combination of flows it was possible to achieve distribution of the film around the complete periphery or to obtain a liquid stream in the bottom of the pipe to represent the conditions which had been observed at exit from the 90° bend of the cylinder head valve port.

Obscuration data for the particle sizer in these tests indicated that no droplets were actually being entrained.

6.4. Pulsating flow tests.

6.4.1. Disc valve tests.

The arrangement of the test apparatus was described in chapter 5. The inlet to the blower supplying air to the acryllic pipe was covered by a rotating disc in one quadrant of which a kidney-shaped hole was cut so that air flowed through the system in much the same pulsating manner as found in the engine inlet manifold. Tests were carried out over the range of airflow Reynolds number and air/film mass flow ratios which is met in the inlet manifold of an engine. It was found that the rotational frequency of the disc had little effect on air flow rate from the blower and this was controlled by adjustment of the blower discharge valve. Some roll wave shearing was observed. The laser beam was adjusted to pass through the entrained droplets while the remainder of the film dribbled vertically down from the open exit of the horizontal pipe.

Obscuration data for the particle sizer in these tests showed that very few droplets were being entrained. Operation of the sizer at these levels of signal is not recommended and reference has already been made in chapter 5 to the checks which were carried out using fine silica sand and glass beads at similar obscuration levels to ensure that the particle sizer analysis was giving credible results. In this situation comparison with the solid particle results showed that analysis by the log normal distribution gave more representative results than the RosinRammler distribution. Repetition of the readings showed that it was essential to clean the lenses thoroughly to eliminate erratic results.

Figs. 6.1a to 6.1i show the effect of air/film mass ratio on droplet size for a range of Reynolds numbe, indicating that there is a steady reduction as the proportion of liquid is reduced but little change with increasing frequency of disc rotation, which corresponds to the frequency of pulsations in the flow. The results from the complete series of tests using the rotating disc are shown in fig. 6.2. These tests were carried out over a wide range of Reynolds number, valve frequency and air/film mass ratio and when lines of approximately constant air/film ratio are drawn it is clear that this parameter has great influence on the size of droplets produced, particularly at higher Reynolds numbers. In general it may be said that droplet size reduces as air/film mass ratio and Reynolds number increase. It has already been observed that disc frequency has little effect on air flow: it is apparent that it had little effect on the size of droplets.

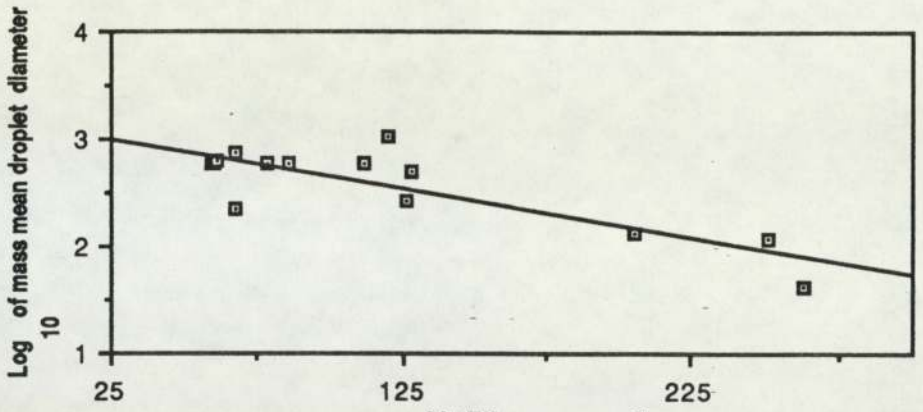

Figure 6.1.a., 320 r.p.m.

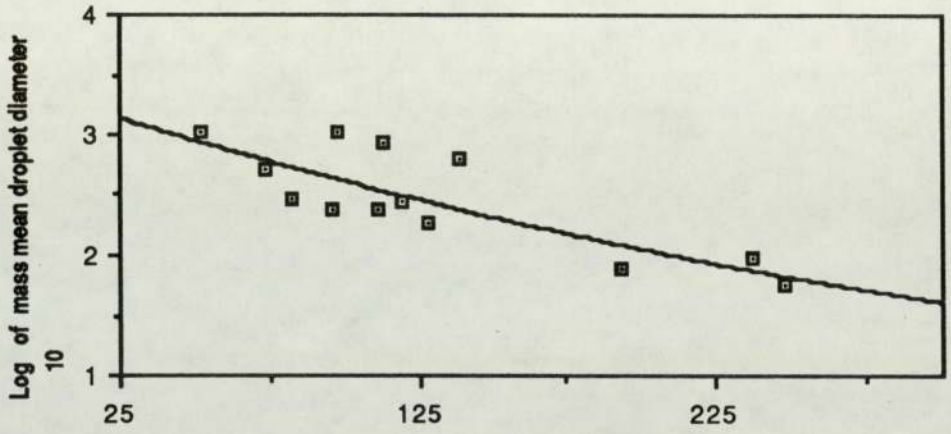

Figure 6.1.b., 350 r.p.m.

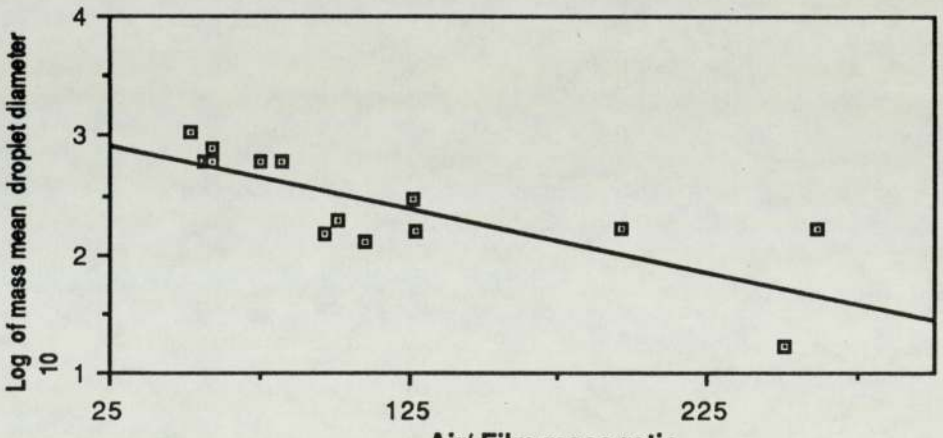

Figure 6.1.c., 400 r.p.m.

Figure 6.1., Droplet entrainment from the wall film in pulsating flow, variation of mass mean diameter with air film mass ratio

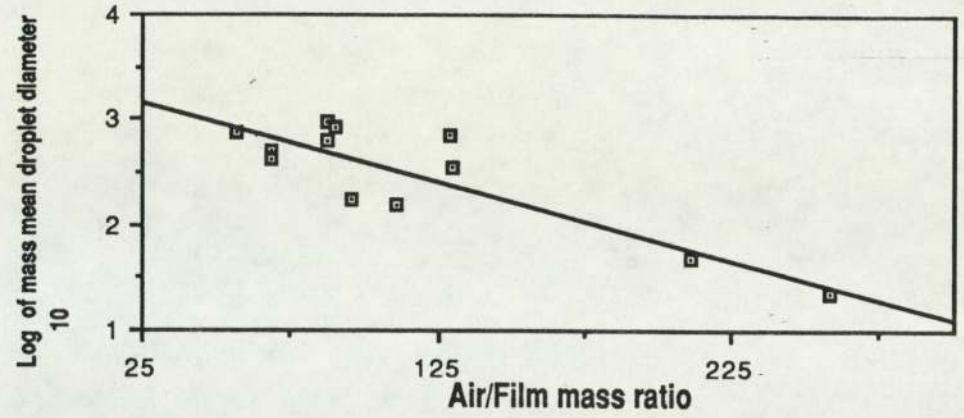

Figure 6.1.c., 480 r.p.m.

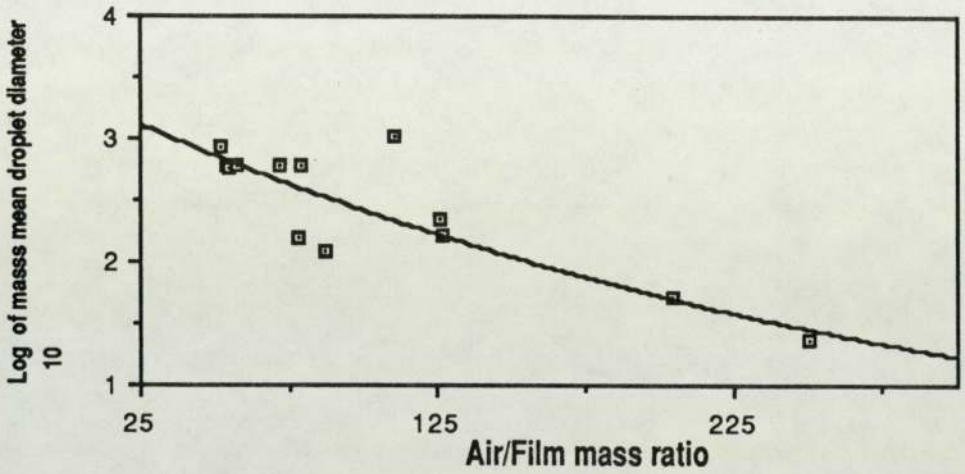

Figure 6.1.e., 600 r.p.m.

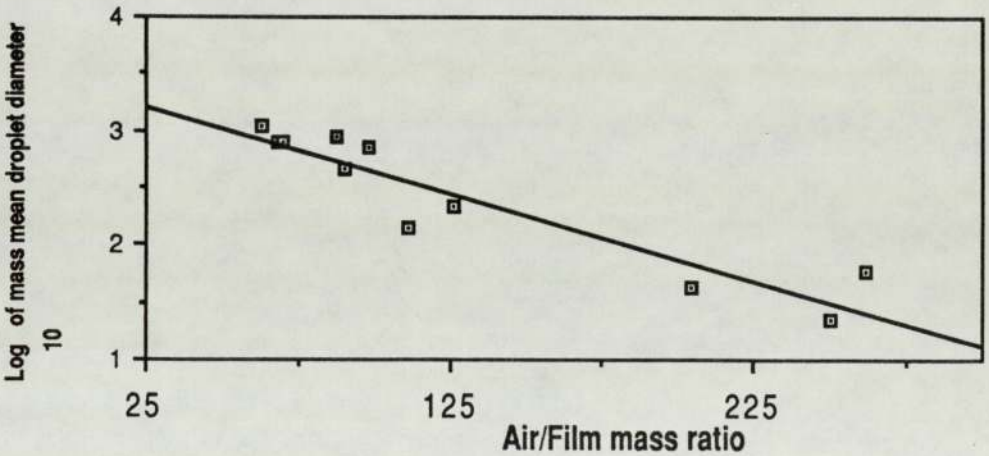

Figure 6.1.f., 700 r.p.m.

Figure 6.1., Droplet entrainment from the wall film in pulsating flow, variation of mass mean diameter with air film mass ratio

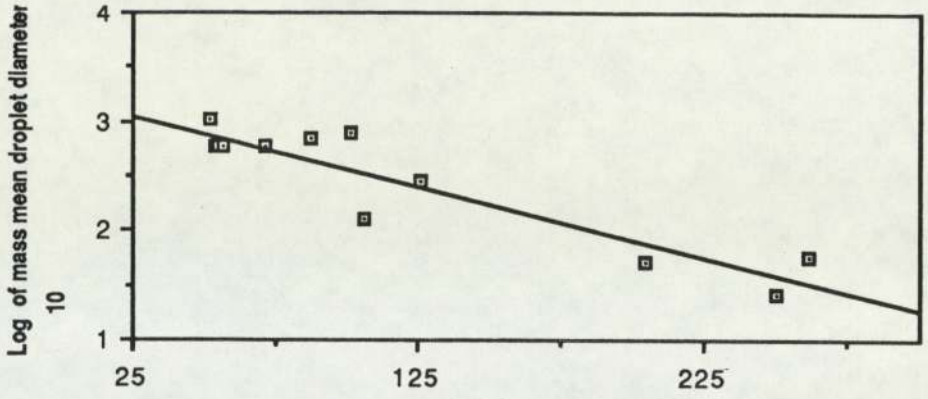

Figure 6.1.g., 860 r.p.m.

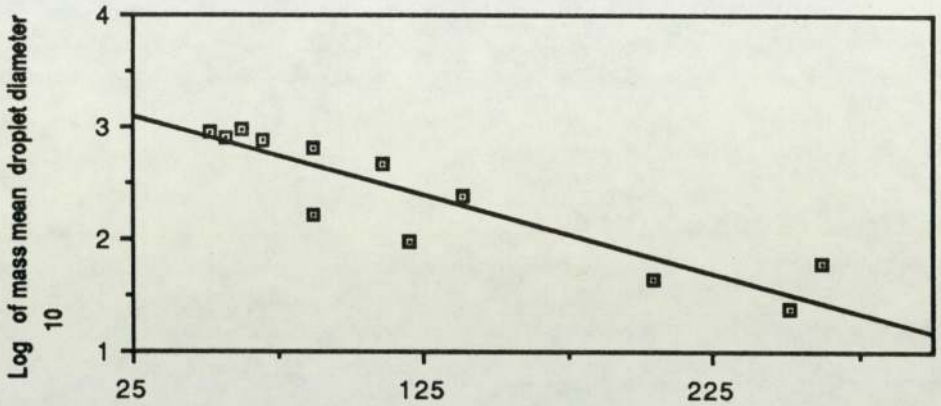

Figure 6.1.h., 960 r.p.m.

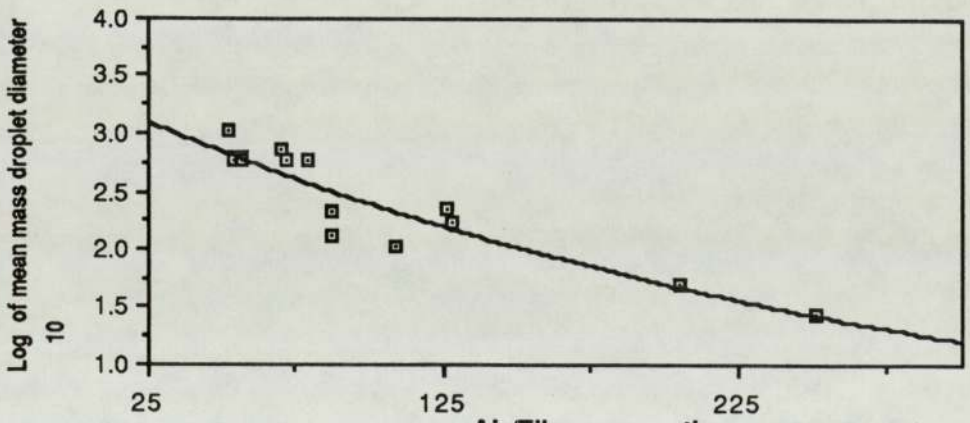

Figure 6.1.i., 1030 r.p.m.

Figure 6.1., Droplet entrainment from the wall film in pulsating flow, variation of mass mean diameter with air film mass ratio

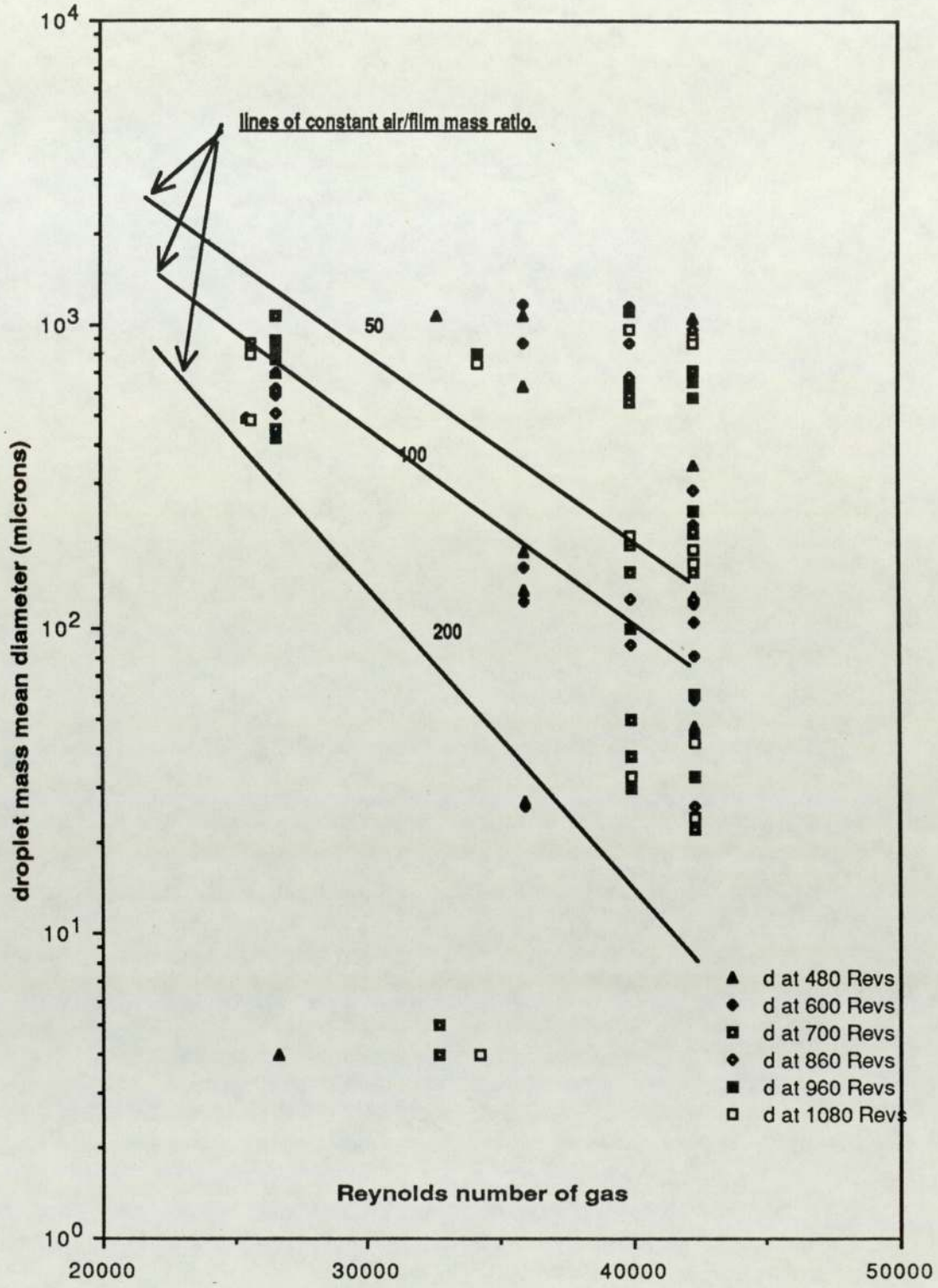

Figure 6.2., droplet size variation with pulsating flow.

(all results of droplets entrained from wall film)

6.4.2. Inlet valve tests.

The results from the tests which were conducted using the system described in 5.3.2 are shown in fig. 6.3a to 6.3i and plates 6.1 and 6.2a to 6.2h. The plates show very clearly that the high rates of shear acting on the liquid during unsteady flow through the inlet valve produced high concentrations of droplets, many more than were produced by roll wave shearing. Obscuration levels for signals analysed by the particle sizer were always within the acceptable range.

In these tests the airflow was measured using a viscous flow element and the rate was again controlled by use of the blower discharge valve. The airflow rate was not greatly influenced by the frequency of operation of the inlet valve, although a slight reduction in flow was apparent when the valve oscillated at the frequency which excited weak pressure waves in the blower and pipework.

At a fixed valve frequency, for which typical results are shown in figs. 6.3e and 6.3f, the particle sizer results indicate that there is a small reduction in Sauter mean diameter of droplets as the air to liquid mass ratio is increased. Such a result would be anticipated, since the shear forces will remain of similar magnitude, due to the fixed airflow rate, while the liquid film becomes thinner and, in accordance with the theories of droplet formation which have been reviewed, smaller diameter droplets form from the sheets and ligaments of liquid on which these forces act.

The spread of results about the mean lines shown in figs.6.3a to 6.3i gives an indication of the accuracy and repeatability of the tests. The use of a semi-logarithmic plot follows the practice of previous investigators in the field of two phase flow. In a number of cases it is apparent that the results are very repeatable, yet there are instances where the Sauter mean diameter measured at similar air/film flow rates varies from approximately 75μm to 150 μm.

The occurrence of these data would be more readily understood at higher rates of air/film flow, where it was found that the discharge of droplets was visibly and audibly inconsistent from one cycle to the next. Consequently it was necessary to use a long scan interval to obtain average readings from the particle sizer. The visualisation tests had shown that there is no continuous film or flow of rivulets at low rates of liquid flow and consequently there are occasions when there is no liquid in the region of the inlet valve at the time when it opens. A similar situation was apparent at the valve frequency which corresponded to the natural frequency of waves travelling in the system, referred to above, but this was approximately 400 rev/min and the discrepancies in the results shown in fig. 6.3b are not especially marked.

The above observation may be the key to understanding the origin of cycle to cycle variation in cylinder performance. Fig. 6.4, taken from an internal report, shows the way in which the variation in cylinder pressure was affected when the wall film was removed immediately downstream from the carburettor of a four cylinder engine. If the

actual quantity of wall film entering the cylinder varies from one cycle to the next, or if the size spectrum of droplets into which the film ruptures varies from cycle to cycle, then it is evident that the cylinder performance will change. In the present tests the varying quantities of film arriving at the inlet valve during operation in high air/film flow conditions led to the discharge of a varying mass of droplets from cycle to cycle, but the method of particle sizer analysis which was employed gave no indication of the consistency of the size spectrum since the sample was scanned over a large number of cycles.

The complete set of results for unsteady flow through the operating inlet valve is presented in fig. 6.5, where the Sauter mean diameter of the droplets is plotted as a function of the air/film mass flow ratio. Attempts to superimpose lines of constant Reynolds number were abandoned when it was shown that this parameter has little significance. The equally negligible effect of valve operating frequency has already been discussed in relation to figs. 1a to 6.1i. The effect of air/film mass ratio is more important, but a six-fold increase in the value of this parameter produces only a 30% reduction in the Sauter mean diameter of droplets over the full range of tests conducted with the induction valve mechanism in operation. These results indicate that the Sauter mean diameter will be greatest in conditions which produce the largest quantity of wall film.

If it is assumed that use of the choke in cold starting leads to an overall air/fuel mass ratio of 10/1 then the 50% of total petrol in the

wall film found by Nightingale and Tsatsame corresponds to an air/film mass ratio of 20/1. This is lower than the minimum value used in the present tests, but extrapolation of the least squares mean line of fig 6.5 would indicate that the Sauter mean diameter of droplets in these conditions would be approximately 150μm. In half throttle operation the wall film quantity has been reported as 25% of total petrol. Assuming that the engine is running with an air/fuel mass ratio of 16/1 in these conditions then the air/film mass ratio would be 64/1, which is still less than the minimum of the present test range.

6.5. Droplet size distribution.

Observation of the droplets streaming through the path of the laser beam, which illuminated them sufficiently to be visible to the naked eye, showed that there were substantial numbers of large drops present in the stream. The series of photographs taken with flash illumination against a dark background confirmed the existence of these drops and also showed how the size distribution varied as the valve opening increased. These photographs are shown in plates 6.1a to 6.1h and it is apparent that in the early stages of valve opening the drops which are formed are very small. As the valve opening increases so the size of droplets increases until, with the valve in the fully open position, the indication is that droplets are being formed principally by the action of roll wave shearing within the manifold. Thus the spectrum of droplets changes continually with the motion of the valve and the long term average which the particle

sizer recorded over 0.3 to 0.5 minutes will be the true average for any one cycle of operation.

The photographs referred to above were taken to verify the existence of large drops, since it is possible for the evaporation of liquid from a droplet surface to produce a surrounding cloud of vapour which diffracts the laser beam to produce a false image on the receiver of the particle sizer, which the instrument interprets as caused by a larger drop.

6.5.1. Effect of the valve operating mechanism.

The valve was actuated by means of a Scotch yoke mechanism, which acts as an eccentric and therefore opens and closes the valve more slowly than would the cam of an normal engine inlet valve. It may be expected that the droplet distribution would be similar for a given valve opening and air/film mass ratio, but the very rapid acceleration which is characteristic of engine valves would reduce the proportion of time for which small flow cross sections exist in the complete valve motion cycle. The photographic evidence suggests that a correspondingly higher proportion of the cycle time would be in the conditions where larger droplets were formed by the reduced shearing effects at greater valve openings. It is therefore possible that the normal engine valve mechanism will cause an even less desirable spectrum of droplets to be formed from the wall film liquid.

6.6. Effect of wall film droplets on unburned hydrocarbon emissions.

Use of the model independent analysis to obtain the distribution of droplet diameters showed that the large droplets accounted for a high proportion of the total mass and that the overall size distribution was bimodal. This implies that if either the log normal distribution or the Rosin Rammler distribution is assumed as the basis for the analysis of the diffraction pattern then the mean value which is calculated will be larger than that which would be obtained from the model independent analysis. The consequence of this will be to suggest that a greater proportion of the wall film remains unburned than is actually the case.

The Sauter mean diameter values which are shown in fig. 6.5 are in the range from 100μm to 130 μm and the value which Hasson's predictions showed to be critical for complete combustion is only 35μm. If the evaporation and reaction rates of the droplets during the combustion stroke were known, then it would be possible to calculate the additional mass of unburned hydrocarbon vapours present in the exhaust from an engine.

Using the 'd^2' law for burnout time, discussed in chapter 3 it may be predicted that only 18% of the wall film liquid will be combusted. In cruising conditions, when perhaps only 1% of the petrol enters as wall film liquid, then some 0.8% of the total petrol mass will be emitted as unburned hydrocarbons. This has to be put in the context of a typical cruising air/fuel ratio of 16/1 and leads to the conclusion

that some 0.05% of the emissions will be unburned hydrocarbons coming from the wall film, ie. 500 parts per million. The situation will be markedly worse when greater proportions of the petrol enter from the wall film, as in cold start conditions or slow moving traffic.

The figure of 500 parts per million is typically quoted for engines operating in cruising conditions, yet in that case includes the discharge of unburned hydrocarbons from crevices and quench layers. Some part of the explanation for this discrepancy lies in the use of the log normal and Rosin Rammler distributions when analysing the results obtained from the Malvern particle sizer.

It should be recalled that the big droplets which were noted to form around the exit piping due to the Coanda effect (sticking to the wall), took many cycles to form and were only shed off when the action of gravity exceeded that of surface tension. They were neither catered for when measurement was carried out, nor in the estimation of the unburned hydrocarbon due to the film, because it is expected that such an effect woud not exist in a firing engine.

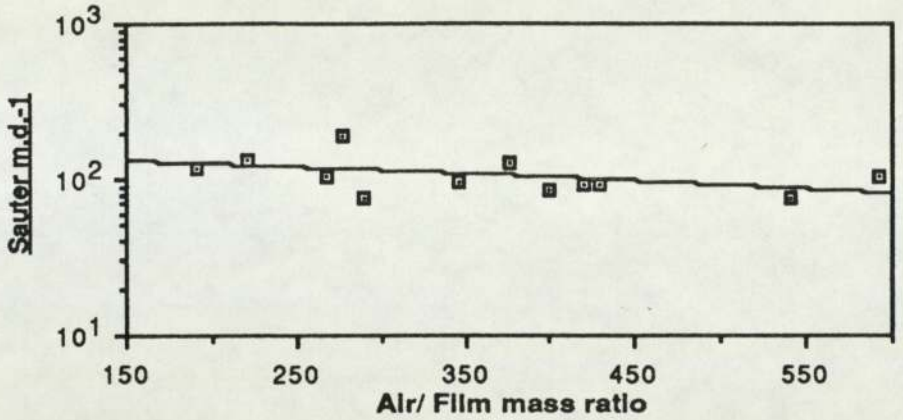

Figure 6.3.a., 90 rev./min.

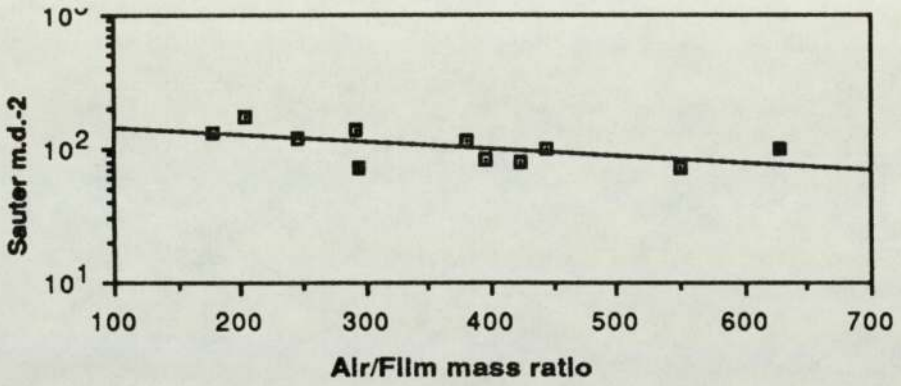

Figure 6.3.b., 400 rev./min.

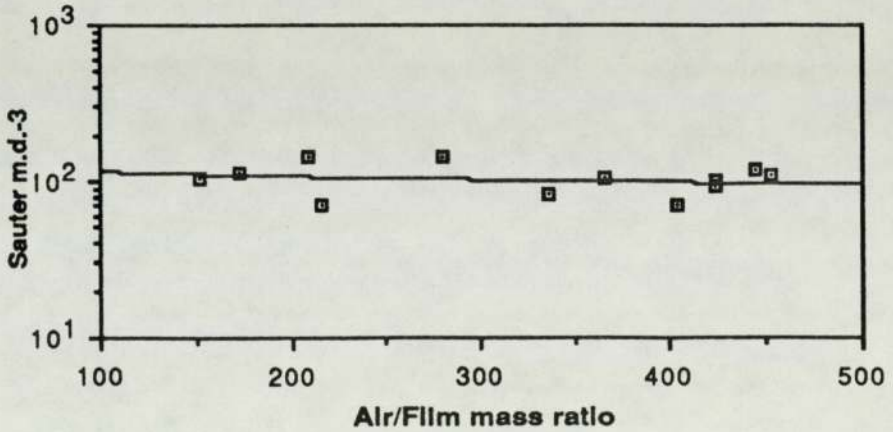

Figure 6.3.c., 490 revs./min.

Figure 6.3., Sauter mean diameter of droplets formed from the wall film by operation of the engine Inlet valve.
(variation with air/film mass ratio)

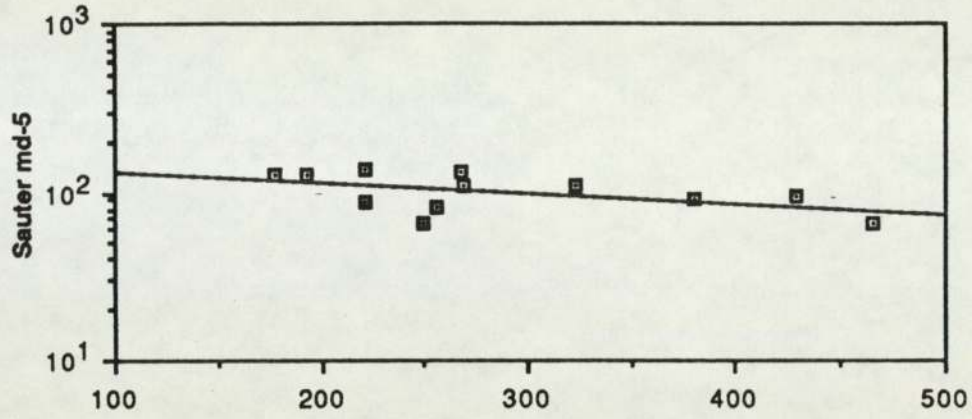

Figure 6.3.d., 510 revs./min.

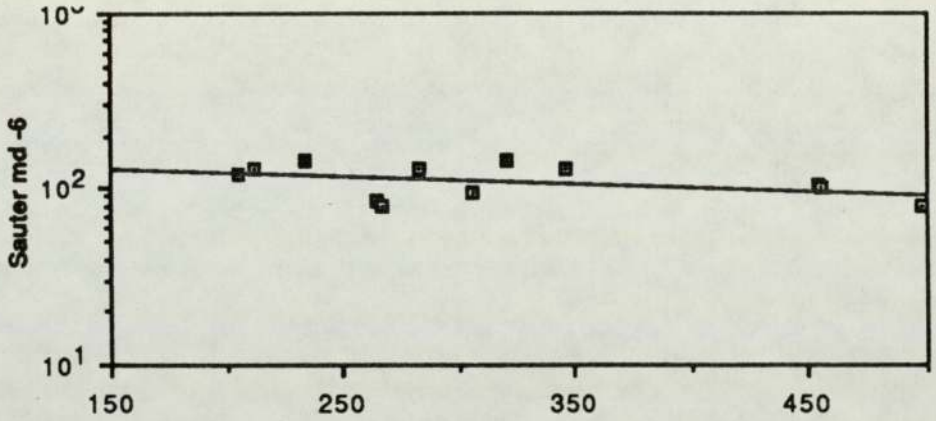

Figure 6.3.e., 740 revs./min

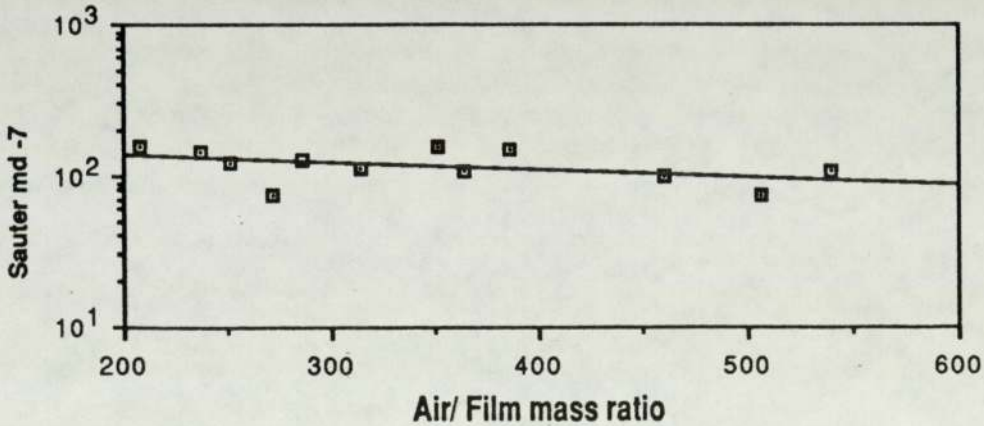

Figure 6.3.f., 875 revs./min.

Figure 6.3., sauter mean diameter of droplets formed from the wall film by operation of the engine inlet valve (variation with air/film mass ratio)

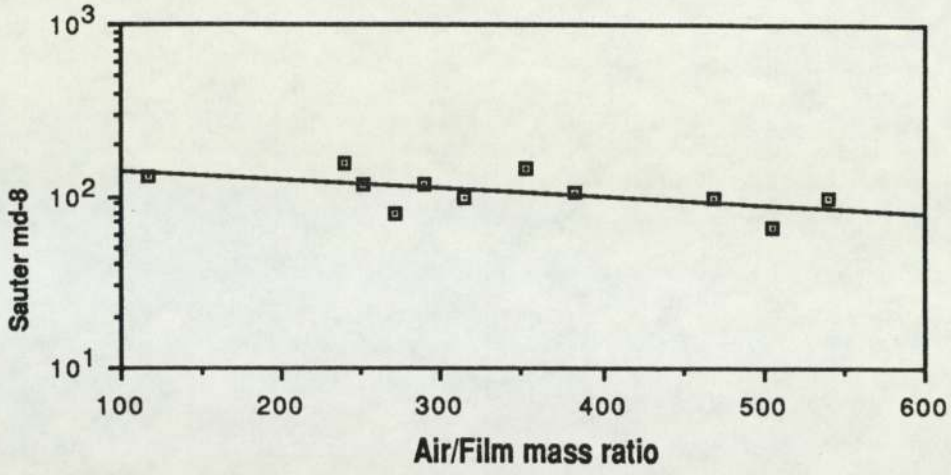

Figure 6.3.g., 960 revs./min.

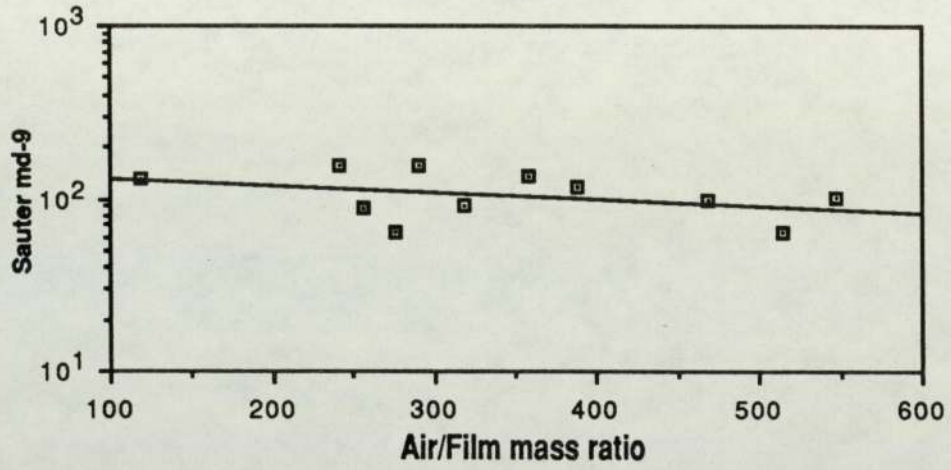

Figure 6.3.h., 1030 revs./min.

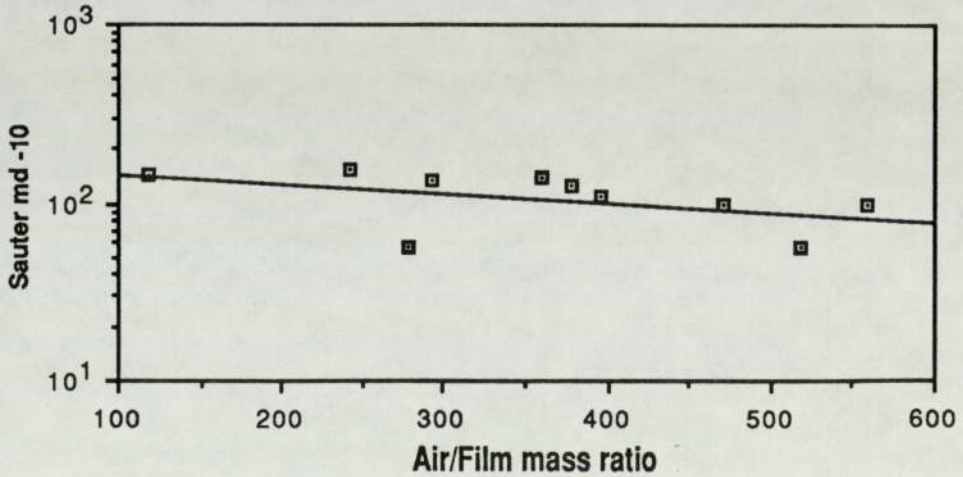

Figure 6.3.i., 1100 revs./min.

Figure 6.3., sauter mean diameter of droplets formed from the wall film by operation of the engine inlet valve (variation with air/film mass ratio)

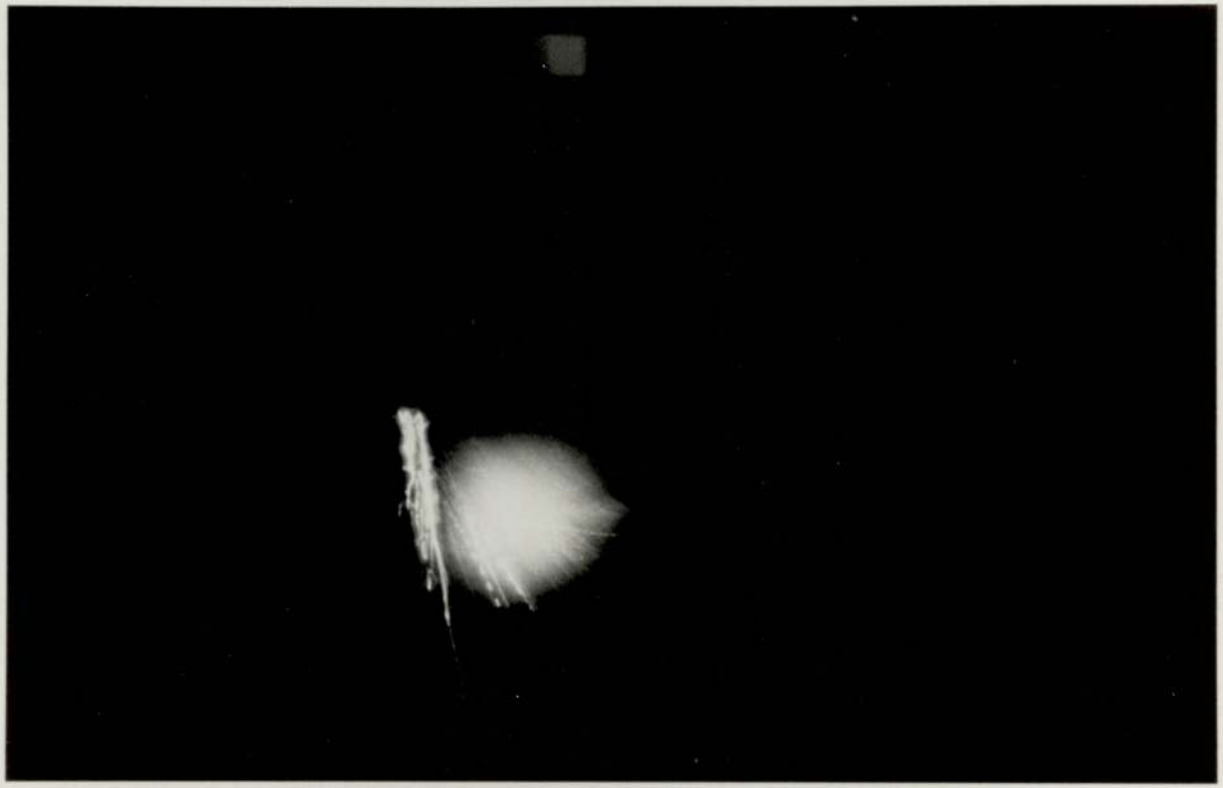

Pl. 6.1
Time Exposure showing Paths
of Droplets, illuminated by the
Laser Beam

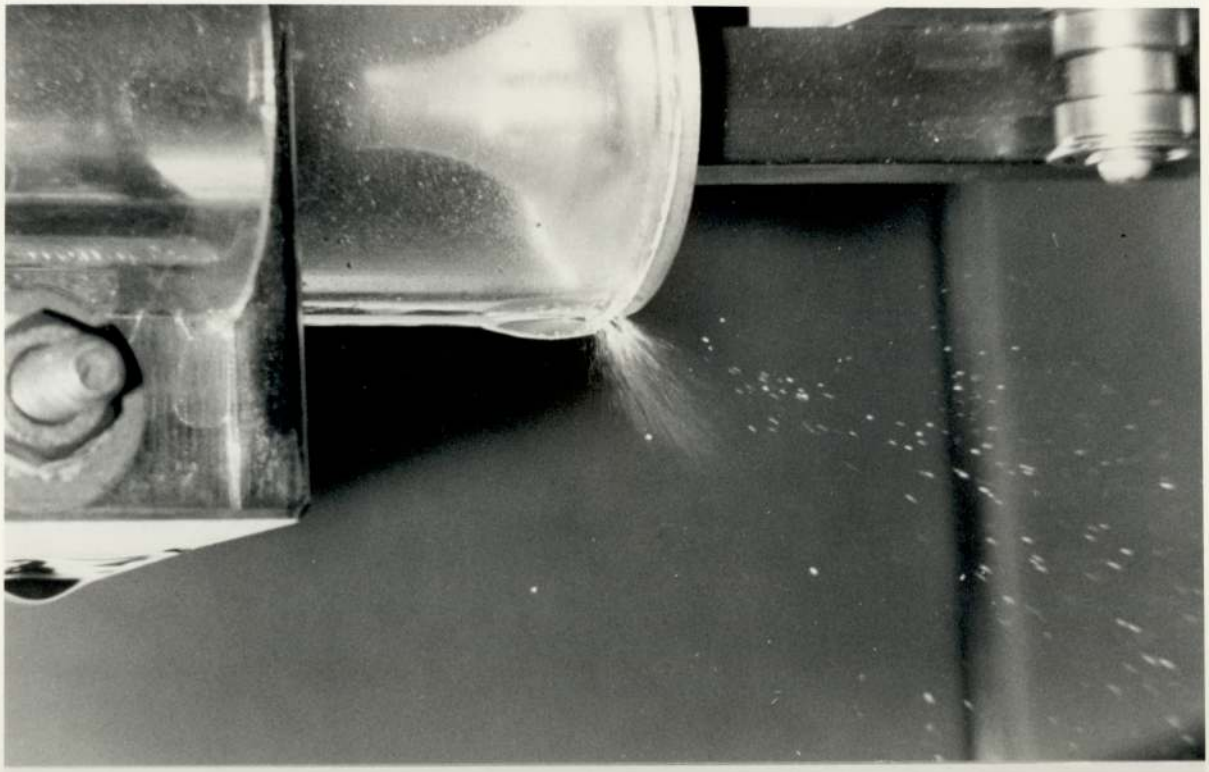

Pl. 6.2a.
Valve Lift Commences

Pl. 6.2b.
Valve Lift Continues.

Pl. 6.2c.
Valve nears Mid-Lift

Pl.6.2d.
Valve beyond Mid-Lift.

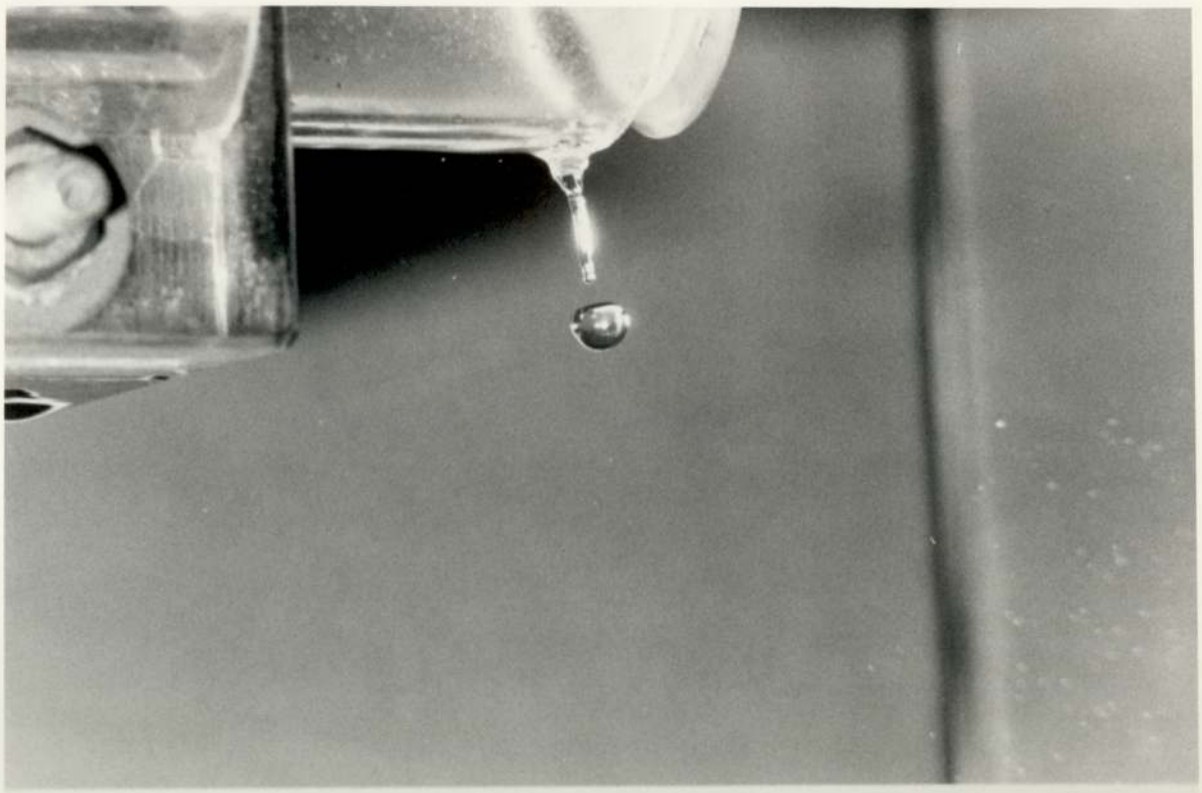

Pl. 6.2e.
Valve nears Fully Open.

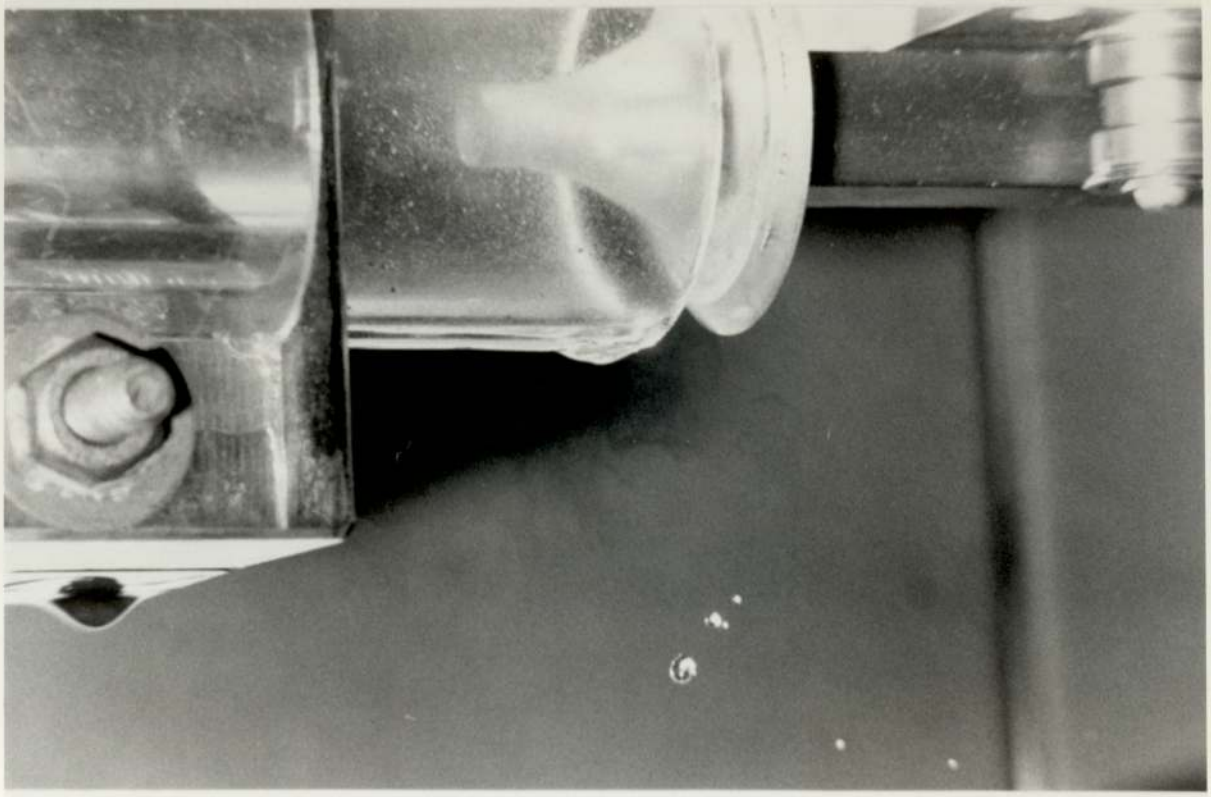

Pl. 6.2f.
Valve Fully Open.

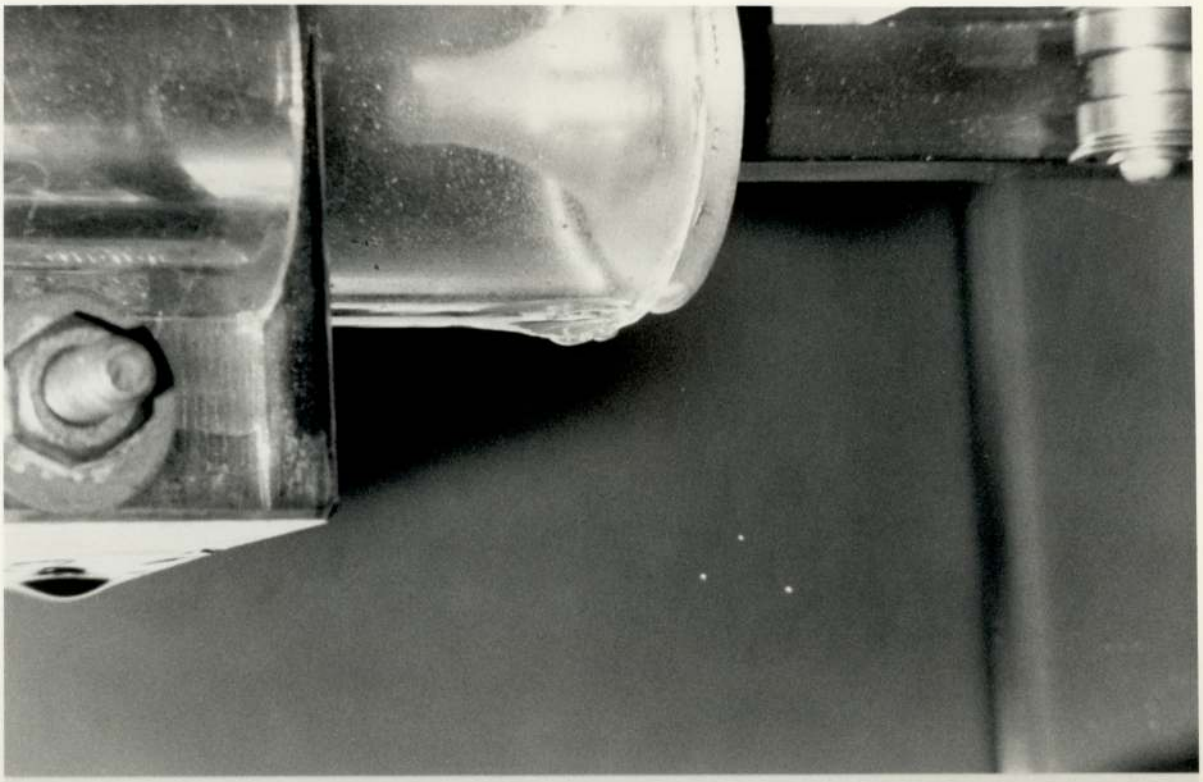

Pl. 6.2g.
Valve Approaching Closure.

Pl. 6.2h.
Valve Closure Imminent.

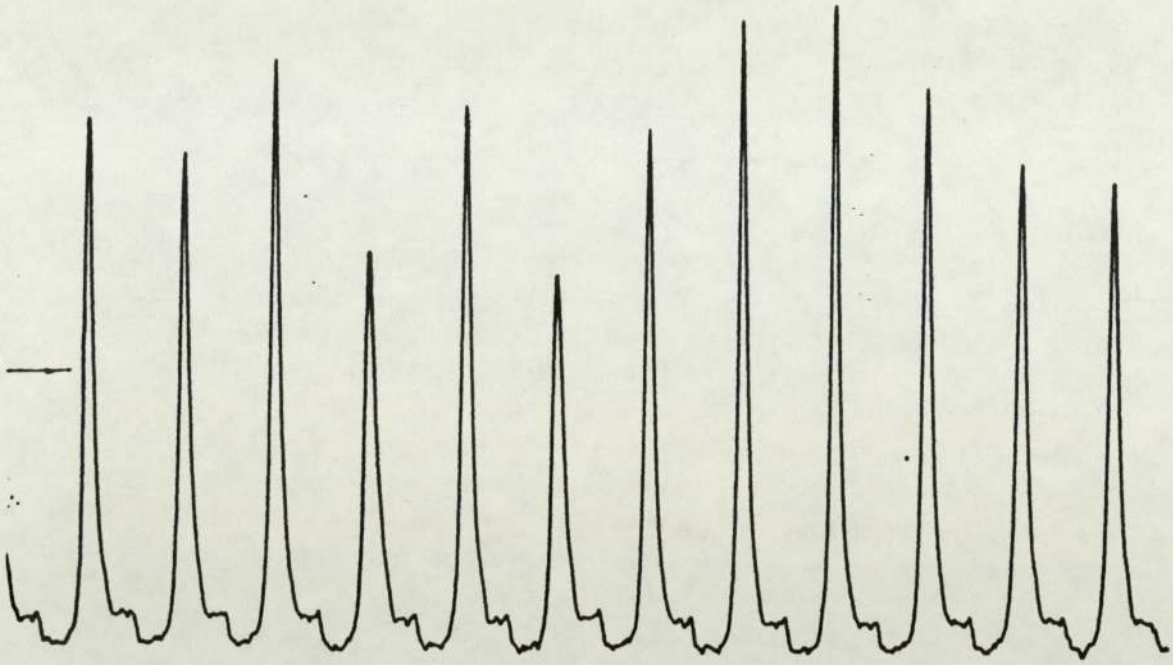

(a) 2000 rev/min, 3.9 kW -- normal carburetter

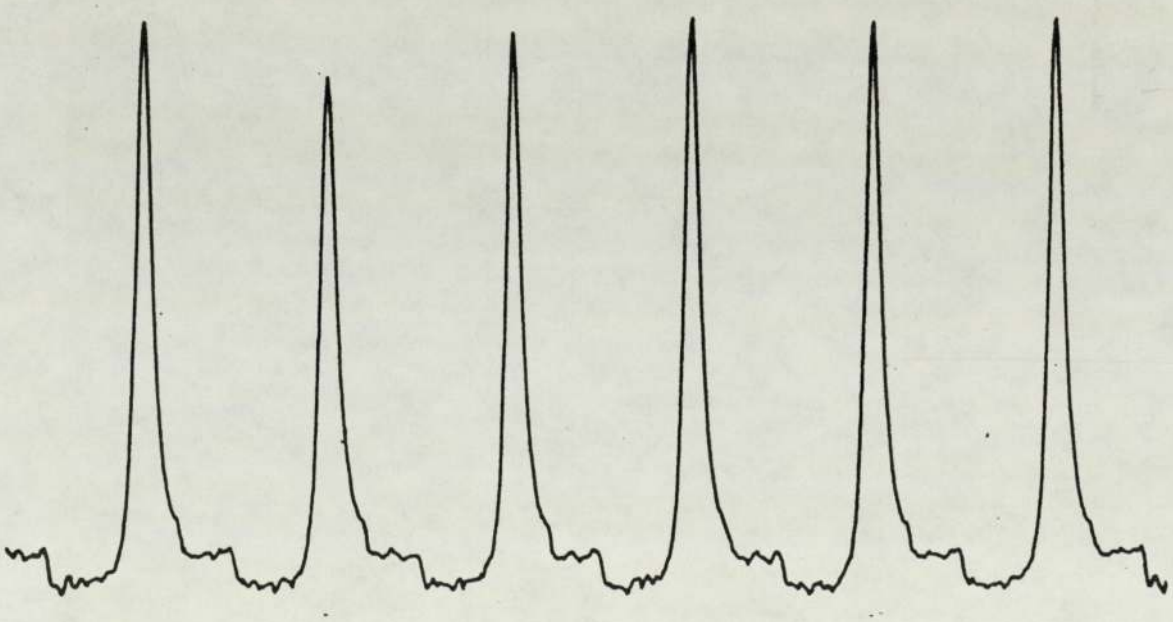

(b) 2000 rev/min, 3.9 kW -- separator gap 1 mm

Figure 6.4., Cyclic Dispersion of Cylinder Pressure

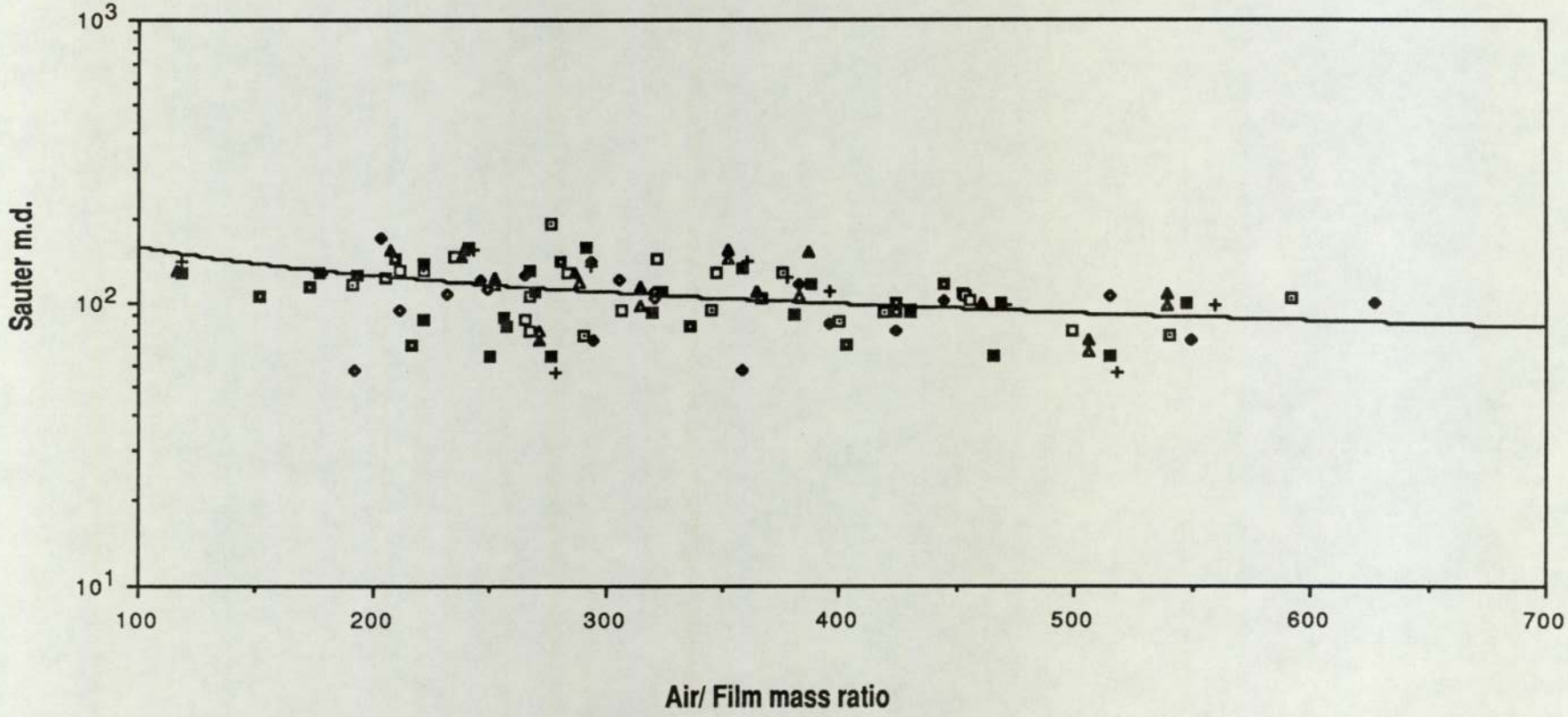

Figure 6.5., s.m.d. of droplets formed at the inlet valve.

(Variation with air/film mass ratio for all frequencies)

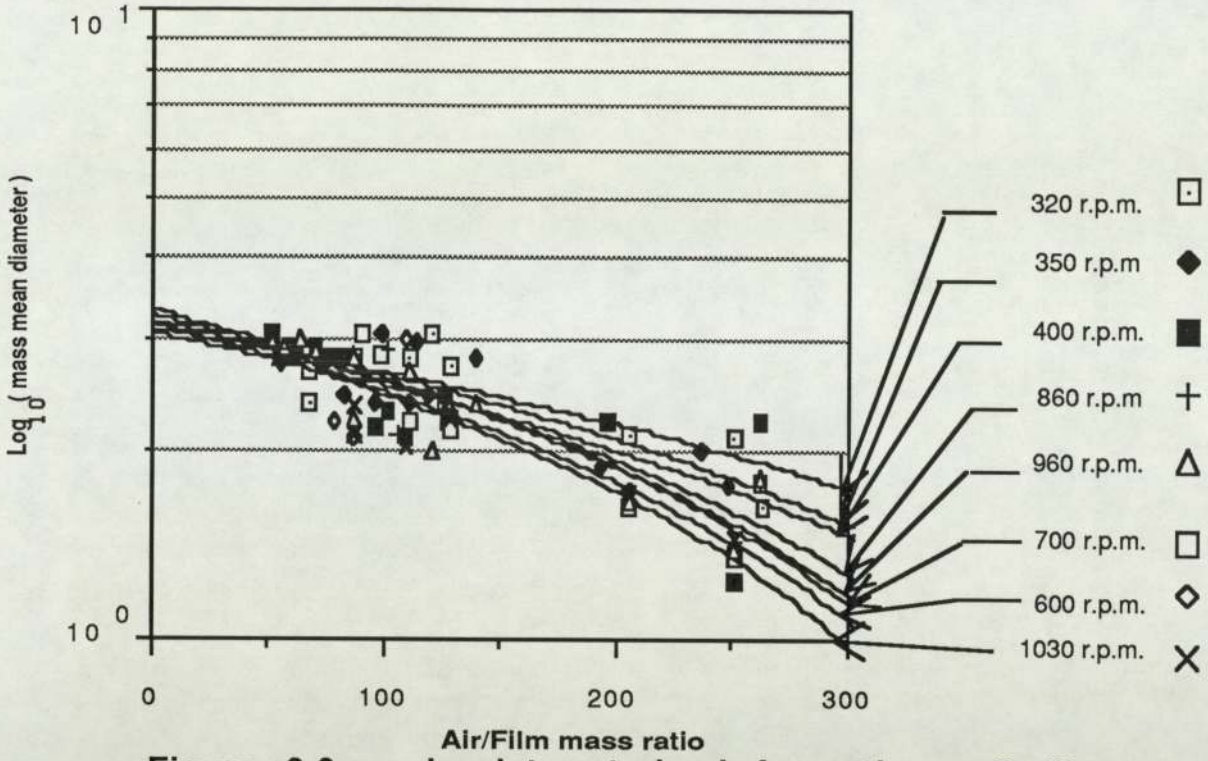

Figure 6.6.a., droplet entrained from the wall film in pulsating flow.

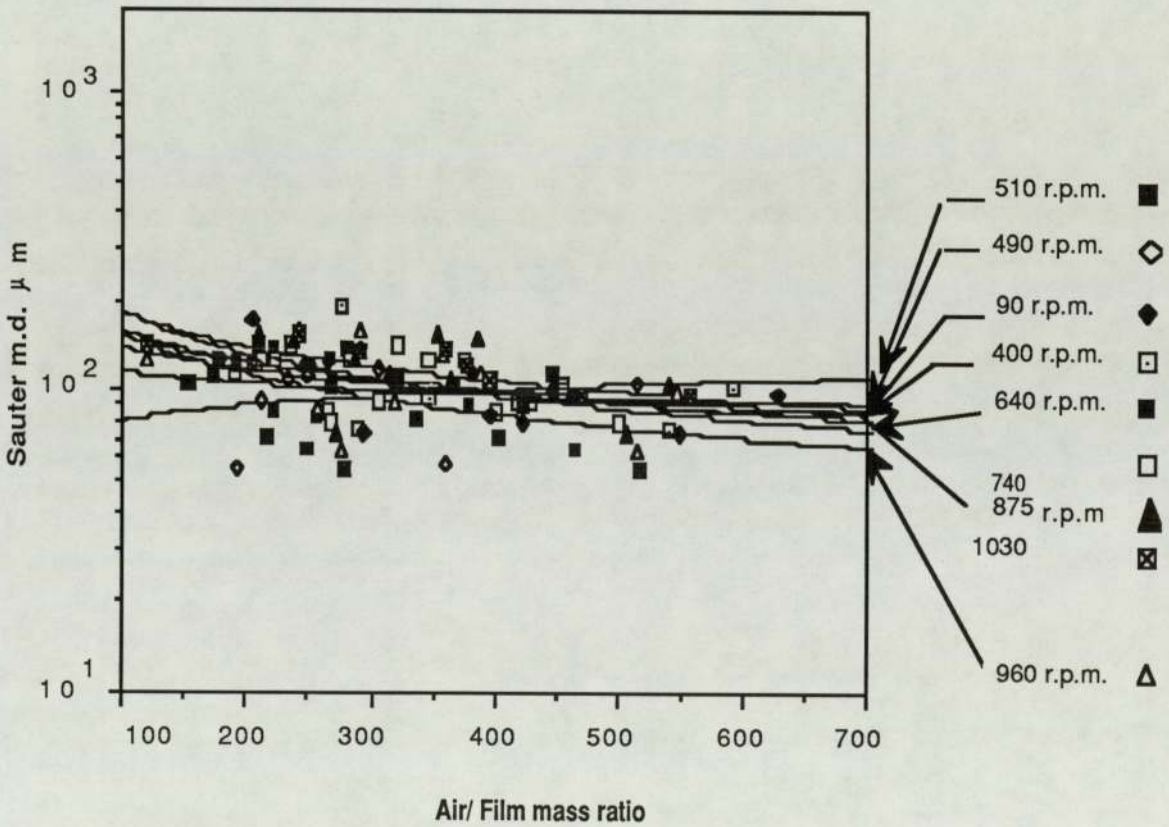

Figure 6.6.b., droplets formed at engine inlet valve.

Figure 6.6., comparison of entrained droplet and inlet valve droplet spectra.

CHAPTER 7

CONCLUSIONS AND SUGGESTIONS FOR FURTHER WORK

7.1 Conclusions.

1. The liquid wall film in the inlet manifold of a carburetted spark ignition engine is broken into a wide spectrum of droplets as is passes through the inlet valve port and into the cylinder.
2. The spectrum appears to change throughout the motion of the valve. Very small droplets are formed at low valve openings, due to the high shear forces between the core flow and the liquid, but the droplet size increases with valve lift. At full lift the formation of droplets might depend solely on roll wave shearing from the liquid surface. Flow pulsations alone did not cause significant droplet formation: only the shear flow at low openings of the valve throat.
3. The size of droplets is controlled principally by the mass ratio of core flow to film flow: neither core flow Reynolds number nor the frequency of valve operation showed any significant effect on the spectrum over the range of the tests carried out.
4. The Sauter mean diameter of droplets formed from the film varies between approximately 75 μm and 150 μm in the conditions which are known to exist in the typical manifold.
5. The literature indicates that droplets greater than 35μm diameter will not burn completely: the remaining heavy fractions of the petrol evaporating to form unburned hydrocarbon emissions. Using the 'd^2' law for burnout time it is estimated that a droplet spectrum with 100 μm Sauter mean diameter will

cause 500 parts per million unburned hydrocarbons to be formed from the wall film in normal cruising conditions, where the air/film mass ratio is known to be approximately 1600/1.

6. The phenomenon of two phase annular flow is too complex to yield analytical solutions. The literature contains adequate correlations for droplet entrainment and deposition in fully developed flow along straight ducts but this is only established after some 200 pipe diameters.
7. Entrainment increases with the core flow Reynolds number, but at a logarithmically decreasing rate in straight ducts: the presence of a smooth bend increases deposition; a mitre bend may cause significant re-entrainment.
8. The formation of very large droplets, due to the Coanda effect would not arise in a firing engine since their formation on the test rig developed over many cycles.

7.2. Suggestions for further work.

1. The range of tests should be repeated using the equipment which was designed during the present research programme to investigate the spectrum of droplets entering from a typical cylinder head with operating valve mechanism, discharging into a representative cylinder and with the flow induced under vacuum conditions.
2. The full potential of the Malvern particle sizer should be exploited to examine the development of the droplet discharge, using the pulsed scan facility to determine the relationship between valve opening and droplet spectrum.
3. Research should be undertaken to examine suitable means for ensuring that the wall film liquid is broken into droplets which are below the accepted maximum diameter capable of burnout in the spark ignition engine.
4. The tests should be repeated using a cam operated engine inlet valve to determine the extent to which the rapid acceleration of normal valve motion produces a larger mean droplet diameter.
5. An investigation should be undertaken to determine the extent to which wall film is formed in spark ignition engines using electronically controlled port injection systems.

APPENDIX 1

Examination of safety aspects.

A1 Introduction

The hazard of explosions to human beings and to material assets cannot be underrated. The hazards are aggravated since potentially explosive gas mixtures do not in general signal their imminent danger.

The main concern here is to study the concept of safety within the aims of this research and arrive at a safe design for the rig that will be used to cope with a fuel/air mixture.

Fires and explosions are very complex chemical reactions and it is no surprise that not all features are well understood. Sources of information are very scattered and some have proven difficult to locate. Yet fundamental knowledge is needed for the present case and the attempt made here is intended to bring about a safer approach when dealing with the fuel air mixture which will flow in the test rig designed to allow examination of the droplets formed when the wall film enters the engine cylinder.

Not all combustible gas mixtures are with air, they could be with pure oxygen, chlorine or hydrogen. If there is too little fuel the reaction will cease because insufficient heat is produced; there is a

minimum fuel concentration that will produce a self sustaining reaction under given condition. That concentration represents the lower flammable limit for a given fuel and oxidant. Compositions containing less fuel are non flammable. At higher fuel concentrations there is a minimum oxidant concentration under given conditions that will produce a marginal self sustaining reaction. The concentration represents the upper flammable limit for a given chemical composition of fuel and oxidant. Compositions containing less oxidants are non flammable.

All gas compositions between the lower and upper limits are readily ignited. The energy produced by the combustion reaction is minimum at the limits and proceeds with increasing magnitude to the maximum energy at the stoichiometric composition at which reaction is ideally complete.

The rate at which a flame propagates through an inflammable mixture depends on a number of factors such as the pressure, temperature, composition, conductivity, intensity of heat generated and type of event that caused the reaction.

A1.1. Literature.

In an experiment carried by Stull [64] on a known composition of reactants in a gas mixture, placed in a vessel at a known temperature and pressure subjected to a spark and observed for

reaction (a reaction is normally identified by the production of light, heat, often sound and a chemical analysis of the product gas) a series of measurements carried out on methane/air mixtures at different initial temperature and pressure produced the data shown on fig. A1.1 . The relation between flammability and non flammability is identified by the solid circles. The widening of the flammable range with temperature is very distinct. The flammability limit shrinks to zero at:

1 125 mm of mercury and 0 C.

2 110 mm of mercury at 250 C.

3 90 mm of mercury at 500 C.

These measurements will vary within one or two percent from one investigator to another because of the uncertainty of composition analysis.

A1.2. Burning velocity:

The flammability limits at atmospheric temperature are normally given as volume percentage at atmospheric temperature and pressure in the gas/air mixture. The explosive range is the range at which an ignition source can initiate a self sustaining reaction under these conditions.

The burning velocity is the velocity of the propagation of the flame front with respect to the unburnt gases. If the propagation rate is less than the speed of sound in air (subsonic) the flame is called a

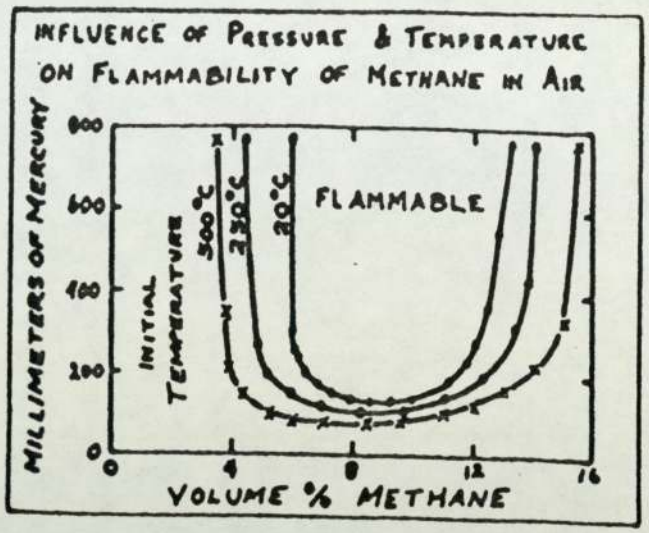

Figure A.1.1, influence of temperature and pressure .

on flammability of gas/ air mixtures

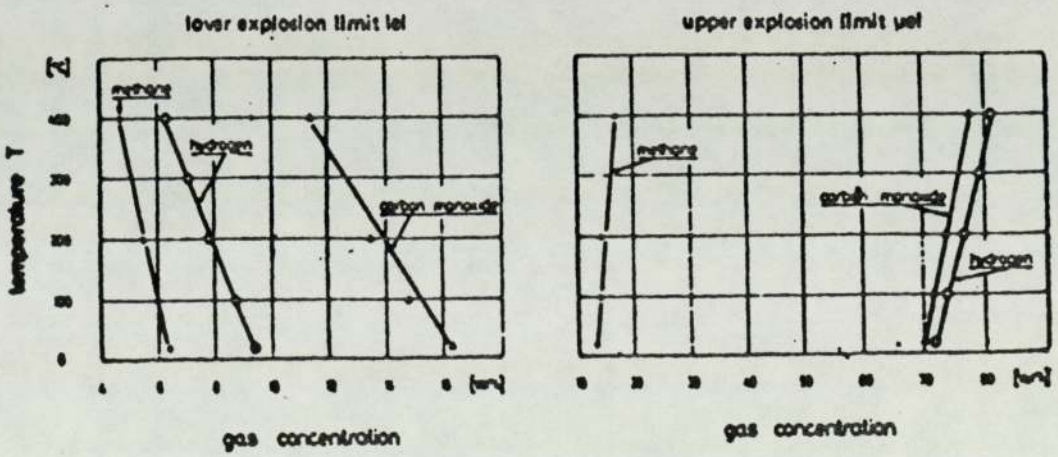

Figure A.1.2, upper and lower explosion limits

[after Barktnecht (65)]

deflagration, but if the propagation exceeds the speed of sound in air (supersonic), then the reaction wave is called a detonation.

The influence of the initial temperature can also be shown in fig.A1.2. by Barktnecht [66], which indicates that for the lower explosion limit gas concentration reduces with temperature and for the upper explosion limit it increases with temperature.

A.1.3. Combustion studies

Studies have been carried out for numerous vapours in air or oxygen enriched air. For instance, [64] quotes that 10% volume of methane in air require 0.5 millijoules (0.0005 Ws) of spark energy to initiate a reaction at the lower flammable limit. If the air is enriched with oxygen, then the minimum spark energy decreases until at 100 % oxygen with 25 % volume methane, the spark energy is about 0.01 of the initial activation energy. This indicates the small amount of energy required to initiate a reaction in oxygen enriched atmospheres.

Studies on quenching distances for numerous mixtures have shown that if the spark electrodes are too massive, or if the spark is near a colder container wall, or if the temperature of the gas to be ignited is too far below the reaction threshold, then the self propagating reaction will be quenched and a self sustaining reaction will not take place. Methane in air can be quenched in about 5 mm.

quenching distance as shown in fig A1.3. As the air is enriched with oxygen, at 25% by volume, the quenching distance has shrunk to 0.3 millimeters. This shows that the oxygen enrichment makes the process easier.

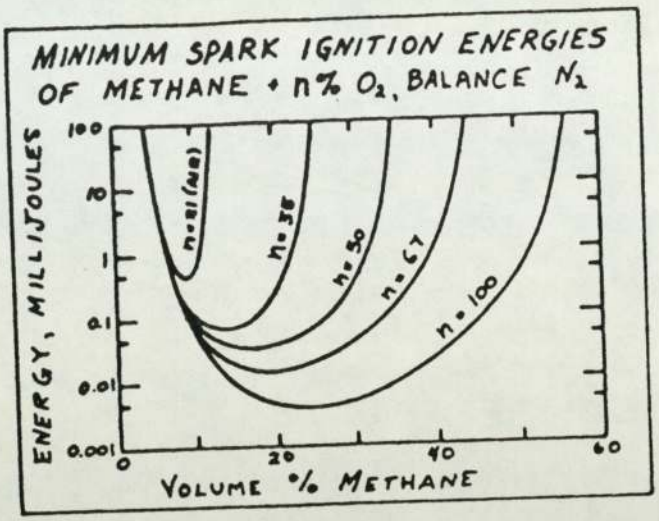

Figure A1.3.a., minimum spark ignition enrgies for mixtures

[after Stull (64)]

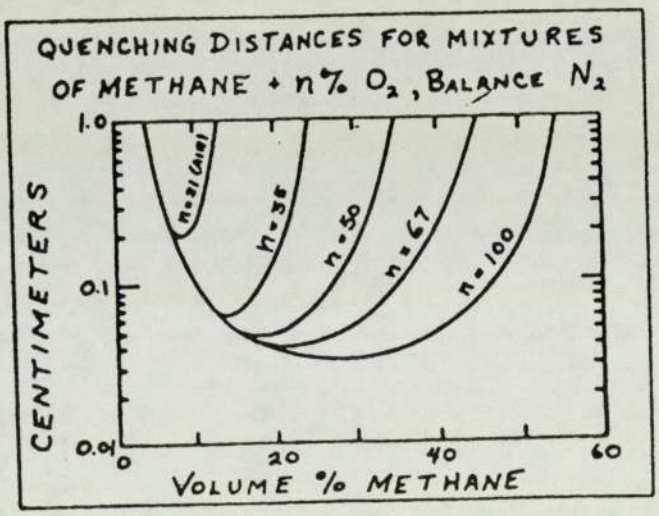

Figure A1.3.b., quenching distance for air/gas mixtures.

[after Stull (64)]

Chance and probability play an important role in the accidental ignition case. The process may form a composition in the flammable range, but because one or more of the necessary factors were not in a "Go" position ignition will not take place. When all factors confirm a "Go" condition, then an ignition will take place. Then a process formerly considered as safe because of repeated successful operations will become unsafe because of a concentration of the required factors.

A1.4 Semnoff thermal theory of ignition

"Temperature and pressure effect"

States that the rate of heat loss by conduction to the surroundings is proportional to the difference between the temperature of reaction and temperature of surroundings, and is represented by the three rate of heat lines when $T_1 < T_2 < T_3$ fig.A1.4.

Since the Arrhenius equation represents the rate of reaction, the rate of heating is an exponential function of the reaction temperature. With a surroundings temperature of T1 any rate of heating less than C is cooled to A , where the reaction temperature is stable at a temperature below ignition. With a surrounding temperature T2 any rate of heating less than B is stablise at B . With a surroundings temperature of T3 any rate of heating to the right of B produces a temperature increase to ignition.

The Arrhenius equation referred to above has the form:

$$K \text{ (mole/s)} = 2.6 \times 10^{16} e^{-53,700/RT} s^{-1}$$

Semnoff showed that for a given temperature the reaction rate is proportional to the square of the reaction pressure Fig. A1.5 . The rate of the loss of heat by conduction is given by the line of temperature T_0. The rates of heating are proportional to the reacting pressures $P_1 < P_2 < P_3$. At low pressure P_1 any temperature less than T_3 cools to T_1 where the reaction is stablised at a temperature below ignition. At intermediate pressure P_2 any temperature less than T_2 stablises at T_2: any rate of heating to the right of T_2 produces a temperature rise to ignition. At a higher pressure P_3 there is insufficient cooling to prevent ignition. This shows that pressure has an accelerating effect on the reaction rate and also on temperature rise. Fig. A1.6.

A1.5. Auto-ignition of liquids

Liquids can be looked upon as condensed gases. Generally liquids have some time lags before igniting and it is assumed that they need to vapourise and mix with air or oxident to become ignited.

Auto ignition temperatures represent a threshold below which

chemicals and combustibles can be handled safely.

A1.6. Impact and compression

Impact and compression can also cause liquids to ignite, but because the two effects are difficult to interpret there is no method to establish a hard and fast rule by which scientific, decisions be made on them. The avoidance of detonation depends on experience and smooth handling.

A1.7. Influence of volume on explosion :

The influence of the vessel on the maximum rate of pressure rise for a given flamable gas or vapour is characterised by the cubic law:

$$(dp/dt)_{max} * V^{1/3} = \text{constant} = K_G$$

It states that the product of the maximum rate of pressure rise and the cube root of the vessel volume is constant . K_G (bar m/s) is a specific material constant valid only for the same shape of vessel, the same degree of turbulence of gas/air mixture, the same mixture concentration and the same ignition source. Thus it is not sufficient to quote the maximum rate of pressure rise , the volume must also be stated .

Fig. A1.6 shows the effect of the violence of explosion, but it must be mentioned that the maximum pressure is not affected by the volume of the vessel. In this effect the volume variation is

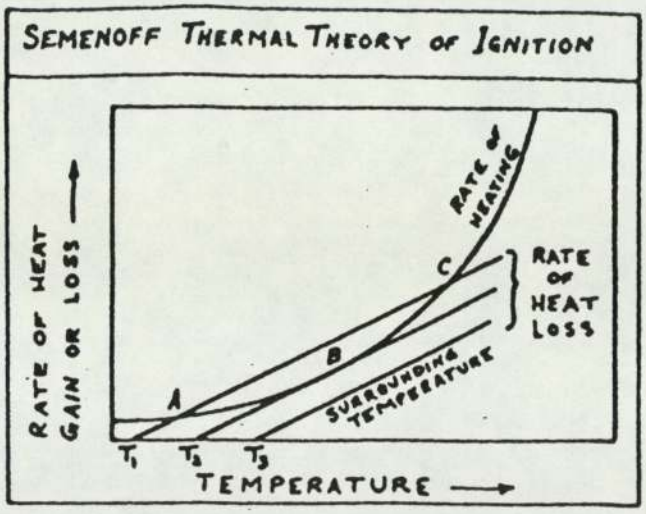

Figure A.1.4, Semnoff theory of ignition.

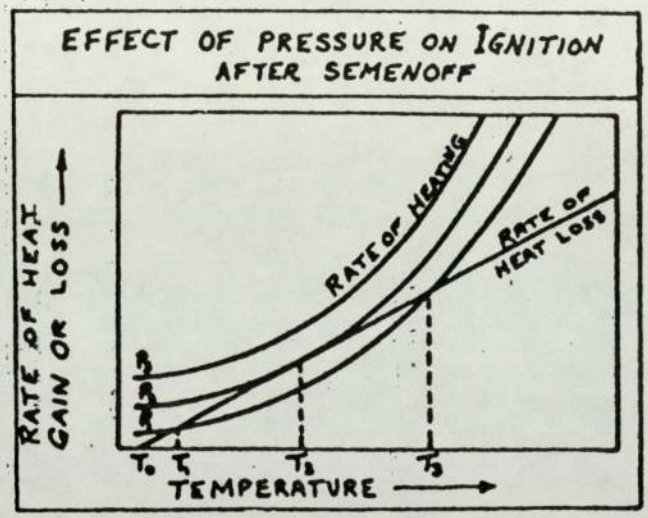

Figure A.1.5,., effect of pressure on ignition.

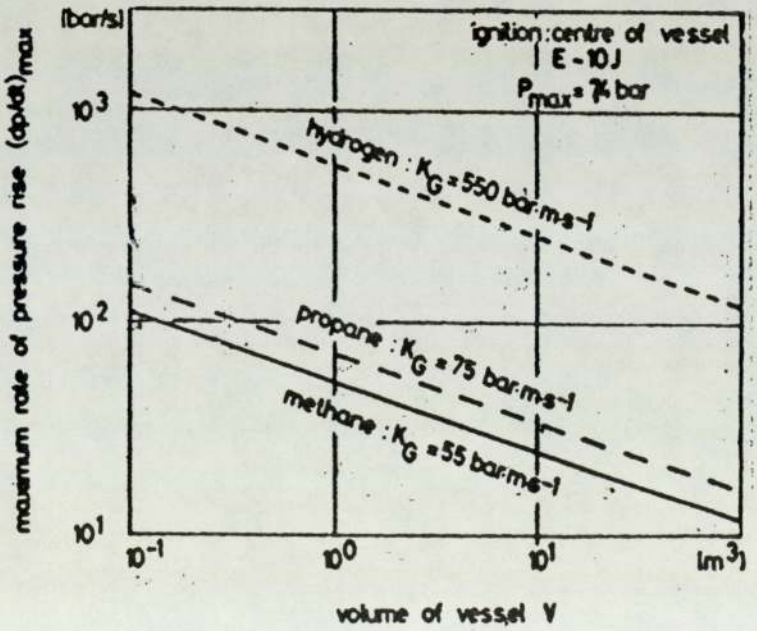

Figure A.1.6,. explosion pressure/ volume relations.

[after Barktnecht (65)]

contrary to the pressure because the initial pressure does determine the maximum explosion pressure that can be reached. Reducing the initial pressure below normal pressure will correspondingly cause a decrease in the explosion data (the pressure and dp/dt_{max}) until finally an explosion can no longer propagate.

A1.7. Influence of turbulence.

In non-turbulent conditions, the propagation of the flame is spherical, but it is severely distorted in turbulent conditions. At high turbulence unburned zones of the mixture are reached by the flame much faster: the rate of a methane explosion can be increased almost 9 fold, the maximum explosion pressure is raised by approximately 20 % and the explosion range is widened slightly. Bartknecht (65). fig 1.8a

A1.9. Effect of pipeline size.

Although the literature available indicates that no comprehensive tests have been carried out in, yet it seems there is a critical diameter below which autonomous propagation of the explosion is no longer possible; all that is said about this critical diameter is that it is in the range of centimeters.

Some critical diameters have been mentioned by Mullins and Penner (66), but they are impractically small for present purposes and have no bearing in the survey unless taken as a guide line to insert

some kind of laminar flow baffle in the suggested rig to hinder the progress of an explosion, although a wire mesh might successfully do the job.

Mullins and Penner report that in general the flammability range widens as the tube diameter is made wider, but the change for diameters above 5 cm. is very small, rarely exceeding one percent. They also report that White [67] found that the narrowing of this range at the weak limit becomes marked. Payman and Whealer [68] found that reducing tube diameter below 0.9 cm caused the flammable range to narrow towards a critical diameter when no propagation could take place. For methane air mixtures this critical diameter was found to be 0.36 cm. and for hydrogen air mixtures it was 0.09 cm.

A1. 10. Le Chatelier's law.

When several flammable gases and vapours are to be considered, the explosion limits can be estimated by the application of Le Chatelier's law, providing that the explosion limits of the components are known.

If P_n is the fraction of a mixture, the lower explosion limit, Lel_m, for the mixture is:

$$Lel_m = \frac{P_1 + P_2 + P_3}{\frac{P_1}{Lel_1} + \frac{P_2}{Lel_2} + \frac{P_3}{Lel_3}} \quad \text{Vol \%}$$

The upper explosion limit is :

$$Uel_m \qquad \frac{P_1 + P_2 + P_3}{\frac{P_1}{Uel_1} + \frac{P_2}{Uel_2} + \frac{P_3}{Uel_3}} \qquad \text{Vol \%}$$

The validity of the law has been proven.

A1.11. Explosion prevention:

The literature has given an insight as to different methods or procedures that are applied to prevent or soften the effect of an explosion. These can be applied singly together according to the discretion of the designer, considering economical limitation without jeopardising safety. Some of these measures are listed as:

A1.11.1. Inerting:

In addition to fuel and oxidant a combustion reaction requires a quantity of energy to initiate it, i.e an ignition source. An explosion can be prevented by breaking this hazard triangle **fig. A1.8.** Inerting of a flamable gas mixture can be achieved by replacing the oxygen in the air by some inert gas such as nitrogen, carbon dioxide or halogenated hydrocarbons.

The consequences of the explosion [max. explosion pressure, max. rate of pressure increase $(dp / dt)_{max}$] will be reduced to a certain degree dependant on the type of inhibitor used. The effectiveness of the inert gases mentioned increases in the order,

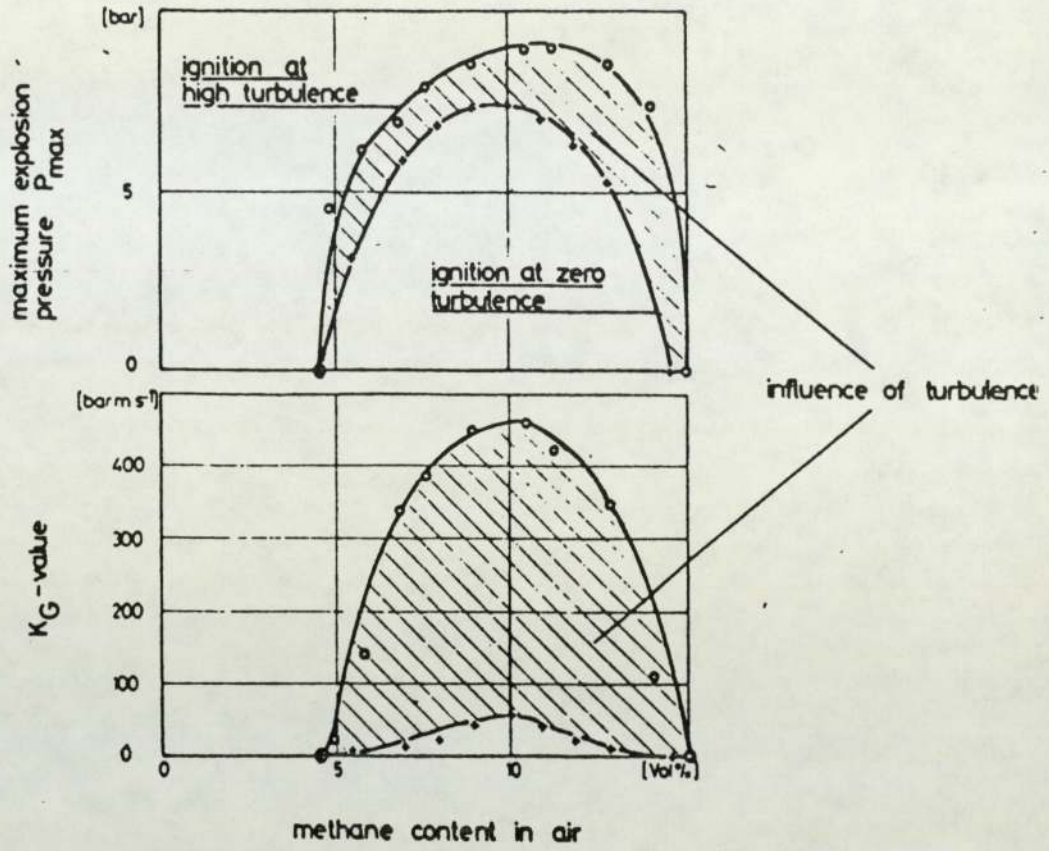

Figure 1.8.b., Turbulence effect on ignition

[after Barktnecht (65)]

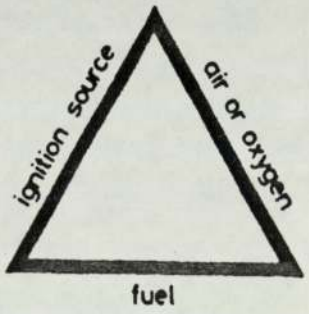

Figure 1.8.b., "Safety Triangle" for explosions

nitrogen - carbon dioxide - halogenated hydrocarbons.

It is not necessary to replace all the oxygen in the air to exclude an explosion. The maximum allowable oxygen varies according to the effectiveness of the inhibitor used. In the case of propane, which is used as a yard stick for relevant combustible gases, the maximum allowable oxygen concentrations by volume are 11 % in nitrogen, 13.5 % in carbon dioxide and 18 % in halons.

A1.12. Pressure venting equipment.

Explosion doors, relief valves and rupture discs are employed when it is anticipated that explosions might occur. They are set to release the pressure before any drastic damage may be done to the equipment. The choice of the relieving device depends on the type of process equipment onto which it is fitted, the location and the atmosphere where it is applied. The detailed study of these devices and their application is beyond the scope of this survey .

A1.12. Pressure relieving area

For venting requirements, it is necessary to have a minimum venting area requirement for a certain volume. One or more rupture discs can be used to provide the total cross sectional area required.

According to nomograms found in the literature the advisable relief area is approximately 1 m^2/ 100 m^3 Ludwig **(69)** Barktnecht**(65)**

A1.13. Explosion prevention using water:

Water can be used in spray form at a concentration of approximately 40% by mass of the explosive mixture. The normal procedure is to use water in spray form across the piping or channel in such a manner that the hazardous effluent is quenched homogeneously. However, Mullins [66] does not deny the phenomenon of water vapour causing an explosive mixture with some gases at some concentrations. His exact wording is quoted:

"*Water is capable, under some circumstances of promoting explosions of hydrocarbon-air mixtures rather than inhibiting them.*"

A1.14. Use of flame arrestors

A device which permits the flow of gases under normal or explosive conditions, without allowing the passage of flame or gases at high temperature, is called a flame arrestor, flame-quenching element or flame trap. A flame trap consists of many passages of small cross sectional area, parallel to the direction of flow and is very effective because it presents a large cooling surface to the flame without inflicting a large pressure drop.

The quenching of flame by proximity to solid surfaces might be purely related to thermal effect due to conduction and convection of heat with the result of cooling of flame gases. A special chemical effect may also be involved where by chain carriers are destroyed thus arresting the chemical reaction. An example of such an effect

is the use of a narrow cylinderical tube in the feed line of a rocket propellant such as ethylene oxide to suppress detonation completely. It has been reported that 120 wire gauze was also used for flame arresting early in the 19th century in coal mines safety lamps and was only successful because of the low temperature of the mixture beyond the gauze.

Mullins (66) quotes Helmore (70) has developed a flame trap for fitting to the induction pipe of spark ignition engines. On investigation, Helmore found that thermal conductivity of the material was relatively unimportant and that a bank of parallel tubes was superior to gauzes. To insure flame arrest he concluded that the reduction in tube length dictated a reduction in the cross sectional area of the tubes.

It was found in flame arrestors using single layers that flames passed through the gauze if the speed of approach exceeded a critical value which was approximately inversely proportional to the width of the gauze. With multiple layers of coarse gauze faster flames could be quenched as the number of layers was increased .
It is reported that wire gauzes are capable of quenching flames from oil mist - air explosions, and it is also claimed that a wire gauze could arrest detonation. (66)

A1.15. Preparatory work before the final design of the rig.

In process systems where separators are used to separate lighter gases from heavier ones, the separation is normally done at high pressures. Liquid and gas separation can be carried out either at high or low pressure. In this work the system will operate under vacuum. To disengage the gas from liquid a specific volume and a liquid-free height is normally required in order to minimise carry-over. The lighter fluid is drawn off at the top, except in cases where the separation process is incomplete. To suppress as far as possible the carry over of liquid with the gas, a wire mesh or soft pad of spongy texture is used suitable to agglommerate liquid droplets in the process involved. If no pad is used an extra height should be allowed in order to get the same gas purity.

A1.15.1. Separator design.

Determination of petrol and air flows.

The cylinder head to be used in the tests is from a Ricardo E6 variable compression engine. From engine manual:

Fuel consumption varies between 0.55 - 0.64 lb/hp h

1- relative to 1000 rev/min. X 5.9 bhp = 3.245 lb / h

2- relative to 3000 rev/min X12.0 bhp = 7.68 lb / h

In kilograms:

1- 3.245 lb/h = 1.475 kg /h

2- 7.68 lb/h = 3.4836 kg /h

The stochiometric level is approximately 1 /15 fuel/air ratio by mass

Air flow system varies between:

1- 1.475 X 15 = 22.125 kg / h

2- 3.4836 X15 = 52.254 kg / h

V olumetric flow at 60 °F (15.4 °C)

Density of air at 60 °F (15.4 °C) = 0.07635 lb / ft. ^{3}

Ist. limit volume in m ^{3} / h

22.125 X 35.310 X 0.07635 / 2.205 = 27 m ^{3} / h

2nd. limit volumetric flow :

52.254 X 35.31 X 0.07635 / 2.205 = 63 . 9 m ^{3} / h

Allow 20% for excess air

63.9 X 120 / 100 = 76.68 m ^{3} / h

S A Y = 80. 0 m ^{3} / h

From Joshi **(71)** :

Given $R_d = \dfrac{V/A}{0.0172 \sqrt{((\rho_l - \rho_v)/\rho_v)}}$

where V = volumetric flow rate of vapour in m ^{3} / s air

A = cross sectional area of the drum in m ^{2}

ρ_l = liquid density in kg / m ^{3}

ρ_v = vapour density in kg / m^3

Take the mogas. gravity as 0.74 at 60 °F. (15.4 °C)

density of mogas. at 60 °F, ie. ρ_l = 740 kg / m^3

density of air at 60 °F (15.4 °C) = 0.07635 X 35.31 / 2.205

= 1.22 kg / m^3

Take air density as 1.29 kg /m^3

$$R_d = \frac{70/3600}{A}$$

$$0.0172 \times \sqrt{(740 - 1.29)/1.29}$$

Take R_d = 0.5 = $\frac{70/3600}{A \times 0.0172 \times 23.93}$

A = 0.0943 m^2

d = 0.346 m

Diameter of vessel without a pad:

Take R_d as 1.3 and calculate same as above to arrive at a diameter d of 0.215 m.

Quoting Backhurst and Harker **(72)** :

" Vessels operating at pressures between 0 and 10 lbf/in^2 and temperatures in the range 600 °F to 1000 °F [design pressure specified as 40 lbf/in^2 -275 kN / m^2] " Vessels operating between -20 °F and 650 °F design temperature may be taken as the operating temperature + 50 °F"

The vessel thickness may be approximated from the relation:

$$t = P r / [S - 0.6P] + C$$

Where:

P = design pressure lb / in ^{2}

R = Internal diameter in metres.

S = allowable working stress lb / in ^{2}

C = corrosion allowance in metres.

t = wall thickness in metres.

(welded joint efficiency is normally taken as 0.75 or 0.80 or 0.95). There is a minimum wall thickness beyond which the vessel will not remain a rigid structure.

$$t = (R + 100)/1000$$

$$= (2.54 + R)/1000$$

For settling height L / D is normally taken in the range 4 to 5. L could also be determined using Joshi's (71) recommendation .

The shell thickness $t = 40 \times 0.324^{*} / 95^{¥} / [(0.0703 - 0.6)] + C^{\#}$

= 1 cm (approximately)

* This is the diameter calculated following the recommendation of Bartknecht (65)

¥ Is the allowable working stress for carbon steel from tables recommended by Joshi (71)

\# Allowance for corrosion neglected because use of equipment is expected to be short lived in the present investigation.

Calculating the thickness using the recommendation of Ludwig (70)

$$T = t = 6PD/S$$

where P = working pressure (lbf / in ^{2})

D = diameter of cylinder (ft)

S = allowable working stress (lbf / in ^{2})

gives the thickness as $T = \frac{6 \times 40 \times 32.4 / 30.5}{95 / 0.0703}$

= 0. 1887 in (approximately)

Net thickness assuming joint efficiency to be 75 %

T = 0.1887 / 0.75 X 2.5 = 0.629 cm.

In this case one would take the thickness obtained from the first equation i.e., the thickness of the vessel separator is 1 cm. Figure A.1.7 shows details of the separator.

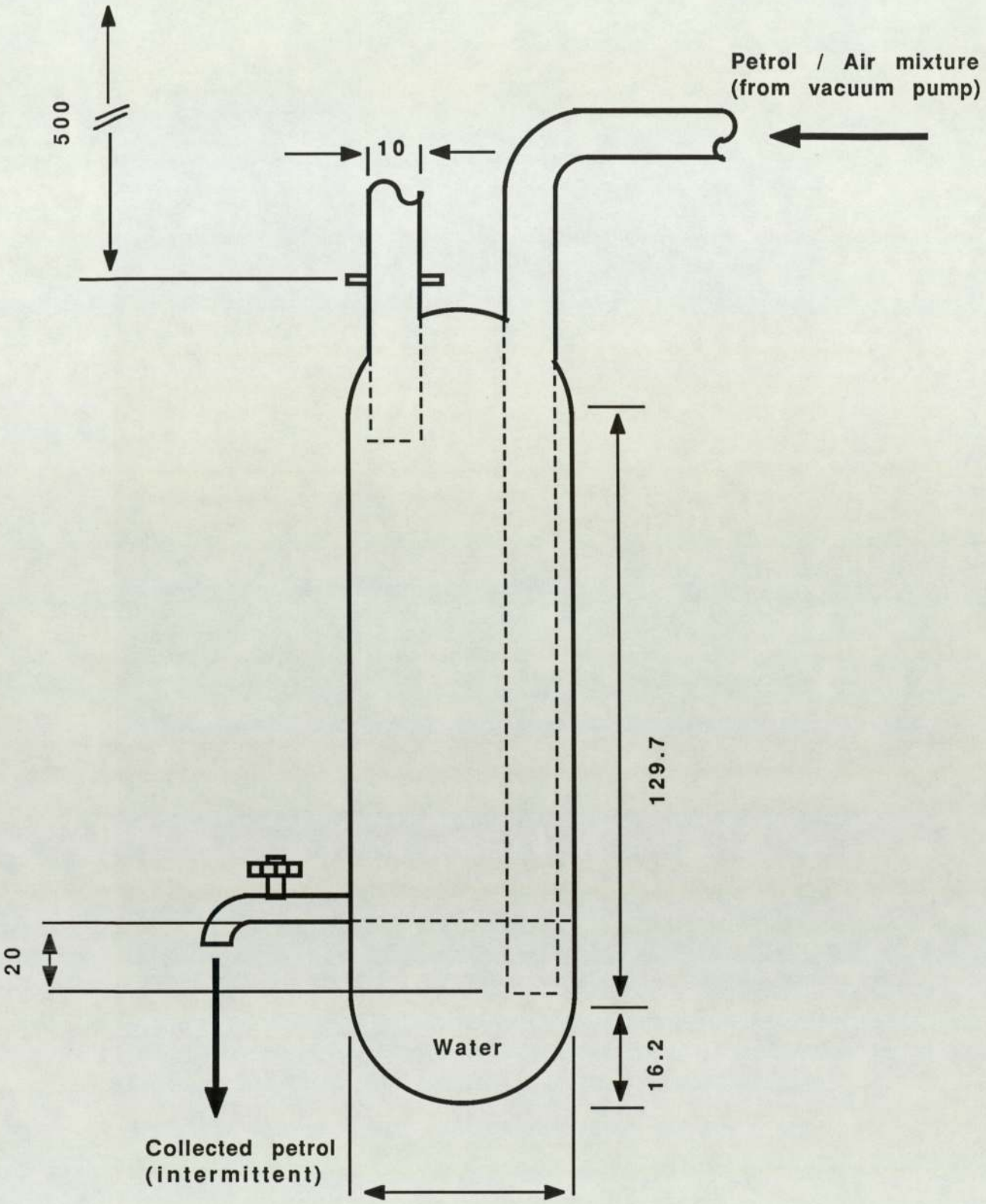

Figure A.1.7., safety vessel (separator) dimensions recommended by Barktnecht.(65).

(agrees with calculated version)

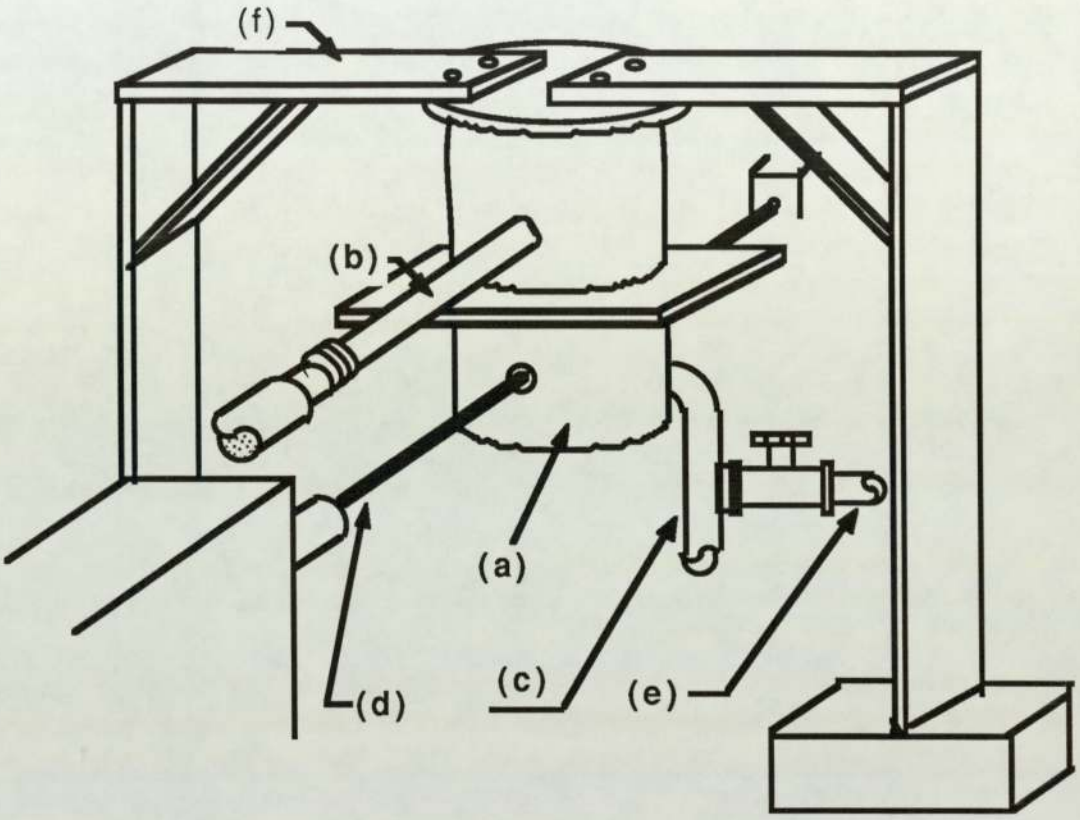

Figure A1.10. Schemetic for flow visualisation rig

Set up of main components

Executed, checked, but not used.

(a) Cylinder & cylinder Head
(b) Induction system
(c) Effluent piping
(d) Laser path
(e) Excess air
(f) Supporting system

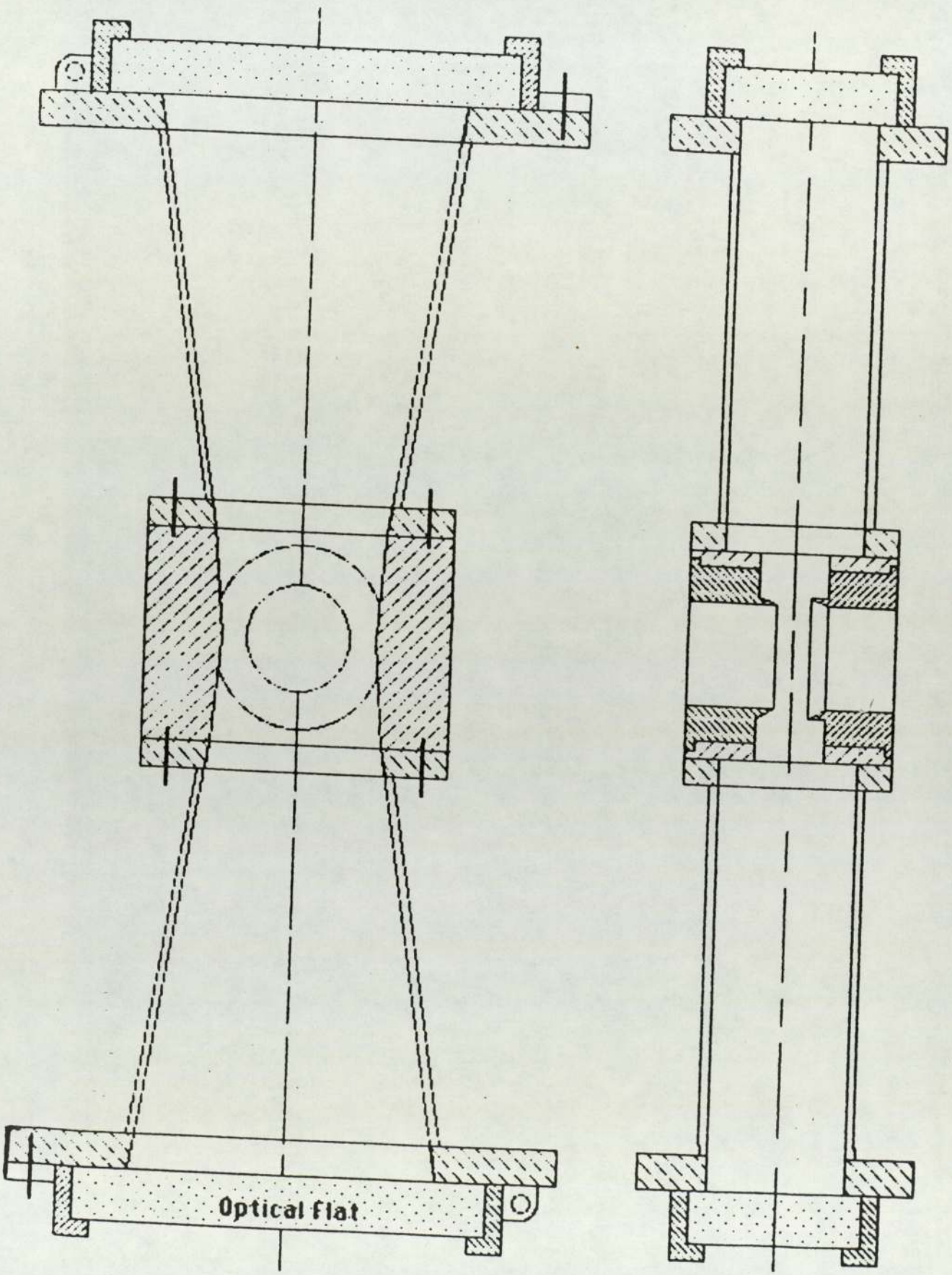

Figure A1.9, proposed viewing system for use with laser.

APPENDIX 2.

Calculation of parameters used in experiments

1 - Core flow and film Reynolds numbers

The following equation was used to calculate the gas and film Reynolds Numbers:

From Ludwig [69] we have :

$$Re = 50.6\ Q\ \rho\ /\ d\ \mu$$

$$= 6.31\ W\ /\ d\ \mu$$

Q = gals. / min. (flow rate).

W = mass flow rate lb / h

d = inside diameter inches.

μ = absolute viscosity (centipoise)

EXAMPLE:

For a flow of air of 10.5 l /sec:

$$R_{eg} = \frac{60 \times 50.6 \times 10.5 \times 0.2199 \times 0.07635}{1.5 \times 1808 \times 10^{-4}} = \underline{\mathbf{19734.9}}$$

2 - Calculation of pressure drop to determine Martinelli parameter:

Martinelli parameter:

$$X = [\Delta P_L / \Delta P_G]^{1/2} = 0.069\ R_e^{0.39}$$

To calculate the pressure drop, it is required to either calculate or find the pipe flow friction factor from the Moody

chart

ΔP_G or $\Delta P_L = 3.36 f L W^2 (10^{-6}) / d^5 \rho$

ε / d = relative roughness (from chart)

f = 0.0115 [Moody chart]

Could be checked against Colebrook's :

$1 / \sqrt{f} = -2 \log_{10} [(\varepsilon / d) / 3.7 \quad 2.51 / R_{tp} \sqrt{f}]$

For a flow of 10.05 l / s and $Re_G \equiv 20 \times 10^3$

$\Delta P_G = 3.36 \times 10^{-6} \times 0.0115 (83.35)^2 / 1.5^5 \times 0.07635$

$= 4.63 \times 10^{-4}$ lbf / in^2

$\Delta P_L = 3.36 \times 10^{-6} f_L (3.078 \times 3600\ 2.205) / 1.5^5 \times 62.32$

$f_L = 64 / Re_L = 64 / 84.58 = 0.76$

$\Delta P_L = 3.36 \times 10^{-6} \times 0.76 \times 5.94^{-4} / 1.5^5 \times 62.32$

$= 8.61 \times 10^{-11}$ lbf / in^2

$X = (\Delta P_L / \Delta P_G)^{1/2}$

$= (8.61 \times 10^{-11} / 4.63 \times 10^{-4})^{1/2} = 4.312 \times 10^{-4}$

f_G can be checked by substituting in the Stanton Pannel relationship:

$1 / \sqrt{f} = 2 \log 10\ Re \sqrt{f}^{-0.8}$

which in this case gives a difference of 10 % .

$$X = 4.312 \times 10^{-4} = 0.069\ R^{0.39} = 2.3 \times 10^{-6}$$

18 points were plotted (using the computer) for the line fit and the graph is shown in fig. 5.2.a . A polynomial version of the graph is also shown , a logarithmic graph is shown for the lower part to show the readings between zero and (2500×10^{-10}) From the experimental results other graphs have been plotted by the computer, for example wall film rate versus air flow, gas Reynolds number versus wall film rate, gas Reynolds number versus film Reynolds number.

APPENDIX 3.

Models to Predict the Entrainment Rate

A3.1. based on Azbel and Liapis [62]

Basically mathematical.

Assumptions:

1- The gas (air) phase is turbulent.

2- The liquid (film, Petrol), is viscous.
The two phases are assumed to be affected by stresses that occur at the interface.

3- The liquid film, petrol, is assumed to be incompressible and described by the following equation:

$$du_{fi}/dt + u_{fk}\, du_{fi}/dx_k = -1/\rho_{f^*} dp_{f}/dx_i + \{ \mu_f/\rho_{f^*} (d^2u_{fi}/dx_k dx_{k)} \} + g \quad (1)$$

where

u_{fi} is the velocity vector of the liquid

x_i is the Cartesian coordinate vector

ρ_f is the liquid density

p_f is the liquid pressure

μ_f is the liquid dynamic viscosity

and g is the acceleration due to gravity.

The above is the Navier-Stokes equation written in the Cartesian

tensor notation, so:

$$d^2/dx_k\, dx_k = d^2/dx^2 + d^2/dx^2 + d^2/dy^2 + d^2/dz^2$$

and the continuity equation for the liquid is :

$$du_{fi}/dx_i = 0 \qquad \text{---------- (2)}$$

For the gas phase a similar approach is applied, the viscous term is replaced by the apparent turbulent stress term and the gravitational force is neglected

$$du_i'/dt + u_k'\, du_i'/dx_k = -1/\rho_g * dp_g'/dx_i - du_i''\, u_k''/dx_k \qquad \text{--- (3)}$$

where

u_i' is the time averaged gas velocity vector and u_i'' is the is the fluctuating gas velocity vector, $u_i = u_i' + u_i''$. The term p_g' is time averaged gas pressure.

The continuity equation for the gas is:

$$du_i'/dx_i' = 0 \qquad \text{---------- (4)}$$

The balance of normal stress at the interface is used to couple the liquid and gas equations which are in turn coupled by boundary conditions as follows:

$$-p_f + 2\mu_f * du_{f3}/dx_3 = p_g' - \rho_g u_3''^2 - \sigma\,(\,i/R_1 + 1/R_2\,) \qquad \text{-------- (5)}$$

where the index 3 refers to the coordinate normal to the interface and indices 1 and 2 refer to conditions parallel to the interface. The main radii of curvature of the interface are given by R_1 and R_2; and σ is the surface tension. The second terms on each side of the equation

are the normal viscous and turbulent stresses, respectively.

For the shear stresses

$$\mu_f(du_{fi}/dx_2 + du_{f3}/dx_i) = \rho_g \, u_2" u_3" \qquad \text{------ (6)}$$

The left hand side of the equation represents liquid viscous shear and the right hand represents gas turbulent shear.

Equations (3) and (6) describe thoroughly the two-phase motion, but their simultaneous solution poses great difficulties. At this stage the authors introduce dimensionless analysis by which they generate dimensionless groups useful in analysing experimental data. The dimensionless functions are:

$$U_{fi} = u_{fi}/v_s, \quad U_i' = u_i'/v_s, \quad Ui" = u_i"/ v_s$$

$$p_f = p_f/\Delta p, \quad p'g = p'g/\Delta p$$

$$T = t/\tau, \quad X = x/h_s, \quad R_{oi} = Ri/h_s$$

V_s is the gas superficial velocity; Δp is a typical flow system pressure difference (eg. between the walls of a chamber, or pipe); τ is a characteristic time and h_s is distance above the free liquid level. Using the dimensionless functions in the equations above leads to

$$v_s/\tau *(dU_{fi}/dT + v_s^2/h_{s*}(U_{fk} dU_{fi}/dX_k) =$$

$$-dp/\rho_f h_{s*}(dp_f/dX_i + \mu_f v_s/\rho_f h_s^2 *(d^2U_{fi}/dX_k dX_k) = g \text{----(7)}$$

$$V_s/h_{s*} (dU_{fi}/dX_i) = 0 \qquad \text{-------(8)}$$

$$v_s/\tau (dU_{fi}'/dT + v_s^2/h_{s*} (U_{gk} dU_i/dX_k) =$$

$$-dp/\rho_g h_{s*}(dp_g'/dX_i - v_s^2/h_{s*}(dU_i" U_k"/dXk) \qquad \text{---------(9)}$$

$$V_s/h_{s*}\ (\ dU_i''/dX_i) = 0 \qquad \text{----------(10)}$$

$$-\Delta p\ (p_f)+ \mu_f V_{s/} h_s*(2dU_3/dX_3)= \Delta p(p_g')-\rho_g v_s^2\ (U_3''^2)- \sigma/h_s\ (1/R_{01}+1/R_{03})$$

----------(11)

In the above relations all the terms in parentheses are of the order unity, so in any study of the relative influence of pressure, viscosity, surface tension, gravity and time variations , it is only needed to consider the coefficients in front of the parentheses.Only equations (7) and (11) need to be used for that.

Therefore

$$v_S/\tau_*\{0(1)\}+v_s^2/h_s*\{0(1)\} =-\Delta p/\rho_f v_s 2*\{0(1)\}+\mu_f v_s/\rho_f h_s^2*\{0(1)\}+ g \text{--(12)}$$

$$h_s/v_s\tau *\ \{0(1)\}+\{0(1)\}=-\Delta p/\rho_f v_s^2 *\{0(1)\} + \mu_f v_s/\rho_f h_s v_s *\{0(1)\}+gh_s/v_s^2$$

----------(12a)

So,

$$-\Delta p\ \{0(1)\}+\ \mu_f v_s/h_s *\{0(1)\} = -\Delta p\ \{0(1)\} - \rho_g v_s^2\ \{0(1)\}-\sigma/h_s *\{0(1)\}\ \text{-(13)}$$

$$-\Delta p/\ \rho_f v_s^2* \{0(1)\}+\ \mu_{f/}\ \rho_g h_s v_s * \{0(1)\}=$$

$$-\Delta p/\ \rho_f v_s^2* \{0(1)\}-\ \rho_{g/}\ \rho_f * \{0(1)\}_-\ \sigma\ /\rho_g h_s v_s^2 \qquad \text{---------(13a)}$$

In the above ,0(1) denotes that the term is of the order unity. It is obvious from equation 12a and 13a that we have several important nondimensional groups in the two-phase flow described by the initial equations:

$$\{\Delta p/\ \rho_f v_s^2, \rho_f h_s v_{s\ /}\ \mu_{f,} v_s^2/\ gh_{s,}\ \rho_g v_s^2 h_{s/}\ \sigma, v_s\tau\ /h_{s,}\ \rho_{g/}\ \rho_{f}\}$$

These can be written as [Eu, Re,Fr,We,Ho, ρ_g/ρ_f]

where

Eu = $\Delta p/\ \rho_f v_s^2$, the Euler number, ratio of pressure to inertial forces

Re = $\rho_f h_s v_s / \mu_f$, the Reynold number, ratio of inertial to viscous forces

Fr= v_s^2 / gh_s, the Froude number , ratio of inertia to gravitational forces

We= $\rho_g v_s^2 h_s/ \sigma$, the Weber number, ratio of inertial to surface tension forces

Ho= $v_s \tau / h_s$, the Homochronity number, ratio of spatial to temporal inertial forces

All these functions are independent except the Euler number because it expresses the relation between the pressure and velocity fields, once the velocity field is given the pressure is determinable and visa versa , hence:

Eu = Eu(Re,Fr,We,Ho,ρ_g/ρ_f) ----------(14)

The above relationship not only hold for the Euler number but also for any dependant quantity .For example for the entrainment coefficient $Y= \Sigma M_f/M_g$, where ΣM_f denotes the total liquid (droplet) entrainment per unit cross sectional area and time(mass flux/time) and M_g is the

mass flow rate of gas, then:

$$Y = Y(\ Re,Fr,We,Ho,\rho_{g/}\rho_f\ ) \qquad \text{---------(15)}$$

The authors[62] declare that experimental determination of such a relationship presents serious difficulties, but experience indicates that this set of dimensionless may successfully be Combined into groups

Hence it can be written

$$A = Fr^{1/2}We^{3/2}\ \rho_g\ /Re^2\ (\ \rho_f - \rho_g\ )$$

$$= (v_s^2/\ gh_s)^{1/2}\{(\rho_f - \rho_g\ )*v_s^2 h_{s/\sigma}\ \}^{3/2}{}_*\ \rho_g/\ [(v_s h_s)/v_f\ ]^2{}_*\ (\rho_f - \rho_g\ ) \qquad \text{----------(16)}$$

Or

$$A = v_f^2\ v_s^2\ \rho_g\ /g^2\ \{\ \sigma\ /g*(\rho_f - \rho_g\ )\}^{\ 3/2}{}_*(\rho_f - \rho_g\ ) \qquad \text{----------(16a)}$$

In the above ρg has been replaced by $(\rho f - \rho g\ )$which is an alternative definition of the Weber number.

Also

$$= v_s\tau\ \sigma^{\ 1/2}/\ h_s^{\ 2}\ \{(\rho_f - \rho_g\ )g\ \}^{1/2} \qquad \text{------(17)}$$

The authors declare that in most applications the Homochronity number is taken as unity. Therefore,

$$\tau = h_s/\ v_s \qquad \text{-----(18)}$$

Equation 17 may be written as

$$B= \{\ \sigma/g\ (\rho_f - \rho_g\ )\ \}^{\ 1/2}\ /\ h_s \qquad \text{----(19)}$$

The value of factor A in equation 16 in any system is determined by the magnitude of gravitational, viscous and surface tension forces

during droplet generation and also determined by inertial and gravitational forces during droplet motion in the gaseous region. Factor B in equation 17 is determined by the relative magnitude of gravitational, inertial and surface tension alone. Equation 15 in terms of the two factors A and B is

$$Y = C\, A^m\, B^n \qquad \text{------- (20)}$$

C,m and n are constant to be determined experimentally. The authors report that the validity of the equation has been checked and tested on various fluids and that the results correlated by a straight line and their final correlation was as follows

$$Y = 3.7 * 10^{13} \left\{ v_f^2\, v_s^2\, \rho_g / g^2\, (\rho_f - \rho_g) \right\}^{1.4} \Big/ \left\{ \sigma / g(\rho_f - \rho_g) \right\}^{1.2} * h_s^{3.2}$$

****

A3.2. Basically experimental

Hewitt and Taylor[43] also report a correlation which has been suggested by Paleev and Flippovich for liquid entrainment on which the authors superimposed the results of Truong and Quang Minh for water and alcohol, Cousins etal -1965, Cousins and Hewitt-1968, Gill et al -1964 and Cousins and Hewitt-1968

Although the Paleev and Flippovich[63] correlation does not include the effect of the diameter it has been included to provide a means of comparison and because of the very limited progress of analysis and correlation in this field.

quantities:

1 - g =9.82 m sec^{-2}

2 - νf= 1.6*10 $^{-6}$ $m^2 sec^{-1}$

3 - V_s= 36.6 m sec^{-1}

4- ρ_g =1.29 kg m^{-3}

5- ρ_f = 820 kg m^{-3}

6- σ = 2.4*10 $^{-3}$ N m-1

7- h_s= 1.375 * 2.54*10 $^{-2}$ m

Substituting in above correlation Entrainment factor =1.74Kg/kg /m^2

Weight of air passing /h =9.58*10 $^{-4}$ *36.6 *1.29 =162.83 kg/h

Entrainment quantity for this mass flow= 0.27138

a typical example of one of the liquid flows is 0.7236 kg/h

therefore entrainment % 0.27138/0.7236 37 %

The Paleev and Flippovich correlation has been used for the same conditions to estimate the discrepancy between the predictions (see fig. A.3.1.)

Data from Troung Quang Minh **(73)** plot and ibid- 1965.

Extarpolation was first attempted from the water results , processed through the computer and best fit was correlated into the following:

$y\ (1-E) = 1.4445 * x^{-0.2667}$

where

x = Paleev and Flippovich correlation

$= \rho_{gc} / \rho_l * (\mu_l v_g)^2 / (\sigma * 10^4)$

where

x = Paleev and Flippovich correlation

ρ_{gc} = assumed to be equal to ρ_g = gas density

ρ_l = liquid density

μ_l = liquid viscosity

v_g = gas velocity

σ = surface tension

E = Entrainment ratio

Taking the same example as before and substituting in the correlation

$$x = 59$$

$$Y\ 48.5 = 1 - E = \underline{51.5\ \%}$$ see fig. A3.1

For alcohol the same conditons give

$$y = 1-E = 0.7821 * 10^{-0.002x} = 0.596$$

Entrainment $= 100 - 59.6 = \underline{40.4\%}$

Using the alcohol plot for the same conditions

$$y = 1-E = 0.8626 * 10^{-0.002x} = 69.4$$

$\therefore$ E % $= 30.6$

Assuming the entrainment to lie within the two limits for alcohol and water, since gravities also lie between the two limits and since entrainment greatly depends on the density of the liquid .

$\therefore$ average entrainment between the two limits = 40.4+ 30.6/2

$= \underline{35.5\%}$

Which is favourably fitting the result estimated by the other method.

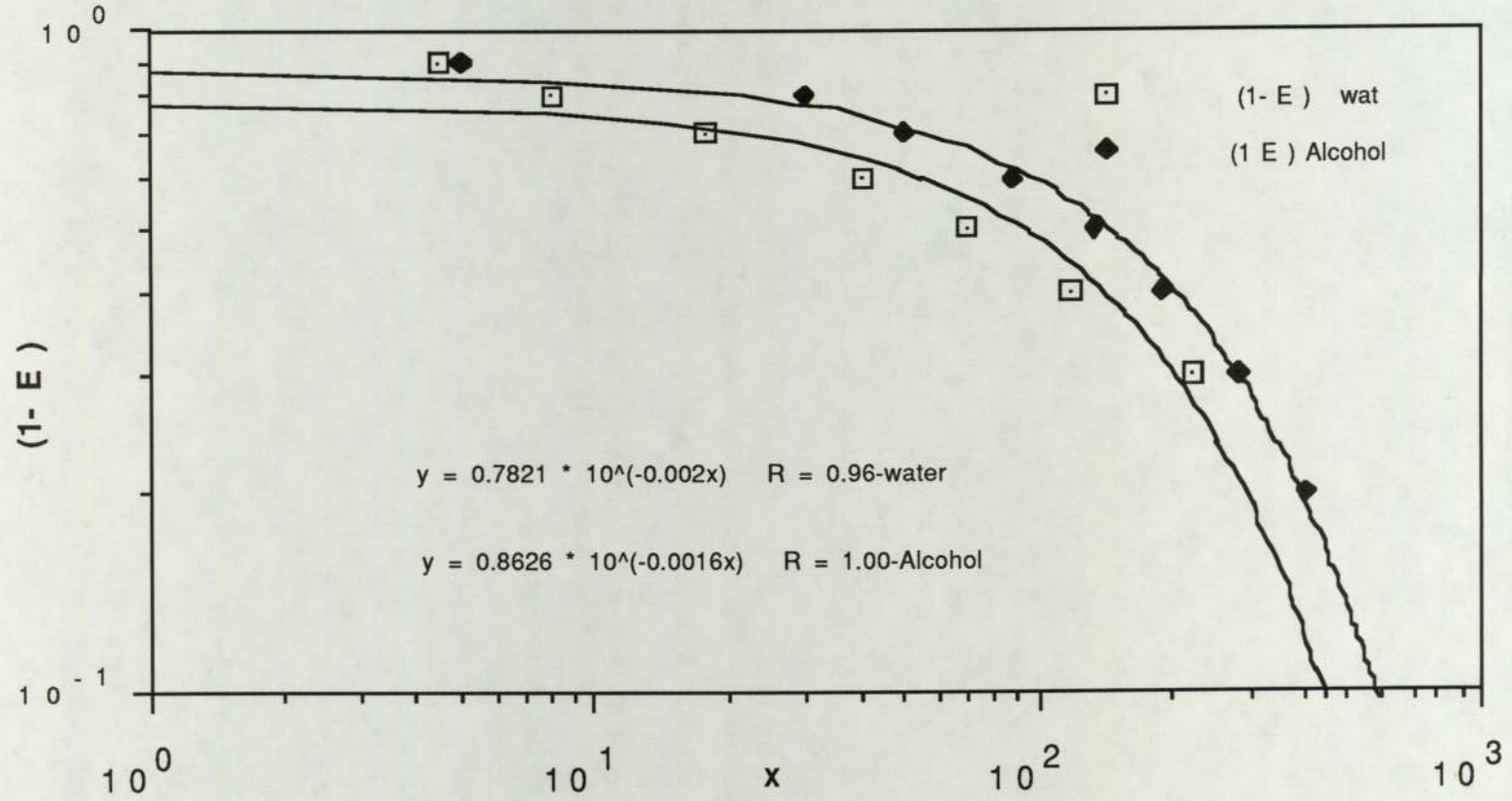

Figure A3.1, Data from "Entrainment correlation."

Truong,Cousins&Hewitt, et al. { Ref. (47) }

All based on Paleev & Flippovich Correlation

TABLE 1

	R	X
1	6.8	26.2
2	360.0	8.6
3	55.1	4.1
4	1260.0	13.9
5	560.0	10.4
6	1770.0	15.9
7	23000.0	43.1
8	690.0	11.0
9	250.0	7.4
10	738.0	11.3
11	120.0	5.5
12	520.0	10.0
13	15800.0	37.4
14	5.2	1.6
15	110.0	5.4
16	5.7	1.7
17	19.0	2.7
18	211.0	6.9

MARTINELLI VS WICKS & DUKLER PARAMETERS (Current Research)

Steady Flow Tests Results and Calculations

TABLE 2

	Re Gas x 10^3	F.Rate (ml/s)	% film	Ref	W. Flow (ml/s)	Air flow (l/sec)	Air Flow	Conditions
1	2.15	3.06	100	84.14	3.03	2.029	1	
2	4.57	2.80	92.4	76.99	3.03	2.43	2	A. Temp. 20 C
3	5.34	2.83	93.4	77.82	3.03	2.840	3	
4	6.66	2.86	94.4	78.64	3.03	3.490	4	
5	7.63	2.86	94.4	78.64	3.03	4.058	5	P.75.3cm. Hg
6	8.69	2.83	93.4	77.82	3.03	4.626	6	
7	9.53	2.83	93.4	77.82	3.03	5.072	7	(Fac. 0.97388)
8	10.53				3.03	5.600	8	
9	11.44	2.80	92.4	76.99	3.03	6.087	9	
10	12.59				3.03	6.700	10	
11	13.58				3.03	7.223	11	
12	14.64	2.83	93.4	77.82	3.03	7.791	12	
13	15.64				3.03	8.319	13	
14	16.78	2.79	93.4	77.72	3.03	8.927	14	
15	17.76	2.78	91.7	76.44	3.03	9.450	15	
16	18.91	2.78	91.7	76.44	3.03	10.063	16	

Steady Flow Tests Results and Calculations

TABLE 3

	Air flow l/s	w. fl-ml/sec	fm.fl. - ml/se	% film	Re Gas x 10^3	Re film	Air flow	Condition	Remarks
1	2.022	3.061	3.109	>100.00	3.8	85.49	1	Baro press	Decided
2	2.426	"	3.099	"	4.56	85.22	2	Amb. temp.	to use a
3	2.831	"	3.093	"	5.34	85.05	3	Press. & temp.	rotometer
4	3.478	"	3.036	99.18	6.54	83.48	4	corr. fact.	mains water
5	4.044	"	3.055	99.8	7.6	84.01	5	753 mm Hg.	supply
6	4.61	"	3.093	>100	8.66	85.05	6	21 deg. C.	
7	5.055	"	3.036	99.18	9.5	83.48	7	0.970569	
8	5.581	"	3.046	99.51	10.49	83.76	8		
9	6.673	"	3.061	100	12.54	84.17	10		
10	7.765	"	3.030	98.99	14.59	83.32	12		
11	8.897	"	3.030	98.99	16.72	83.32	14		
12	10.029	"	3.009	98.30	18.85	82.74	16		

Steady Flow Tests Results and Calculations

TABLE 4

	Air flow- l/se	w. flow- ml/s	fm.flow-ml/se	% film	Re Gas x 10^3	Re film	Air flow	Column 8	Remarks
1	2.026	2.985	3.0076	(!)>100	3.81	84.58	1	Baro. press	It is obvious
2	2.43	"	3.092	"	4.57	85.02	2	& Amb.	that the air
3	2.84	"	3.125	"	5.34	85.93	3	temp press	flow is too
4	3.49	"	3.092	"	6.56	85.02	4	correction	small to
5	4.62	"	3.03	"	8.68	83.31	6	factor	inflict
6	5.59	"	3.03	"	10.51	83.31	8	752 mm Hg.	disengagement
7	6.69	"	3.024	"	12.57	83.15	10	20 deg. C.	of droplets, the
8	7.78	"	3.024	"	14.62	83.15	12	0.9725	mains pressure
9	10.05	"	3.00	"	19.73	82.49	16		fluctuation

Steady Flow Tests Results and Calculations

TABLE 5

	Air flow l/s	w. flow- ml/s	film - m l/s	% film	Re Gas x 10^3	Re film	Air flow	Condition	Remarks
1	2.03	1.25	0.87	70	3.81	23.92	1	Pressure &	Test
2	2.43	"	0.77	62	4.57	21.17	2	temperature	discontinued
3	2.84	"	0.59	47	5.34	16.22	3	correction	because of
4									irregularity of
5									mains water
6									
7									
8									

Steady Flow Tests Results and Calculations

TABLE 6

	Air flow l/s	w. flow- ml/s	fm.flow-m l/s	% film	Column 5	Re film	Re Gas x 10^3	Air flow	Remarks
1		3.125	3.125	100	85.9			0	at flow 10
2	2.43	"	3.03	97	4.57	83.29	4.57	1	film increased
3	2.84	"	3.04	97	5.34	83.46	5.34	2	
4	3.49	"	3.02	97	6.56	82.96	6.56	4	
5	4.62	"	3.00	96	8.68	82.47	8.68	6	
6	5.59	"	2.94	94	10.51	80.82	10.51	8	
7	6.69	"	3.02	97	12.57	83.13	12.57	10	
8	7.78	"	3.99	96	14.62	82.19	14.62	12	
9	8.92	"	2.96	95	16.77	81.37	16.77	14	
10	10.05	"	2.94	94	18.89	80.82	18.89	16	

Steady Flow Tests Results and Calculations

TABLE 7

	Air flow-l/s	w. flow - ml/s	film - fl ml/s	% film	Re Gas x 10^3	Re film	Air flow	Conditions	Remarks
1	2.03	1.736	1.49	86.0	3.81	40.97	1	Pressure %	More air
2	2.43	"	1.38	79.5	4.57	37.95	2	temperature	needed.
3	2.84	"	1.32	75.8	5.34	36.30	3	factor	Very
4	3.49	"	1.27	73.3	6.56	34.92	4	0.9725	difficult to
5	4.05	"	1.20	69.0	7.61	32.94	5		take
6	4.62	"	1.17	67.4	8.68	32.17	6		measurement
7	5.07	"	1.15	66.2	9.53	31.62	7		with
8	6.08	"	1.12	64.4	11.43	30.72	9		existing
9	7.21	"	1.11	64.0	13.55	30.52	11		equipment
10	8.31	"	1.07	62.0	15.62	29.42	13		
11	8.67	"	1.06	61.0	16.30	29.15	15		
12									

TABLE 8

PULSATING FLOW TEST DATA

DROPLET ENTRAINMENT FROM WALL FILM WITH PULSATING FLOW FOR RANGE OF DISK SPEED

	A/F 320	Log Dr. 320	A/F 350	Log Dr. 350	A/F 400	Log Dr. 400	A/F 600	Log Dr. 600	A/F 700
1		2.1644			78		78	2.2014	98
2		1.9777	96	2.3765	112		112		251
3	251	2.0719	237	1.9822	196	2.2068	196		262
4	120	3.0322	113	2.9400	96	2.1644	96		205
5	263	1.6232	248	1.7559	101	2.2945	101		126
6	205	2.129	193	1.8921	251	1.2304	251	1.3617	70
7	126	2.4161	119	2.4518	120		120		70
8	67	2.3598	82	2.4564	262	2.2201	263		68
9	67	2.8820			205		205	1.7243	90
10	78	2.7868			126	2.4639	126	2.340	52
11	86	2.7782			87		87	2.083	128
12	61	2.7910			151		151		111
13	60	2.7731		1.8633	132		132		
14	59	2.7745	98	3.0322	166		166		
15	59	2.7810	139	2.8041	143		143		
16		1.9823			82	2.7782	67		
17		2.8280	52	3.0220	75	2.7803	54	2.7900	
18	128	2.7103	87		59	2.7917	79	2.7760	
19	111	2.7839	128	2.2718	59	2.9030	72	2.7803	
20			111	2.367	59	2.7796	57	2.7868	
21					58	2.7796	55	2.7709	
22					56	2.7896	54	2.7902	
23					63		63		
24					52	3.0320	52	2.9410	
25					127	2.1959	87		
26					110	2.0969	127	2.2095	
27							110	3.0220	
28									

TABLE 9

PULSATING FLOW TEST DATA

DROPLET ENTRAINMENT FROM WALL FILM WITH PULSATING FLOW FOR RANGE OF DISK SPEED

	Log Dr. 700	A/F 860	Log Dr. 860	A/F 960	Log Dr. 960	A/F1030	Log Dr. 1030	A/F 1080	Log Dr. 108
1	2.8500	87		87		87	2.3243	87	2.2788
2	1.3424	124		124		124		124	
3	1.7782	218		218		224		218	
4	1.6334	106	2.1104	87	2.8089	109	2.0172	106	2.2945
5	2.3243	101	2.8820	101		101		101	
6	2.9074	251	1.4.50	251	1.3802	251	1.4472	251	1.3802
7	2.8920	120		120	1.9868			120	1.9868
8	2.6580	262	1.7709	262	1.7853	205	1.6989	205	1.6232
9	3.0320	205	1.7243	205	1.6435	126	2.3385	125	2.2201
10	2.9395	126	2.4518	139	2.3856	87	2.1072	87	2.2648
11	2.1553	87	2.8451	87	2.8082	174		147	
12	2.2175	167		174		70		174	
13		147		70		70	2.8633	70	2.8751
14		634		70	2.8751	79	2.7716	70	2.9009
15		166		57	2.9031	72	2.7752	55	2.6857
16		67		57	2.9042	57	2.7825	65	2.8357
17		793		111	2.6730	57	2.7774	124	
18		72	2.7760	129		54	2.7818	63	3.0322
19		57	2.7752	63	2.9868	54	2.7782	52	
20		55	2.7782	52	2.9410	63		87	2.4533
21		54	2.7825	87	2.2253	52	3.0322	128	
22		54	2.7774	128		87		90	
23		63		111		128	2.2253		
24		52	3.0220			111			
25		87							

TABLE 10

ENGINE INLET VALVE RESULTS

	Air/Film - 1	Sauter md - 1	Air/Film - 2	Sauter md - 2	Air/Film - 3	Sauter md - 3	Air/Film - 4	Sauter md - 4
1	399.6	86.1	423.5	79.74	423.5	99.3	305.5	120.4
2	276.3	192.1	292.8	141.2	423.5	92.1	211.2	94.3
3	419	93.1	444.4	101.8	444.4	117.5	320.6	110
4	345.3	95.3	366	-	366.0	103.4	249.2	111.5
5	592.0	103.1	627.4	99.1	452.6	108.1	192.3	56.8
6	375.0	127.7	381.9	116.9	280.0	140.2	358.4	57
7	289.9	76.3	294.6	74.1	216.1	71.3	232	108.8
8	540	76.3	549	74.1	402.8	71.3	265.1	125.3
9	190.9	116.0	178.0	129.5	151.5	105.8	320.4	104.4
10	221.1	130.3	203.4	171.5	173.1	113.8	514.8	106.3
11	267.2	105.2	245.8	122.1	209.2	143.6		
12	429.4	92.7	395	84.2	336.2	82.5		

TABLE 11

ENGINE INLET VALVE RESULTS

	Air/Film - 5	Sauter md - 5	Air/Film - 6	Sauter md - 6	Air/Film - 7	Sauter md - 7	Air/Film - 8	Sauter md - 8
1	256.4	82.4	306.2	94.4	364.1	110.4		
2	177.3	128.8	211.6	130.5	251.7	122.7	251.7	117.2
3	269.1	110.4	321.3	143.0	386.1	153.3	382.1	106.1
4	221.6	86.6	264.6	86.6	314.7	115.3	314.7	98.5
5	379.9	91.2	453.6	106.0	539.4	107.6	539.4	98.5
6	323.2	111.1	346.4	128.4	351.8	154.9	351.8	143.4
7	249.4	64.8	267.3	79.9	271.4	74.2	271.4	79.2
8	464.9	64.8	498.2	79.9	505.9	74.1	505.9	66.3
9	193.5	126.4	205.0	123.2	207.5	156.1	116.6	130.1
10	221.1	139.3	234.3	145.5	237.1	146.6	238.9	154.5
11	267.2	129.6	283.1	129.2	286.5	128.3	288.6	117.9
12	429.4	95	454.9	101.7	460.5	99.4	468.2	98.9

TABLE 12

ENGINE INLET VALVE RESULTS

	Air/Film - 9	Sauter md - 9	Air/Film - 10	Sauter md - 10
1	369.5		377.2	123.6
2	255.5	88.6	260.8	
3	387.8	115.7	395.9	110.2
4	319.3	93.1	326.0	
5	547.4	100.5	558.9	98.5
6	357.9	133.1	360.2	140.8
7	276.2	64.8	278.0	56.0
8	514.8	64.8	518.0	56.0
9	117.74	128.4	118.0	142.3
10	241.1	158.6	242.3	154.7
11	291.4	158.4	292.8	135.0
12	468.4	99.4	470.4	98.9

Nomenclature

The symbols listed below are those used most commonly througout the text, where different symbols are used in relationships quoted within the literature reviews of chapter 2, 3 and the appendix; the symbols are defined locally in the text.

B breadth of wave

B empirical constant (defined by equation 19 ch.3)

C droplet concentration (defined by equation (2) Ch.3)

Cd drag coefficient

C_p specific heat

D pipe diameter

D droplet diameter

D' mass diffusivity

d droplet diameter

d_{32} sauter mean diameter

E entrained fraction

E activation energy

E_p eddy diffusivity

G mass flux (mass flow/area)

g gravitational force

H height of channel

h height of air annulus

h heat transfer coefficient*

h_m average film thickness

k thermal conductivity

f friction factor

K_d mass transfer coefficient

K_{dv} deposition rate constant

N mass rate deposition /unit area

Nu Nusselt number, (h*d/k)

Pr Prandtl number, ($c_p \mu$/k)

Re Reynolds number, (v D/μ)

Sc Schmidt number ($\mu/\rho D'$)

We Weber number ($\rho u^2 d/\sigma$)

T temperature

t temperature

t thickness

u velocity

v main stream velocity

Y Total mass of liquid / total mass of gas

y distance normal to channel or main stream bed.

Z axial distance from onset point of the two fluids

δ film thickness

μ dynamic viscosity

ρ density

σ surface tension

Subscripts

f film or liquid
G gas
g gas
l liquid
L liquid
vm volume mean

REFERENCES

1. **Yukio Hohsho, Tushikazu Kadota, Ken Kado, Kadowaki, Kazuhitu MAKINO and Satoshi KOTERA**

   "Evaporation of Group of Droplets Under Sub Atmospheric Pressure", Bulletin of JSME, Vol 29, N0. 255 Sebtember 1986.

2. **Ricardo, H.R.**

   "The Internal Combustion Engine", Volume 2 - High Speed Engines. Publishers Blackie and Son Ltd., 50 old Bailey London - Glasgow and Bombay.

3. **Harrow, G.A.**

   "The Effect of Mixture Preparation on Fuel Economy", Editted By **Blackmore, D.R.** and **Thomas, A.**, Published by the MacMillan Press.

4. **Beale, N.R. and Hodgetts, D.**

   "The Effect of Mixture quality on the Exhaust gas Emissions of a Petrol Engine", Cranfield Report A.S.A.E., number 1, Cranfield Institute of Technology.

5. **Boam, D. J. and Finlay, I. C.**

   "A Computer Model of Fuel Evaporation in the Intake System of the Carburetted Petrol Engine", Paper Number C 89 / 79 , 1 Mech. Eng. Conf. (March 1979 - 9)

6. **Hasson, D.**

   "Mixture Preparation Combustion in Spark Ignition Engines", Ph.D. Thesis, Aston University 1986.

7. **Trayser, D.A., Creswick, F.A., Gieseke, J.A., Hazard, H.R. and Weller, A.E.**

"A Study of the Influence of Fuel Atomisation, Vaporization and Mixing Processes on Pollutant Emissions from Motor Vehicle Power Plants", Batlle Memorial Inst., Research Report PB 185886, 1969.

8. **Hughes, D.W. and Goulburn, J.R.**

"Fuel Vaporization - Economy with Reduced Exhaust Emissions", Proc. Inst. Mech. Engrs., Vol. 190, 1976.

9. **Peters, B.D. and Quader A.A.**

" 'Wetting' the appetite of spark ignition engines for lean combustion", SAE Paper No. 780234

10. **Germane, J.G, Hess, C.H., Wood., C.G.**

"Lean Combustion Spark-Ignited Internal Combustion Engines - a Review", SAE Paper 831217.

11. **Mizutani, Y. and Nakajima, A.,**

"Combustion of Fuel Vapour - Drop Air Systems.", Combustion and Flame 21, pp. 343-35, 1973.

12. **Subba Rao, H.N. and Lefebvre, A.H.**

"Ignition of Kerosine Fuel Sprays in a Flowing Air Stream.", Combustion Science and Technology Volume 8, pp. 95 - 100, 1973.

13. **Lefebvre, A.H.**

"An Evaporation Model for Quenching Distance and Minimum Ignition Energy in Liquid Fuel Sprays.", Presented at Fall Meeting of the Combustion Institute (Eastern Section 1977)

14. **Elwakil, M. M., Priem, R.J., Brikowisky, H.J., Myeres,P.S., Uyehara, O.A.**

"Experimental and Calculated Temperature and Mass Histories of Vapourizing Fuel Drops", NACA TN - 3490 (1956)

15. **Be'er, J.M. and Chigier. N.A.**

"Combustion Aerodynamics", Applied Science Publications Ltd., 1972.

16. **Williams, A.**

"Mechanism of Combustion of Droplets and Sprays of Liquid Fuels" ,Oxidation and Combustion Reviews, 1, 1-1968

17. **Williams, A.**

" Combustion Flame ", 21, 1- 1973

18. **Agoston,G.A., Wise, H. and Rosser, W.A.**

Sixth Symposium International on Combustion, p 708, Reinhold, New York, 1957.

19. **Sjognen, A..**

Fourteenth Symposium (International) on Combustion p. 919. The Combustion Institute Pittsburgh, 1973.

20. **Williams, A.**

"Fundamentals of Oil Combustion", Energy and Combustion Science, Selected Papers from Progress in Energy and Combustion Science -Pergamon Press - Editted by **N.Chigier -** 1979.

21. **Putnam, A.**

"ARS J. 3, 1467-1468 (1961) "

22. **Faeth, G.M.**

"Current Status of Droplet and Liquid Combustion.", Energy and Combustion Science, Selected Papers from Progress in Energy and Combustion Science -Pergamon Press - Editted by **N.Chigier -**1979.

23. **Ranz, W.E. and Marshall. W.R.**

"Evaporation from Drops", Chemical Engineering Progress 1952, 48, pp141-146,173-180.

24. **Caddock, B.D.**

"The Effect of Physical Properties of Gasoline on Fuel Economy.", Editted By **Blackmore, D.R.** and **Thomas, A. -** 1978, Published by the MacMillan Press.

25. **Goodger, E.M.**

"Petroleum and Performance in Internal Combustion Engines" Published by Butterworth, 1953.

26. **Andreussi, P. and Azzoprdi, B.J.**

"Droplet Deposition and Inter Change in Annular Two-Phase flow", International Journal Multi-Phase Flow, Vol.9., No.6, pp.681-695, (1983)

27. **James, R.P.W., Hewitt., G.F. and Whally, P.B**

"Droplet Motion in Two-Phase Flow", U K A E Report-R 9711.

28. **Heywood, J.B.**

"Pollutant Formation and Control in Spark Ignition Engines"Selected Papers from Progress in Energy and Combustion Science- Pergamon Press, 1979.

29. **Heywood, J.B.**

"Fluid Motion Within the Cylinder of Internal Combustion Engines", the 1986 Freeman Scholar Lecture, Journal of Fluids Engineering, March 1987.

30. **Sandia Report.**

"Sources of Unburned Hydrocarbons from homogeneous Charge, Automotive Engines", Printed September 1983 - Sand. 83-8241.

31. **Blackmore, D.R.**

"The Effect of Emission Controls on Fuel Economy", Fuel Economy of 'The Gasoline Engine', Editted By **Blackmore, D.R.** and **Thomas, A.**

32. **Hayashi, S. and Sawa, N.**

"A Study of the Transient Characteristics of Small S.I. Engines," Bull. JSME, Vol. 27, No. 224, 1984.

33. **Servatti, H.B. and Yuen, W.W.**

"Deposition of Fuel Droplets in Horizontal Intake Manifolds and the Behaviour of Fuel Film on its Walls", SAE Paper NO 840239.

34. **Nightingale, C.J. E. and Tsatsami, V.**

"Seminar on Mixture Preparations on Wall film Measurement", UICEG Meeting, UMIST, June 1984.

35. **Finlay, I.C., McMillan T. and Bannel, J.L.K.**

"Liquid Fuel Distribution in the Region of Throttle Plate of an Air Valve Carburettor,"

36. **Nukiyama S. and Tanasawa, Y.**

"An Experiment on the Atomization of Liquid by Means of an air Stream", A lecture Delivered at Science Lecture Conference of the 40th Rounding Aniversary of the Engineering Society Oct.17, 1937.

37. **Wigg, L.D.**

"Drop Size Prediction for Twin Fluid Atomizers", J. Institute Fuel 37, 500-505, 1964.

38. **Mullinger, P.J. and Chigier, N.A.**

"The Design and Performance of Internal Mixing Multijet Twin fluid Atomizers", J. Institute of Fuel, 47, 25 - 261 (1974)

39. **Woodmansee, D.E.**

"Atomization from Flowing Horizontal Water Film by A Parallel Air Flow, " Ph.D. Thesis in Chem. Eng., University of Illiinois (1968). 12.

40. **Taylor, H. N.S. et al.,** Chemic. Engng. sci. 18 (1963-8), p.537

41. **Dombrowiski, N.**

"Biochhemical and Biological Engineering Science", vol 2, Ch. 16 Academic Press London and New York, 1968.

42. **Zanelli, S. and Hanratty, T.J.**

"Relationship of Entrainment to Wave Structure and Liquid Film," Paper-1, International Symposium on Two-phase Systems Augest 29 Sebt 2, Technicon city, Haifa.

43. **Taylor,G.I.**

"Generation of Ripples by Wind Blowing over a Viscous Fluid", The Scientific Papers of Sir G.I.Taylor, III (Edited by G.K. Batchelor), 244, Cambridge University Press(1963).

44. **Lockhart, R.W.and Martinelli, R.C.**

"Proposed Correlation Data for Isothermal Two-Component Flow in Pipes", Chemical Engineering Progress, Vol.45, No.1, pp. 39-45, January (1949).

45. **Krasikova.**

"Some Characteristic Flows of Two- Phase Flow in Horizontal pipe," Zuhrnal Techichisokoi Fiziki vol. 22 No. 4, 1952 page 656.

46. **McManus, Jr., H.N.,**

"Local Liquid Distribution and Pressure Drop in Annular Two-Phase Flow", ASME Publications, 61-HYD-20, (1961).

47. **Hewitt, G.E. and N.S. Hall Taylor,**

"Annular Two-phase Flow", Chemical Engineering Division A.E.R.E Harwell, England 1970.

48. **Koji Akagawa, Turushige FUJII, Junichi Ito, Yukio HAMANO, Takashiro HORIUCHI.**

"Horizontal Mist Two-Phase flow", 2nd Report, Droplet Deposition and Entrainment Rates." Bulletin of J.SM.E. vol. 28 Number 236. 1985.

49. **Gill, L.E., Hewitt, G.F., Hitchon, J.W. and Lacey, P.M.**
"Sampling Probe Studies of the Gas Core in Annular Two -Phase Flow -1.", Chemical Eng. Sci., vol. 18, pp. 525- 35, 1963.

50. **Gill, L.E., Hewitt, G.F., Hitchon, J.W. and Lacey, P.M.**
"Sampling Probe Studies of the Gas Core in Annular Two-Phase Flow-2" Chemical Eng. Sci., vol. 19, pp. 665-82, 1964

51. **Ueda, T.** Trans. of JSME. (in Japanese) 45-389(1979 -1), p.1", Quoted by Akagawa et al[48]"

52. **Dallman,J.C. and Hanratty, T.J.,**
"Interpretation of Entrainment in Annular Gas-Liquid Flows" Technical Paper of 6th IHIC, (1978).

53. **Wicks, M. and A.E. Duckler,**
"In situ Measurements of Drop Size distribution in Two Phase flow : A New Method for Electrically Conducting Liquids", Paper at International Heat Transfer Conference, Chicago, III. (1966).

54. **Alexander, L.G. and Coldren, C.L.**
"Droplet Transfer from Suspending Air to Dust walls", Ind. & Engng Chem. vol 43, No. 6, pp. 1325- 133, 1951.

55. **McCoy, D.D. and Hanratty T.J.**
"Rate of Deposition of Droplets in Annular Two-Phase Flow," Int. J. Multiphase Flow Vol. 3., pp319-33 1 (1977).

56. **Tatterson, D.F.**
"Rates of Atomization and Drop Size in Annular Two-Phase Flow," Ph.D. Thesis University of Illinois (1975).

57. **Hinze, J.O.**
"Fundamentals of the Hydrodynamic Mechanism of Splitting in Dispersion Process", A.I.CH.E Journ. 1, 289 (1955)

58. **Sekoguchi,K., et al.**

Trans. of JSME (in Japanese) 39 -317, (1973 -1), p. 313", Quoted by **Akagawa et al** [48]"

59. **Isao Kataoka, Mamoru Ishi and Kaichiro Mishima,**

"Generation and Size Distribution in Annular Two-Phase Flow," Transactions of the ASME, Journal of Fluids Engineering, 230/vol. 105, June 1983.

60. **Azzopardi, P. J.**

"Drop Sizes in Annular Two-Phase Flow", Experiments in Fluids,vol 3, pp. 53-59 (1985)

61. **Finlay, I.C., McMillan, T., Bannell, J.L.K., Nightingale, C.J.K.**

"The measurement of droplet sizes leaving the throttle plate of an air valve carburettor ", Dpt. of Industry - National Engng. Lab. Internal report.

62. **Azbel, D. and Liapis, A.I.**

"Mechanisms of Liquid Entrainment", Hand Book of Fluids in Motion Editted by **Cheremisinoff, R. A.** and **Gupta, R.**, 1983, an Arbour Science, the Betterworth Group.

63. **Paleev, I.I. and Flippovich, B.S.**

"Phenomina of Liquid Transfer in Two-Phase Dispersed Annular Flow", International Journal of Heat and Mass Transfer, 9, 1089.

64. **Stull, D.R.**

"Fundamentals of Fire and Explosion", American Inst. of Ch, Eng. AICHE Monograph Series 1977.

65. **Barktnecht, W.**

"Explosion Course Prevention Protection", Springer Verlag-1981.

66. **Mullins, B.P. and Penner, S.S.**

"Explosions, Detonations, Flammability and Ignition", Pergamon Press 1959.

67. **White, A.G.**

"Limits for the Propagation of Flame in Flammable Gas Mixtures pt. 1 Mixtures of Air and One Gas at Ordinary Temperature and Pressure" J.Chem Soc. Tran. 125 (pt. 2), 2387-96 (1924).

68. **Payman, W. and Wheeler, R .**

"Propagation of Flames in Tubes of Small Diameter", J. Chem. Sc. 115, 36, 1919

69. **Ludwig, E.E.**

"Applied Process Design-1", Gulf Publishing Company Houston, 1977.

70. **Helmore, W.**

[Quoted by **Mullins and Penner** (66)]

71. **Joshi, M.V.**

"Process Equipment Design", The McMillan Company of India 1976.

72. **Backhurst, J.R. and Harker, J. H.**

"Process Plant Design" London Heineman Educational 1973.

73. **Truong- Quang Minh.**

"Contribution to the Study of Two Mass Flow in the Annular dispersed Regime" Doct. Ing Thesis, Grenoble.

74. **Mcreath, C.G. and Be'er, J.M.**

"A Review of drop Size Measurement in Fuel Speays", Applied Energy (2) (1976) _ Applied Science Publishers Ltd., England, 1976, 42.

75. **Giffen, E. and Muraszew, A.**

"Atomization of liquid Fuels", Chapman and Hall 1952.

76. **Allen, T.**

"Particle size Measurement", 3rd Edition, Published by Chapman and Hall.

77. **Reynolds, T.W and Gerstein, M.**

"Influence of Molecular Structure of Hydrocarbons on Rate of Flame Propagation", Third Symposium on Combustion, Flame and Explosion Phenomena, p. 192, Williams and Wilkins, 1949.